
Document Number**:** H2020-ICT-52/RISE-6G/D4.4

Project Name:
**R**econfigurable **I**ntelligent **S**ustainable **E**nvironments for **6G** Wireless Networks
(RISE-6G)

# Deliverable D4.4

# Multi-user techniques and connectivity of RIS based communication and mobile edge computing (Final Specifications)

| | | | |
|---|---|---|---|
| Date of delivery: | 30/09/2023 | Version: | 0.1 |
| Start date of Project: | 01/01/2021 | Duration: | 36 months |

# Deliverable D4.4

# Multi-user techniques and connectivity of RIS based communication and mobile edge computing (Final Specifications)

| | |
|---|---|
| **Project Number**: | 101017011 |
| **Project Name:** | **R**econfigurable **I**ntelligent **S**ustainable **E**nvironments for **6G** Wireless Networks |

| | |
|---|---|
| **Document Number**: | H2020-ICT-52/RISE-6G/D4.4 |
| **Document Title:** | Deployment and control strategies of RIS based connectivity (Final Specifications) |
| **Editor(s):** | Paolo Di Lorenzo, Francesca Costanzo (CNIT) |
| **Authors:** | Placido Mursia (NEC), Francesco Devoti (NEC), Vincenzo Sciancalepore (NEC), Fabio Saggese (AAU), Petar Popovski (AAU), Radoslaw Kotaba (AAU), Victor Croisfelt (AAU), Marco Di Renzo (CNRS), Nour Awarkeh (CNRS), Sumin Jeong (CNRS), Hajar El Hassani (CNRS), Kyriakos Stylianopoulos (NKUA), George Alexandropoulos (NKUA), Francesca Costanzo (CNIT), Paolo Di Lorenzo (CNIT), Stefania Sardellitti (CNIT), Minglei You (UNOT), Stephen Creagh (UNOT), Gabriele Gradoni (UNOT), Mattia Merluzzi (CEA), Emilio Calvanese Strinati (CEA) |
| **Dissemination Level:** | PU |
| **Contractual Date of Delivery:** | 30/09/2023 |
| **Security:** | Public |
| **Status:** | Draft |
| **Version:** | 1.0 |
| **File Name:** | RISE-6G_WP4_D4.4_V0.1.docx |

## Abstract

This deliverable provides the results of the RISE-6G proposals on multi-user techniques for RIS-aided communication from work package 4 “RIS for Enhanced Connectivity and Reliability”, as well as final performance evaluations of these proposals.



## Keywords

*Beyond-5G; 6G; RIS; Multi-user; Connectivity; Channel estimation; RIS-profile optimization; Edge computing*

# Contents

# List of Figures

# List of Tables

## List of Acronyms

| | |
|---|---|
| 2D | two-dimensional |
| 3D | three-dimensional |
| 5G | 5th Generation |
| A2G | Air-to-ground |
| AoA | Angle of arrival |
| AoD | Angle of departure |
| AP | Access Point |
| AS | Angle Spread |
| BC | Broadcast channel |
| BCD | Block coordinate descent |
| BER | Bit Error Rate |
| BS | Base station |
| CDF | Cumulative density function |
| CDS | Coherent Modulation Scheme |
| CPU | Central Processing Unit |
| CSI | Channel State Information |
| CSIT | Channel State Information at the Transmitter |
| DDPG | Deep Deterministic Policy Gradient |
| DEA | Dynamical energy analysis |
| DL | Downlink |
| DOF | Degree of freedom |
| DPSK | Differential Phase Shift Keying |
| DQN | Deep Q Networks |
| DRL | Deep Reinforcement Learning |
| DS | Delay Spread |
| E2E | End-to-End |
| EE | Energy Efficiency |
| EH | Energy Harvesting |
| EM | Electromagnetic |
| eMBB | enhanced Mobile BroadBand |
| EMI | Electromagnetic Interference |
| ES | Edge server |
| FDMA | Frequency-Division Multiple Access |
| GHz | Giga-Hertz |
| HRIS | Hybrid RIS |
| IoT | Internet of Things |
| KPI | Key performance indicator |
| LIS | Large intelligent surface |
| LoS | Line of Sight |
| MAC | Multiple Access Channel |
| MEC | Multi-access Edge Computing |

| | |
|---|---|
| MI | Mutual Information |
| MIMO | Multiple-input multiple-output |
| MMSE | Minimum mean squared error |
| MRT | Maximum ration transmission |
| MSE | Mean Squared Error |
| NCDS | Non-Coherent Demodulation Scheme |
| NLoS | Non-line-of-sight |
| NMSE | Normalized Mean Squared Error |
| OFDM | Orthogonal Frequency Division Multiplexing |
| PEC | perfect electric conductor |
| PIN | positive-intrinsic-negative |
| PL | Physical Layer |
| RAT | Radio access technology |
| RCS | Radar cross section |
| RF | Radio frequency |
| RIS | Reconfigurable intelligent surface |
| RISC | RIS Controller |
| RISE | RIS enabled |
| RISO | RIS Orchestrator |
| RL | Reinforcement Learning |
| Rx | Receiver |
| SCA | Successive Concave Approximation |
| SDR | Semidefinite relaxation |
| SE | Spectral Efficiency |
| SEP | Symbol Error Probability |
| SIMO | Single-input multiple-output |
| SINR | Signal to Interference plus Noise Ratio |
| SISO | Single Input Single Output |
| SLNR | Signal to leakage and noise ratio |
| SMSE | Sum mean squared error |
| SNR | Signal to Noise Ratio |
| SotA | State-of-the-art |
| TDMA | Time-Division Multiple Access |
| THz | Tera-Hertz |
| Tx | Transmitter |
| UAV | Unmanned Aerial Vehicle |
| UE | User equipment |
| URLLC | Ultra-Reliable Low-Latency Communication |
| wMMSE | Weighted mean squared error |
| ZF | Zero-forcing |

# 1 Introduction

In the present deliverable, we report the research work carried out by the consortium of RISE-6G on multi-user algorithms and protocols for application to reconfigurable intelligent surface (RIS)-aided smart radio environments. The research findings reported in the present deliverable are in agreement with the initial specifications reported in deliverable D4.1 titled "On deployment and control strategies of RIS based connectivity". The results reported in the present deliverable constitute the final specifications that further elaborate and finalize the intermediary results provided in deliverables D4.2 and D4.3.

## 1.1 Deliverable objectives

The objectives of the present deliverable are the following:

(1) To report specifications and final results on fundamental performance limits in RIS-aided smart radio environments, which account for RIS-aided channel models and the associated control overhead.

(2) To report specifications and final results on the design and optimisation of control signalling protocols, channel estimation algorithms, resource allocation and scheduling policies to support the efficient deployment of RISs in smart radio environments.

(3) To report specifications and final results on the design and optimisation of resilient, energy efficient, and joint communication and computation mechanisms with low electromagnetic field exposure for application to power- and latency-constrained (edge) cloud services.

## 1.2 Deliverable structure

After reviewing the key performance metrics and Key Performance Indicators (KPIs) specified in deliverable D4.1, which drives the development of the research work within WP4 and the RISE-6G project, the present deliverable is logically organized in compliance with the tasks of WP4. More specifically, deliverable D4.4 is organized in three main macro sections that are focused on:

(1) The fundamentals of multi-user network connectivity for RISE systems (i.e., Section 3).

(2) The design of multi-user techniques for RISE communications (i.e., Section 4).

(3) The design of multi-user techniques for RISE mobile edge computing (i.e., Section 5).

In this document, multi-user can refer also to multi-RIS systems, which require coordination techniques as well. Moreover, we remark that with RISE system, we refer to every kind of network including RISs, while with "RIS-empowered" or "RIS-aided" we refer to systems where a single or multiple RISs are used to enhance the achievable performance.

As far as the first macro section is concerned, in Table 3-1 we list 13 main research and technology contributions made by the RISE-6G consortium: four of them were already detailed in D4.2, whereas the remaining nine are novel contributions described by this deliverable. The list of the nine new contributions is as follows: (i) Scattering Aware Reconfigurable Intelligent Surface (SARIS); (ii) Randomized control of coherence time via RIS; (iii) Metrics from direction-resolved signal-to-noise ratios: Analytical characterisation of modes and channels using Slepian method extended to nearfield; (iv) Metrics from direction-resolved signal-to-noise ratios: Channels, mutual information and capacity derived from direction- and position-resolved Signal to Noise Ratio (SNR) using ray-tracing in multi-reflective environments; (v) Model-free channel hardening algorithm with lab-based experiment to evaluate the channel hardening performance in the reverberation chamber environment; (vi) Non-coherent modulation schemes in RIS communications; (vii) Capacity analysis of large-RIS-systems; (viii) On the maximum achievable Sum-Rate of the RIS-aided Multiple-Input Multiple-Output (MIMO) broadcast channel; (ix) Extra degrees of freedom (DOF) in RIS tuning via rotation and movement.

As far as the second macro section is concerned, in Table 4-1 we list 17 main research and technology contributions made by the RISE-6G consortium: 5 of them were already detailed in D4.2, whereas the

remaining 12 are novel contributions described by this deliverable. The list of the 12 new contribution is as follows: (i) Random access protocol with channel oracle enabled by a Reconfigurable Intelligent Surface; (ii) Multi-RIS massive access protocol via scheduling and contention; (iii) Generalized unitary approximate message passing for double linear transformation model; (iv) Direct tensor-based estimation of broadband mmWave channels with RIS; (v) Channel estimation with simultaneous reflecting and sensing hybrid reconfigurable intelligent metasurfaces; (vi) Uplink multiplexing of enhanced Mobile Broadband (eMBB) / Ultra Reliable Low Latency Communication (URLLC) services assisted by RISs; (vii) Distributed sum-rate maximization of cellular communications with multiple RISs; (viii) Autonomous RIS solution with Energy harvesting and Self-configuration (ARES) towards 6G ; (ix) Localization-based Orthogonal Frequency Division Multiplexing (OFDM) framework for RIS-aided systems; (x) RIS-aided URLLC with imperfect device tracking; (xi) Two-timescale design for RIS-aided massive MIMO systems with imperfect Channel State Information (CSI); (xii) RIS area illumination strategies.

As far as the third macro section is concerned, in Table 5-1 we list 6 main research and technology contributions made by the RISE-6G consortium: 4 of them were already detailed in D4.2, whereas the remaining 2 are novel contributions described by this deliverable. The list of the 2 new contributions is as follows: (i) Model-based joint optimisation of RIS, wireless and computing resources for energy-efficient edge inference; (ii) Mixed model-based and data-driven joint optimization of RIS, wireless and computing resources for energy-efficient edge inference.

Finally, the present deliverable is concluded with a summary of the main obtained scientific contributions.

### 1.3 Definitions and taxonomy

The main notation symbols appearing throughout the document are listed in Table 1-1. Miscellaneous self-contained notations introduced in certain contributions will be defined per case. In listed figures and algorithms, the notation may follow that of the corresponding publication, for a consistent presentation.

**Table 1-1: Definition of the main notation symbols.**

| Parameter | Notation | Parameter | Notation | Parameter | Notation |
|---|---|---|---|---|---|
| Total number of UEs | $K$ | Receive signal at UE k | $y_k$ | Transmit symbol for UE k | $s_k$ |
| RIS phase shift matrix | $\boldsymbol{\Phi}$ | Number of RIS elements | $N = N_x \times N_y$ | Base station (BS) precoder | $\boldsymbol{v}$ |
| Power budget at the BS | $P$ | Working wavelength | $\lambda$ | Receiver noise | $n_k$ |
| Sum rate | $R_{tot}$ | Rate of UE k | $R_k$ | Working frequency | $f$ |

# 2 Metrics and KPIs

## 2.1 KPIs for control channels

The metrics considered in this WP have been presented in detail in D4.2. Their definitions and further analysis for the objectives of RISE-6G have been the focus of WP2. Since this deliverable presents this project's final contributions to methodologies for enhanced connectivity, communication, and Multi-access Edge Computing (MEC) systems, this section provides a taxonomy of the metrics considered per contribution, to give an overview of the WP's contributions. A brief description of the metrics considered here is given below and their associated contributions are given in Table 2-1.

- **SNR**: The ratio of the desired signal power to the background noise power, indicating signal clarity and quality, indicating the link quality (Definition: D4.2/2.2).
- **SINR** (Signal-to-Interference-plus-Noise Ratio): An extension of the SNR metric which considers interference from other signals, providing a more accurate measure of signal quality in the presence of interference scenarios, e.g., multi-user communications (Definition: D4.2/2.2).
- **Sum-Rate:** The total data rate achieved by all users in a wireless system, used to assess the overall system capacity (Definition: D4.2/2.2).
- **Mutual Information** (MI): The amount of information that can be reliably transmitted over a channel, considering both the signal power and noise. MI gives an information-theoretic perspective on the optimal link capacity. Specifically, given a transmitted signal $x$ and a received signal $y$, the MI is expressed as

$$I(x;y) = H(x) - H(x|y),$$

where $H(x)$ denotes the entropy of the transmit signal and $H(x|y)$ denotes its conditional entropy when observing $y$. The maximum average mutual information, in an instant of a signaling interval, when transmitted by a discrete memoryless channel, the probabilities of the rate of maximum reliable transmission of data, is termed as the channel capacity.

- **Minimum Rate:** In a multi-user system, this metric is the minimum data rate (i.e., spectral efficiency (SE) – defined in D4.4/2.2) among all participating users. It is used to assess reliability and fairness schemes.
- **Throughput:** The actual data rate achieved in a communication link, accounting for various factors including channel conditions, protocol overhead, and packet loss (Definition: D4.2/2.2).
- **Goodput:** The useful data rate received at the application layer, excluding protocol overhead and retransmissions. The exact definition of this metrics depends on protocol implementations.
- **E2E** (End-to-End) **Delay**: The time it takes for a packet to travel from the source to the destination in a communication network, including all processing and transmission delays. This metric is of particular importance in MEC systems, where computation is offloaded to a remote machine (Definition: D4.2/2.1).
- **Outage Probability**: The likelihood that a wireless link's performance (normally, spectral efficiency, as defined in D4.2/2.1) falls below a specified threshold due to fading or other impairments. This definition is closely related to the definition of reliability in D4.2/2.3.
- **Power Consumption:** The amount of energy used by wireless devices (in particular, RISs) to operate per time unit.
- **Harvested Power:** The amount of power collected from the environment via RF chains of wireless devices (in particular, RISs).
- **Channel Temporal Correlation:** The extent to which the wireless channel's characteristics remain consistent over time. It is based on self-correlation of the channel as a function of the time.
- **Direction-Resolved SNR:** SNR measured and analysed with respect to different spatial directions, considering antenna patterns and beamforming.
- **NMSE:** Normalised mean-squared error between the estimated/received signal or channel matrix and the original signal or channel matrix. In this deliverable, it is used in the context of channel estimation to assess the performance of the proposed schemes (Definition: D4.2/2.6).

**Table 2-1: Metrics per contribution considered in this deliverable.**

| Metric(s) | Primary Contribution Objective | Contribution(s) |
|---|---|---|
| Sum-rate | Capacity Analysis | 3.5.1 |
| Channel Temporal Correlation | Channel Analysis | 3.5.2 |
| Direction-Resolved SNR | Channel Analysis | 3.5.3 |
| SNR | Channel Analysis | 3.5.4, 3.5.5 |
| SINR | System Analysis | 3.5.6 |
| Mutual Information | Capacity Analysis | 3.5.7 |
| Throughput | Multiple Access | 4.4.1, 4.4.2 |
| NMSE | Channel Estimation | 4.4.3, 4.4.4, 4.4.5 |
| Outage Probability | URLLC and eMBB slicing | 4.4.6 |
| Sum-rate | Rate Enhancement | 4.4.7 |
| Power (gained) | Power Harvesting | 4.4.8 |
| Goodput | Resource allocation for ISAC | 4.4.9 |
| Power (consumed) | URLLC | 4.4.10 |
| Minimum Rate | Rate Enhancement | 4.4.11 |
| SNR | Communication with blockage | 4.4.12 |
| E2E delay – Power consumption | MEC classification | 5.1.1, 5.1.2 |

# 3 Fundamentals of Multi-User Network Connectivity for RISE Systems

## 3.1 Joint Active and Passive Beamforming

In this section, we give the most general definition of the multi-user problem in RIS-aided wireless networks. We show how the key aspect is the joint optimization of the (active) beamforming at the BS and the (passive) beamforming at the RIS. In the default settings, a given number of end users (UEs) $K$ is scheduled to be served at the same time-frequency resources.

Focusing on the downlink, let $y_k$ denote the received signal at the (single antenna) UE $k$, which reads as

$$y_k = (\boldsymbol{h}_k^{\boldsymbol{H}} \boldsymbol{\Phi} \boldsymbol{G} + \boldsymbol{h}_{d,k}^{\boldsymbol{H}}) \boldsymbol{v}\, s_k + n_k$$

where $\boldsymbol{h}_k^{\boldsymbol{H}}$, $\boldsymbol{G}$, and $\boldsymbol{h}_{d,k}^{\boldsymbol{H}}$ denote the channel vectors from the RIS to the UE, from the BS to the RIS and from the RIS to the UE, respectively, and all other notations are defined as in Section 2. Here, the BS precoder and the RIS phase-shifting matrix contribute together to the received signal quality. Hence, their optimization must be jointly considered. Let $\boldsymbol{f}(\cdot)$ be the considered network utility function, such that we can define the following optimization problem:

$$\max_{\boldsymbol{\Phi},\boldsymbol{v}} \ \boldsymbol{f}(\boldsymbol{\Phi}, \boldsymbol{v})$$
$$\text{s.t.} \ \ \left|[\boldsymbol{\Phi}]_{i,i}\right|^2 \leq 1, \qquad \left|[\boldsymbol{\Phi}]_{i,j}\right|^2 = 0$$
$$\|\boldsymbol{v}\|^2 \leq \boldsymbol{P}$$

where the first constraint is required to guarantee that the phase-shift configuration at the RIS is given by a diagonal matrix and that the incoming signal is not amplified, while the second constraint limits the

transmit power at the BS. Note that in the most general definition of such problem, the RIS is treated as an *ideal* hardware capable of any continuous phase-shift. However, several existing works consider the more practical case of a discrete set of phase-shifting configurations.

### 3.1.1 Capacity analysis

In [MAD23], by exploiting tools from random matrix theory, the authors characterize the asymptotic achievable capacity of a multi-RIS system, which is valid in the regime of large number of both BS antennas and RIS elements. Specifically, the mutual information between transmitter and receiver is shown to converge to a Gaussian distribution. As a result, an optimal capacity-achieving RIS configuration is derived by exploiting the channel correlation matrices only. Hence, since the optimized RIS configuration can be kept constant for several channel frames, this framework is applicable without the need to acquire costly instantaneous CSI, as is the case for many existing works.
In the sequel, the detailed analytical results in Section 3.5.3 apply in the special case of ray densities that are uniform in the set formed in the receiver phase plane by rays arriving from the transmitter (Tx). Section 3.5.4 considered complex, lossy and metareflective environments, where the density is variable and, although degree-of-freedom estimates outlined in Section 3.5.3 are still valid, the singular values of the channel matrix depend on the detailed variation of this density, which can be used to define a local SNR that is resolved in terms of AoA, as well as position. The methodology used is based on a representation of both Tx and receiver (Rx) correlation functions in terms of (distinct) ray densities, using the Wigner transform. Using ray-tracing approaches such as Dynamical Energy Analysis (DEA), it is possible to propagate the Tx ray density to the Rx, where it is compared with a ray density defined by Rx noise to define a SNR*(x,p)* that depends on AoA (coordinate *p*) as well as position (coordinate *x*).

### 3.1.2 Cascaded/Linear channel model

In this section, we describe approaches to maximize the chosen network utility function under conventional cascaded/linear channel model, i.e., the one described in Section 3.1 where the RIS configuration is represented by a diagonal matrix of phase shifts.

In this regard, the choice of the objective function is of paramount importance, especially for massive access scenarios. Indeed, it must be chosen to provide high-performing solutions while guaranteeing efficiency and scalability. While several existing works focus on maximizing the rate of each UE (see, e.g., [WZ19]), which is a highly-challenging non-convex problem, in [MDS21] the sum mean squared error (SMSE) of the received signal has been shown to have a convex structure in the two optimization variables separately, i.e., $\boldsymbol{\Phi}$ and $\boldsymbol{v}$. Such property allows to obtain an efficient and convergent algorithm via alternating optimization that is shown to outperform conventional state-of-the-art MIMO beamforming techniques in the absence of the RIS, thus demonstrating its potential gains in terms of system sum-rate.

Moreover, in [PTD22], the authors investigate the achievable Sum-rate optimization in a BC in the presence of multiple RISs and with multiple multi-antenna users. Due to the non-convexity of the optimization problem and the possibility that a local optimization method may be trapped in a bad local optimum, the authors exploit the duality between the Gaussian MIMO Broadcast Channel (BC) and the multiple-access channel (MAC), to derive optimization algorithms targeting the users' covariance matrices and the RIS phase shifts in the dual MAC alternatively. The users' covariance matrices are obtained by a dual decomposition method with a block coordinate maximization (BCM), while the phase shifts of the RIS elements are computed sequentially and are formulated in a closed-form expression. Two time-efficient alternatives are also provided, based on approximate alternating optimization and projected gradient.

### 3.1.3 Impedance-based channel model

The signal model employed above is based on conventional communication and antenna theory and assumes absence of mutual coupling (i.e., half-wavelength inter-element distance), far-field, and independence between the signal attenuation and phase shift at each RIS unit cell [HZA19]. Depending on the application environment and the available practical hardware, some of these assumptions may not hold in real-life scenarios.

In this regard, an electromagnetic-compliant and mutual coupling aware channel model was recently introduced in [GD21] (further details can found in D3.3), which is equivalent to a MIMO channel. Under this setting, the above signal model is modified as follows (for the case of single-antenna transmitter)

$$y_k = H_{e2e}\, s_k + n_k$$

where the channel coefficient is given by

$$H_{\boldsymbol{e2e}} = y_0\left(Z_{RT} - \boldsymbol{Z}_{RS}(\boldsymbol{Z}_{RIS} + \boldsymbol{Z}_{SS})^{-1}\boldsymbol{Z}_{ST}\right),$$

with $y_0$ accounting for internal impedance of the voltage generator of the transmitter, load impedance of the receiver, and self-impedance of the transmit and receive antennas, whereas $\boldsymbol{Z}_{X,Y}$ is the (self) mutual impedance between $X$ and $Y$, where $T, R, S$ stand for the transmitter, the receiver and the RIS, respectively. Moreover, $\boldsymbol{Z}_{RIS}$ represents the tunable (diagonal) impedance matrix at the RIS. Under this model, the optimization procedure requires to deal with the inverse operation, which further compounds the complexity of designing optimal RIS strategies [ADD21], [QD21], [MPS23]. In this regard, [MPS23] extends the framework presented in [MDS21] and Section 3.1.2 to this non-linear channel model by exploiting the Neumann series to linearize the expression in small iterative updates of the matrix of tunable RIS impedances $\boldsymbol{Z}_{RIS}$.

A treatment of degree-of-freedom estimation and an accompanying analytical approximation (in 2D) of channel strengths based on the geometry in phase space of the set of rays connecting transmitter to receiver were previously studied, which made simplifying assumptions that the receiver was in the far-field. Section 3.5.3 extended it to near-field geometries for which the relevant ray sets are more complex. This contribution aims to evaluate information metrics in large, complex environments where direct modelling of the propagated wave solution is not feasible. To account for the more general case, a coordinate transformation is found, which deforms near-field geometries into the rectilinear setting for which this conventional Slepian analysis applies, albeit approximately.

### 3.1.4 Channel statistics

Motivated by the growing concerns on the applicability of per-channel frame RIS optimization frameworks that require instantaneous CSI, [CAG22a] and [CAG22b] deal with the design of a non-coherent modulation scheme for a RIS-aided single-input multiple-output (SIMO) network. In this context, the authors propose to exploit the robust nature of Differential Phase Shift Keying (DPSK), which is proven to work well under fast-varying channels. With the proposed framework, the control channel previously used for CSI acquisition is removed, and the corresponding time-frequency resources are used for communication, thus improving the overall network performance. Moreover, thanks to the non-coherent modulation scheme, the RIS configuration can be chosen at random, thus allowing to remove most of the resources dedicated to the RIS control channel and resulting in a simplified design of RIS-aided networks, especially under massive deployment. While the aforementioned works have demonstrated the potential benefits brought by relying solely on channel statistics (see [MAD23], [CAG22a] and [CAG22b]), in [ICS23], the authors investigate how the RIS can be exploited to alter such statistics in a desired way. For instance, the RIS can be used to create artificial time diversity in slow-fading channels. In this way, the RIS may be used to render and control a rich scattering environment.

## 3.2 Static versus Nomadic RIS

In the previous section, we assumed a static RIS position, e.g., mounted on the façade of a building or indoor wall. However, this might not be the case for some novel RIS use cases.

In this regard, consider the newly defined concept of air-to-ground network, whereby aerial devices, such as Unmanned Aerial Vehicles (UAVs), are used to facilitate the communication between a BS and a set of target UEs by flying above obstacles and providing enhanced connection reliability. In this context, RISs can be leveraged to alleviate the limited battery life of such devices, while guaranteeing advanced beamforming capabilities.

Owing to the non-static RIS position, the aforementioned multi-user problem formulation is modified by introducing the variation of the RIS position and orientation over time [DMS22] [SAH22].

However, since UAVs might be subject to unwanted perturbations caused by meteorological phenomena, the system needs to take into account a degree of uncertainty on the (nominal) position and orientation of the RIS [MSL23].

While the aforementioned works study how to counteract the possible misalignments induced by random and unwanted rotations of the RIS surface, in [JAS22], it is proposed to exploit the extra degree of freedom given by the RIS orientation to improve the system performance. Indeed, in this case the RIS orientation is optimized to maximize the received signal power at a given receiver location. The results show that the optimized RIS rotation has a greater impact as compared to the classical RIS positioning problem.

## 3.3 Exploiting the Frequency Domain in RISE Systems

While in Section 3.1, the problem of multi-user network connectivity in RISE systems is treated by designing optimized beamforming techniques both at the RIS and at the BS, advanced RIS hardware design may be exploited to achieve multi-frequency operation, without the need of redundant deployments.

Indeed, novel RIS designs allow to operate on different frequency bands with the same hardware. In this way, the users may be scheduled in the frequency-domain as well and/or multiple RATs may be supported. In [MAM22], the RIS unit cell is replaced by a reconfigurable patch-antenna, i.e., an antenna whose operating frequency may be dynamically configured. By doing so, and depending on the chosen working frequency, the inter-element spacing may be different than the conventional half-wavelength. As a result, the array response may be corrupted by mutual coupling effects. A solution to this problem may be given by selectively turning-off antenna elements, so as to restore independence across the array of antennas. The choice of the elements activation requires additional optimization, which is coupled with the current propagation environment and application scenario.

## 3.4 Autonomous RISs

The above-mentioned methods rely on a control channel between the BS and the RIS, which is used to communicate to the RISC the optimized phase-shift configuration. Moreover, the BS exploits the available CSI at the transmitter (CSIT) to optimize the given network utility metric.

In real-life scenarios, such assumptions may be unpractical or even unfeasible. Hence, recent works have introduced the concept of self-configuring RISs, whereby the RISC exploits only locally available CSI to automatically find the best RIS configuration.

In [ADS22], the authors propose to embed the RIS with basic sensing capabilities and denote it with *hybrid* RIS (HRIS). A fraction of the incident signal is redirected to a sensing branch on the RIS. Both signal components are phase-shifted by the same amount, which is different for each unit cell. During uplink transmission, the power of the signal obtained by summing-up all the outputs of sensing branches across the array can be exploited to infer the location of the intended receiver. Such information, together with the known BS position, is then exploited to self-configure the RIS by aligning it to the direction of maximum power as computed by the sensing branch.

## 3.5 Contributions from RISE-6G

The following table lists the relevant contributions from RISE-6G in the multi-user connectivity design for RISE systems and summarizes the key system parameters.

**Table 3-1 Contribution from RISE-6G on fundamentals of multi-user network connectivity.**

| Title | Scope | Optimization variables | #BS | #RIS | CSI | Continuous/ quantized phase-shift | Deliverable/ Section no. |
|---|---|---|---|---|---|---|---|
| SARIS: Scattering Aware Reconfigurable Intelligent Surface (Optimization of the RIS configuration under the impedance-based channel model) | Minimizing SMSE | BS beamforming configuration and RIS tunable impedances. | 1 | 1 | Perfect | Quantized/bounded. | D4.4/3.5.1 |
| Randomize control of coherence time via RIS | Coherence time | Seed for randomized RIS phase-shifts, RIS number of elements | 1 | 1 | Line-of-sight (LoS) component known | Continuous | D4.4/3.5.2 |
| Metrics from direction-resolved signal-to-noise ratios: Analytical characterisation of modes and channels using Slepian method - extended to nearfield | Near-field degree-of-freedom estimation and analytical approximation of channel strengths | N/A | 1 | 1 | Unknown | N/A | D4.4/3.5.3 |
| Metrics from direction-resolved signal-to-noise ratios: Channels, mutual information and capacity derived from direction- and position-resolved SNR using ray-tracing in multi-reflective environments | Analytical approximation of channel strengths in the case of variable ray densities | N/A | 1 | 1 | Unknown | N/A | D4.4/3.5.4 |
| Model-free channel hardening algorithm with lab-based experiment to evaluate the channel hardening | Maximize SNR | RIS phase-shifts | 1 | 2 | Unknown | Quantized | D4.4/3.5.5 |

| | | | | | | | |
|---|---|---|---|---|---|---|---|
| performance in the reverberation chamber environment | | | | | | | |
| Non-Coherent Modulation Schemes in RIS communications | Analysis of NCDS in presence of RIS | N/A | 1 | Any | Un-known | Both | D4.4/3.5.6 |
| Capacity analysis of large-RIS-systems | Ergodically optimal RIS profiles | RIS phase shifts | 1 | Mul-tiple | Statis-tical | Continu-ous | D4.4/3.5.7 |
| On the Maximum Achievable Sum-Rate of the RIS-Aided MIMO Broadcast Channel | Maximize Achievable Sum-rate | users' covari-ance matrices and RIS phase shifts | 1 | Mul-tiple | Perfect | N/A | D 4.4/3.5.8 |
| Extra Degrees of freedom in RIS tuning via Rota-tion and Move-ment | Analysis of the directiv-ity patterns | RIS rotation and position optimisation. | 1 | 1 | Un-known | Continu-ous | D4.4/3.5.9 |
| Joint active-pas-sive beamforming (RISMA) | SMSE | BS and RIS beamforming configura-tions. | 1 | 1 | Perfect | Quantized | D4.2/3.5.1 |
| A Frequency-Ag-nostic RIS-based solution (FABRIS) | Maximize SLNR | RIS phase-shifts, activa-tion profile, and BS pre-coder | 1 | 1 | Perfect | Continu-ous | D4.2/3.5.3 |
| RIS-Empowered UAV Communi-cations for Robust and Reliable Air-to-Ground Net-works (RiFE) | Maximize Minimum SNR | BS and RIS phase-shifts | 1 | 1 | Statis-tical | Continu-ous | D4.2/3.5.2 |
| A Self-Configur-ing RIS Solution Towards 6G (MARISA) | Maximize Sum Rate | RIS phase-shifts | 1 | 1 | Un-known | Continu-ous | D4.2/3.5.4 |

### 3.5.1 SARIS: Scattering Aware Reconfigurable Intelligent Surface (Optimization of the RIS configuration under the impedance-based channel model)

***Motivation and context***

In this section, we summarize the contribution in [MPS23], which focuses on extending the end-to-end mutual coupling aware and electromagnetic-compliant channel model, which was initially proposed in [GD21] for the case of pure LoS between Tx-RIS and RIS-Rx to the case of complex propagation environments with scattering clusters.

We consider the system model depicted in Figure 3-1, wherein a multi-antenna BS serves multiple single-antenna terminals with the aid of a $N$-element RIS whose antenna elements are spaced by $d$. Moreover, by exploiting the discrete dipole approximation [YH07], we model the scattering clusters as collections of thin-wire half-wavelength dipoles that are assumed to be co-planar with the RIS.

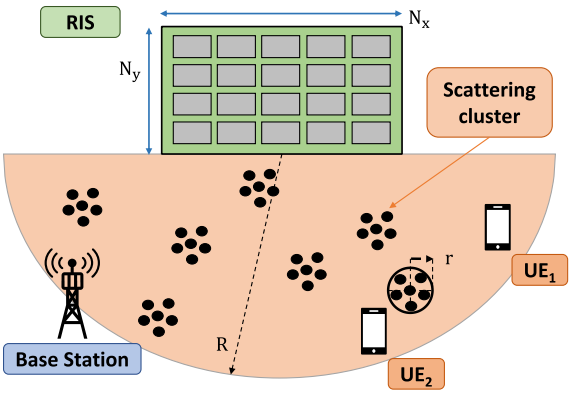


**Figure 3-1 RIS-aided propagation environment with scattering clusters.**

In this setting, we model the end-to-end MIMO channel as

$$\boldsymbol{H}_{E2E} = (\boldsymbol{I}_L + \boldsymbol{Z}_{RR}\boldsymbol{Z}_L^{-1})^{-1}[\boldsymbol{Z}_{RT} - \boldsymbol{Z}_{RE}(\boldsymbol{Z}_{EE} + \boldsymbol{Z}_{SC})^{-1}\boldsymbol{Z}_{ET}](\boldsymbol{Z}_{TT} + \boldsymbol{Z}_G)^{-1} \in \mathbb{C}^{L\times M}$$

$$\boldsymbol{Z}_{EE} = \begin{bmatrix} \boldsymbol{Z}_{OO} & \boldsymbol{Z}_{OS} \\ \boldsymbol{Z}_{SO} & \boldsymbol{Z}_{SS} \end{bmatrix}, \qquad \boldsymbol{Z}_{RE} = [\boldsymbol{Z}_{RO} \quad \boldsymbol{Z}_{RS}], \qquad \boldsymbol{Z}_{ET} = [\boldsymbol{Z}_{OT}{}^T \quad \boldsymbol{Z}_{ST}{}^T]^T$$

$$\mathbf{Z}_{\mathrm{SC}} = \begin{bmatrix} \mathbf{Z}_{\mathrm{US}} & \mathbf{0} \\ \mathbf{0} & \mathbf{Z}_{\mathrm{RIS}} \end{bmatrix}$$

where the code letters $\mathrm{R}, \mathrm{T}, \mathrm{S}, \mathrm{O}$ stand for the Rx, Tx, RIS and scattering objects, respectively. Moreover, $\mathbf{Z}_{\mathrm{US}}$ is a diagonal matrix modelling the loads of each scattering dipole. In this way, by suitably adjusting such load we can model any kind of realistic scattering object. Lastly, the tunable RIS impedance matrix is modelled as

$$\mathbf{Z}_{\mathrm{RIS}} = \mathrm{diag}[\mathrm{R}_0 + jx_n]_{n=1}^{\mathrm{N}}$$

with $\mathrm{R}_0$ a constant value modelling the RIS internal circuit losses, and $x_n$ the tunable reactance of each RIS unit cell.

***Methodology***

In this context, we formalize the problem of jointly optimizing the BS and RIS active and passive beamforming vectors, respectively, via the RISMA framework in [MDS21]. In particular, in this context, the RIS passive beamforming vector is identified via the matrix of tunable impedances $\mathbf{Z}_{\mathrm{RIS}}$. Hence, given the expression of the channel provided above, we have the additional complexity of having the optimization variable inside an inverse matric operation. To deal with this issue, we employ the Neumann series [QD21]. Specifically, at each iteration of our proposed approach, we optimize only a small update of $\mathbf{Z}_{\mathrm{RIS}}$, as $\mathbf{Z}_{\mathrm{RIS}}{}^{i+1} = \mathbf{Z}_{\mathrm{RIS}}{}^{i} + \boldsymbol{\Delta}$. Hence, thanks to the Neumann series we can formulate the inverse matrix

operation and make it linear in $\boldsymbol{\Delta}$, which is now our new optimization variable. Indeed, if $\boldsymbol{\Delta}$ is small enough, we have that $\left(\boldsymbol{A}+\mathbf{Z}_{\mathrm{RIS}}{}^{i}+\boldsymbol{\Delta}\right)^{-1} \approx \boldsymbol{G}^{i}-\boldsymbol{G}^{i}\boldsymbol{\Delta}\boldsymbol{G}^{i}$, where $\boldsymbol{G}^{i}=\left(\boldsymbol{A}+\mathbf{Z}_{\mathrm{RIS}}{}^{i}\right)^{-1}$ for any non-diagonal matrix $\boldsymbol{A}$.

After a series of mathematical reformulations, we can cast the problem in the same bi-convex nature of [MDS21]. The formulated optimization algorithm is dubbed as *SARIS*, which is formally proven to converge to a stationary point in [MPS23].

***Results and outcome***

In the latter, we provide some numerical results of a $\mathrm{L}=2$ UE setting by comparing SARIS with two reference schemes, namely the block-coordinate descent weighted Minimum Mean Squared Error (BCD wMMSE) algorithm in [ADD21] and a *mismatched* model, which corresponds to ignoring the interactions between the RIS and the scattering objects (i.e., by setting $\mathbf{Z}_{\mathrm{OS}}=\mathbf{Z}_{\mathrm{SO}}=\mathbf{0}$). In Figure 3-2 we show the convergence of the considered algorithms for different values of $N$ and $d$ on the left-hand side, while we show the convergence versus the value of $\mathrm{R}_0$ for $\mathrm{N}=64$ and $\mathrm{d}=\lambda/8$. Here, we demonstrate how SARIS is both faster and more stable than reference schemes. In Figure 3-3, we show the achievable sum-rate of the considered schemes versus the number of UEs $L$ (left-hand side) and the number of scattering clusters $\mathrm{N_c}$ (right-hand side), for different values of $N$ and $d$. Details on the numerical results can be found in [MPS23].

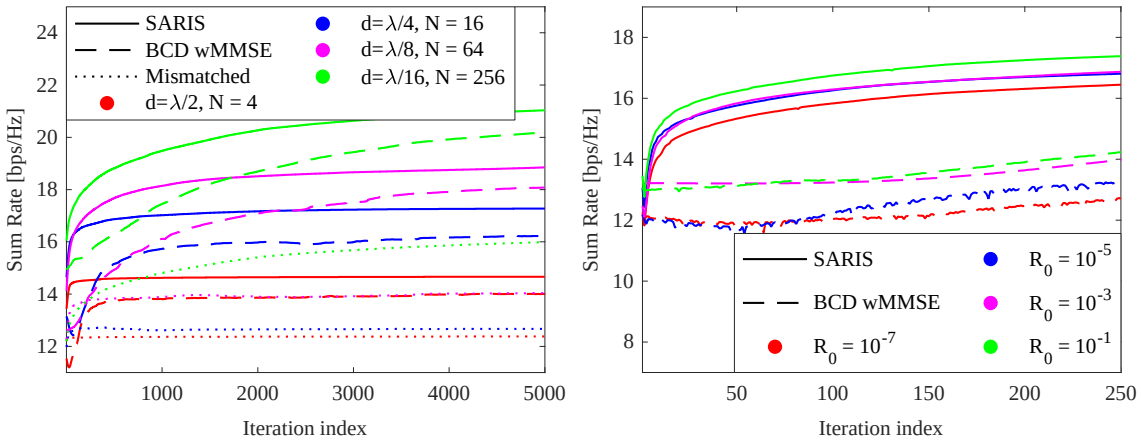


**Figure 3-2 SARIS algorithm convergence for different values of N and d (left-hand side) and $\mathrm{R_0}$ (right-hand side).**

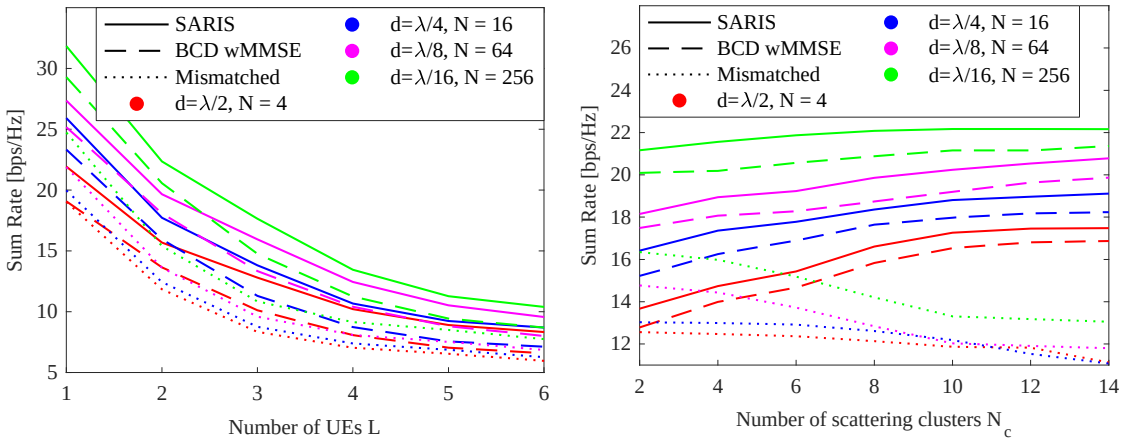


**Figure 3-3 Sum rate obtained with SARIS and the reference schemes versus the number of UEs L (left-hand side) and the number of scattering clusters $\mathrm{N_c}$ (right-hand side), for different values of N and d.**

***Relation to other RISE6G contributions***

This contribution creates a link between advanced channel models derived in WP3, such as the one in [GD21], to optimization methods characterized in WP4, such as [MDS21]. Indeed, it provides a framework for joint active and passive beamforming under electromagnetic compliant and mutual coupling aware channel models, which are intrinsically more complex to tackle as compared to standard cascaded/linear modes, as described in Section 16.

### 3.5.2 Randomize control of coherence time via RIS (Method to control the coherence time of a UE through the change of configuration of an RIS)

***Motivation and context***

In the current literature, there are numerous use cases showing how an RIS can control the wireless propagation to improve the communication performance by maximizing the Quality of Service (QoS). However, relatively few works explore how to use an RIS to shape the temporal channel statistics, such as the channel correlation. Such a control could be used to induce temporal diversity in slow-fading channels, avoiding prolonged unfavourable propagation to the receiver. To study how the RIS can shape the channel temporal statistics, we analyse the scenario with a single transmitter, receiver, and RIS. The RIS configuration changes randomly at every time step, with phase shifts sampled from a uniform distribution over the interval $[\pi - \theta, \pi + \theta]$, parameterized by $0 \leq \theta \leq \pi$.

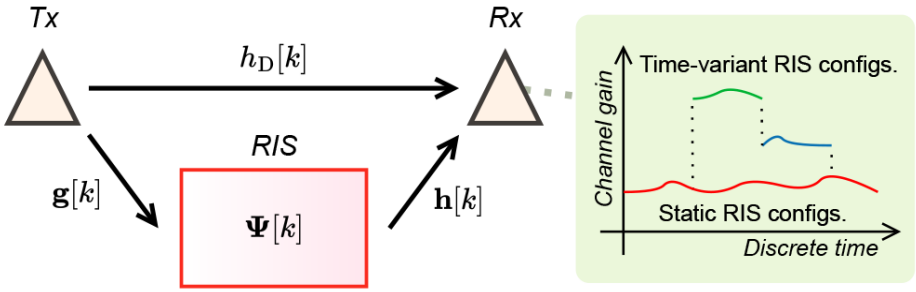


**Figure 3-4 RIS-aided communication system**

***Methodology***

To characterize the channel temporal correlation, we first define the discrete-time-varying channel model. In this model, each complex coefficient representing a channel link comprises a constant LoS component and a time-varying non-LoS (NLoS) component. Especially, the NLoS component is modelled as a stationary first-order autoregressive ($AR(1)$) random process with parameter $0 \leq \alpha < 1$. Given the channel model, we derive the autocorrelation function (ACF) of the equivalent transmitter-receiver channel considering uniformly distributed RIS' phase shifts ([ICS23], eq. 12). Derived from the ACF, the channel temporal correlation ([ICS23], eq. 14) strongly depends on the number of RIS' elements $N$ and the parameter of their phase shifts distribution $\theta$. Therefore, we propose a randomized framework to control the channel correlation by setting $\theta$ and $N$ to yield a target temporal correlation ([ICS23], eqs. 17 and 19). The interested reader can refer to [ICS23] for all the details on the system model, the problem formulation, and the proposed randomized framework.

***Results and outcomes***

Figure 3-5 depicts the channel temporal correlation versus the discrete-time delay, considering different values of the phase shifts distribution parameter. One can observe that, when the RIS has static configurations ($\theta = 0$), the correlation crosses 0.9 at the time delay of 1000 samples. For the other curves, $\theta$ is designed using the proposed framework to yield the correlation of 0.9 at the delays of 750, 500, and 250 samples. Similarly, Figure 3-6 shows the channel temporal correlation, but now considering different values of the number of RIS' elements. In the case when $N = 9$, the correlation crosses 0.9 at the time delay of 50 samples. Using the proposed framework, $N$ is calculated for the other curves to yield the correlation of 0.9 at the delays of 100, 200, and 400 samples. These results demonstrate that, with the proposed randomized framework, channels with a slow decay correlation can be speeded up by increasing

the phase shifts distribution parameter. Conversely, channels with a fast decay correlation can be slowed down by increasing the number of RIS' elements. Finally, Figure 3-7 depicts the channel temporal correlation versus the $AR(1)$ parameter and the Rice factor, showing that the introduced model can represent a wide range of scenarios.

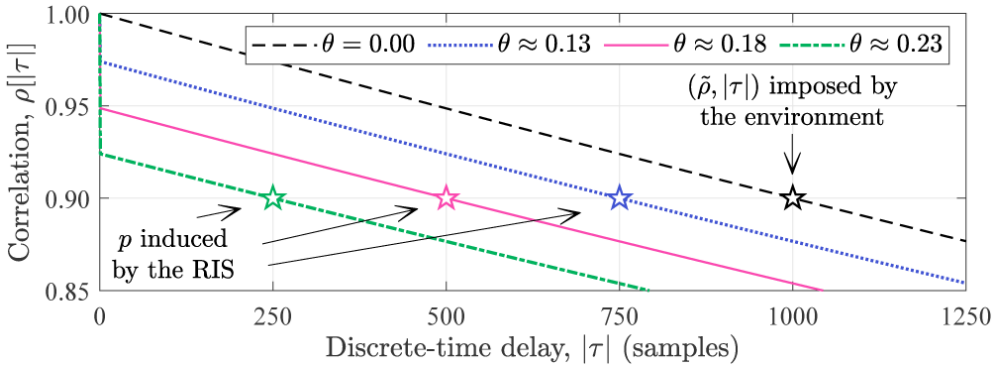


**Figure 3-5 Channel temporal correlation varying the phase shifts distribution parameter θ [ICS23]**

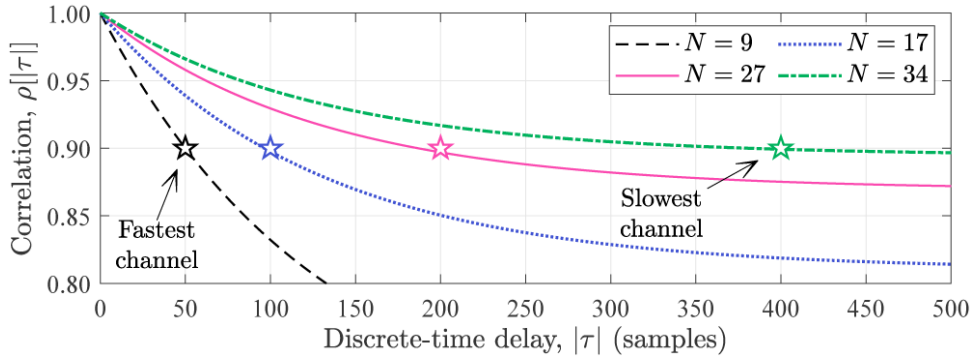


**Figure 3-6: Channel temporal correlation varying the number of RIS' elements N [ICS23]**

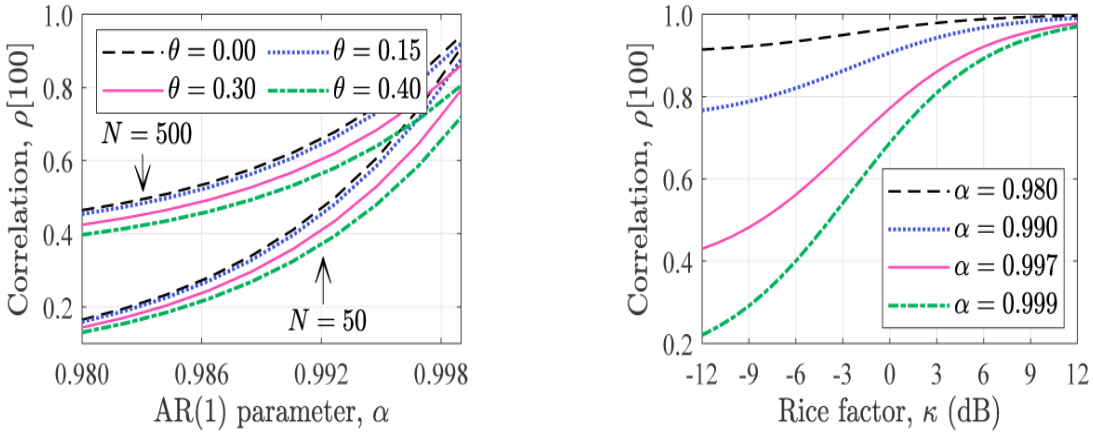


**Figure 3-7: Channel temporal correlation versus (left) the AR(1) parameter and (right) the Rice factor [ICS23]**

***Relation to other RISE-6G contributions***

This works shows the working principles of using the RIS in an alternative way with respect to standard communication techniques, allowing the device to further enhance performance to users having terrible channel condition and high coherence time. We remark that this method can be seen as an instance of an autonomous RIS, because the process is performed by the RIS device without the control of an external

entity. The proposed approach can be used by dedicated RISs installed for this purpose in rich scattering environment. Further study needs to be carried on to provide a feasible hardware with such capabilities.

### 3.5.3 Metrics from direction-resolved signal-to-noise ratios: Analytical characterisation of modes and channels using Slepian method - extended to nearfield

***Motivation and context***

We have previously provided a treatment of degree-of-freedom estimation and an accompanying analytical approximation (in 2D) of channel strengths based on the geometry in phase space of the set of rays connecting transmitter to receiver. Work described here applies to a continuum limit of transmitter and receiver antennae. The previous work made simplifying assumptions about this set that effectively assumed the receiver was in the far-field. These results are extended to near-field geometries for which the relevant ray sets are more complex. This contribution, along with the next, is part of a broader strategy at UNOT of leveraging ray-racing simulations, emerging from approaches such as DEA, to evaluate information metrics in large, complex environments where direct modelling of the propagated wave solution is not feasible.

***Methodology***

As with the treatment of the far-field case previously considered, the underlying methodology is based on a solution of related integral equations using Prolate Spheroidal Wave Functions, due to Slepian. To account for the more general case, a coordinate transformation is found which deforms near-field geometries into the rectilinear setting for which this conventional Slepian analysis applies, albeit approximately.

***Results and outcomes***

Figure 3-8 (left), taken from [CMG23], illustrates the set of rays arriving in the phase plane of the receiver from the transmitter in a near-field LoS setup. Unlike the far-field case, where the edges of this region of the phase plane are nearly straight, the boundary of this set is strongly curved and shows significant left-to-right asymmetry. We derive an area-preserving coordinate transformation so that the ray set forms a parallelogram in the phase plane: a treatment previously published in [CG23a] then applies and predicts singular values accurately, as shown on the right of Figure 3-9.

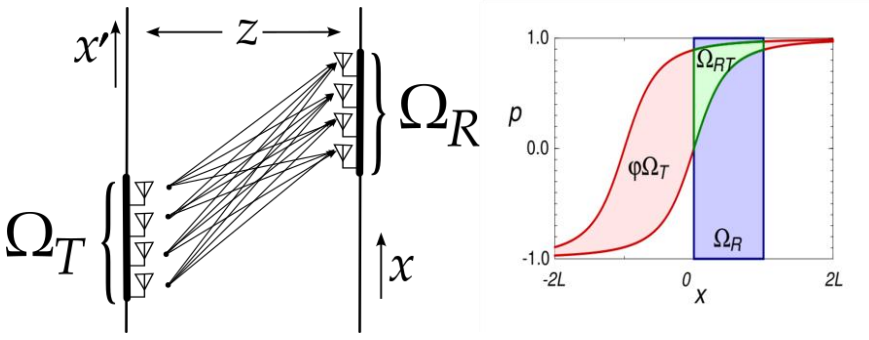


**Figure 3-8 The generalized calculation treats near-field cases (illustrated figuratively on the left), for which the set of rays from transmitter to receiver is considerably deformed: the figure on the right shows an example of such a set, shaded green and denoted in the phase plane of the receiver (parametrized by position and direction/momentum variable where is the angle of arrival at the receiver).**

A key parameter in this treatment is provided by the number of degrees of freedom in the system, determined by the area of the intersecting set. This depends on geometry of the transmitter-receiver system as exemplified on the left of Figure 3-9, where the number of degrees of freedom is plotted as a function of

distance between parallel arrays. The singular values of the channel matrix are then calculated in the same way as in the far-field model, using the tunnelling approach of [CG23b] except that it accounts for the deformed ray set.

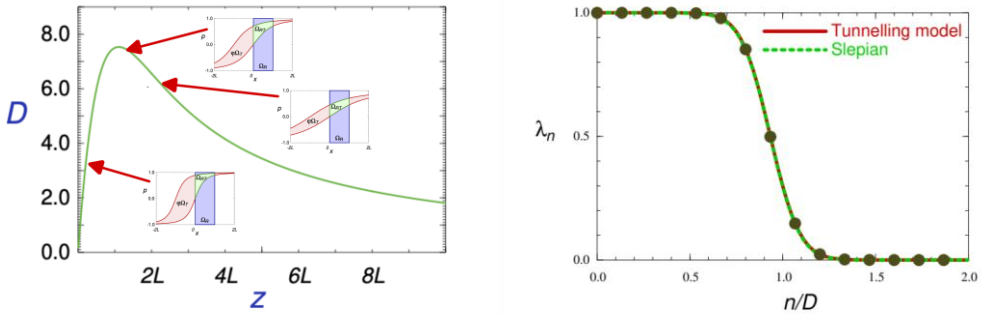


**Figure 3-9 DOF estimates from phase-space geometry are exemplified on the left. The right plot shows an example of the channel strengths of the deformed model, which are well described by the analytical models developed (continuous curves).**

***Relation to other RISE6G contributions***

The direction-resolved signal-to-noise ratio can be served as metrics for the RIS optimization-based studies in WP4, and the sustainable RIS solutions as focused on WP6, especially in supporting the channel model based RIS optimizations.

### 3.5.4 Metrics from direction-resolved signal-to-noise ratios: Channels, mutual information and capacity derived from direction- and position-resolved SNR using ray-tracing in multi-reflective environments

***Motivation and context***

The detailed analytical results in the previous section apply in the special case of ray densities that are uniform in the set formed in the receiver phase plane by rays arriving from the transmitter. In complex, lossy and metareflective environments, the density is variable and, although degree-of-freedom estimates outlined in the previous section are still valid, the singular values of the channel matrix depend on the detailed variation of this density, which can be used to define a local signal-to-noise ratio that is resolved in terms of angle of arrival as well as position.

***Methodology***

The methodology used is based on a representation of both transmitter and receiver correlation functions in terms of (distinct) ray densities, using the Wigner transform. Using ray-tracing approaches such as DEA, we can propagate the transmitter ray density to the receiver, where it is compared with a ray density defined by receiver noise to define a SNR*(x,p)* that depends on angle of arrival (coordinate *p*) as well as position (coordinate *x*).

***Results and outcomes***

We derive a formula (illustrated and implemented here for 2D) for the mutual information of the form in which SNR*(x,p)* is evaluated in closed environments using a DEA approach. A mutual information that is scaled by the degree-of-freedom estimation of the previous section is independent of frequency and allows comparison of results across the spectrum: it is illustrated for a particular, L-shaped 2D enclosure in part (a) of Figure 3-10 using signal-to-noise ratios SNR that have been calculated both for a single realisation (“unaveraged”) and after smearing of ray densities corresponding to an average over a range of frequency. These are each compared with a corresponding direct spectral evaluation of singular values of the channel matrix. This so-defined mutual information can be optimised using a water-filling argument within the ray-density setting [CBG23].

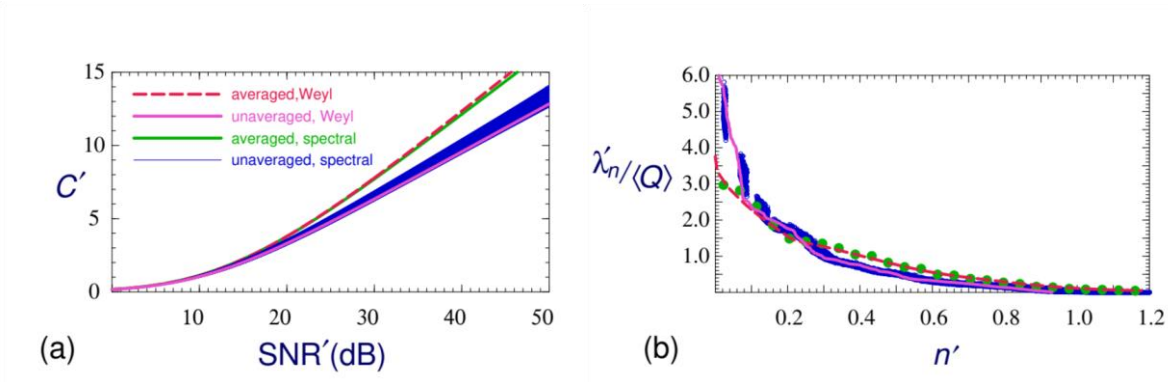


**Figure 3-10 A calculation of scaled mutual information using DEA simulation of a 2D L-shaped enclosure is compared in part (a) with direct spectral evaluation, for both averaged and unaveraged densities. Part (b) illustrates the Weyl estimate of eigenvalues (scaled by a loss factor denoted <*Q*> on which this is based).**

The calculation of mutual information and channel capacity by local signal-to-noise ratio is based on an averaged prediction of eigenvalues using a Weyl counting formula previously reported, which can also be made independent of frequency by an appropriate scaling of counting variables and is exemplified for an L-shaped enclosure in Figure 3-10.

***Relation to other RISE6G contributions***

The channel model and metrics proposed and derived in this work are versatile in supporting optimization-based studies in WP4. The metrics and models are also with great potential in supporting the estimation algorithms for RIS-based localisation and mapping studies in WP5.

### 3.5.5 Model-free channel hardening algorithm with lab-based experiment to evaluate the channel hardening performance in the reverberation chamber environment

***Motivation and context***

RIS devices have emerged as an effective way to control the propagation channels for enhancing the end-users' performance. However, RIS optimization involves configuring the radio frequency response of a large number of radiating elements, which is challenging in real-world applications due to high computational complexity. In this work, a model-free cross-entropy (CE) algorithm is proposed to optimize the binary RIS configuration for improving the SNR at the Rx. One key advantage of the proposed method is that it only requires system performance indicators, e.g., the received SNR, without the need for channel models or channel estimation. Both simulations and experiments are conducted to evaluate the performance of the proposed cross-entropy algorithm. This study provides an experimental demonstration of the channel hardening effect in a multi-antenna RIS-assisted wireless system under rich multipath fading. An RIS-assisted communication system is considered as illustrated in Figure 3-11, where the RIS is equipped with N reflective elements located between the M-antenna BS and the single-antenna UE.

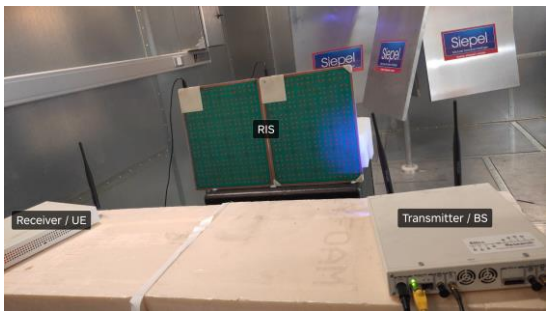


**Figure 3-11 An illustration of the RIS-assisted communication system with N = 152 elements.**

***Methodology***

The objective of the RIS optimization problem is to maximize the SNR of the UE by optimizing the phase shifts of the RIS elements. This problem involving N integers is nonconvex, hence challenging to obtain the solution, especially when N is large. It can be formulated as

$$\max_{\mathbf{x}} \xi(\mathbf{x}), \text{ subject to } \mathbf{x_n} \in \{0, 1\}, n=1, \ldots, N,$$

where $\xi$ denotes the SNR of the UE. $\mathbf{x} = \{x_n\}_{n=1}^{N}$ denotes the phase shifts of N RIS elements, and $\mathbf{x}_n$ denotes the binary phase shift of the n-th element, $x_n = 0$ and $x_n = 1$ represent a 0 and a $\pi$ phase shift, respectively.

The cross-entropy algorithm, denoted in this section as *CE algorithm*, is considered to solve this RIS optimization challenge for the SNR improvement, which mainly depends on the Kullback-Leibler cross-entropy and the importance sampling in an iterative manner [DKM05]. The detailed steps for the binary RIS optimization are given in Algorithm 1. The interested reader can refer to [CYZ23] for further details.

**Algorithm 1:** CE Algorithm for RIS Optimization.

Step 1: Initialize the Bernoulli probability vector $\mathbf{P}^0 = \{P_n^0\}_{n=1}^N$ with $P_n^0 = 0.5$, where $P_n^0$ denotes the initial probability of the $n$-th RIS element to be one. Set the total number of iterations as T and the iteration index $t = 1$.
Step 2: Randomly generate $K$ samples $\{\boldsymbol{x}^j\}_{j=1}^K$ according to Bernoulli distribution with probability $\mathbf{P}^{(t-1)}$, where $\boldsymbol{x}^j = \{x_n^j\}_{n=1}^N$, and $x_n^j$ denotes the binary phase shift of the $n$-th element of the $j$-th sample (RIS configuration).
Step 3: Commit each RIS configuration and collect the corresponding performance indicator, e.g., received SNR.
**for** $j = 1 : K$ **do**
- Commit $\boldsymbol{x}^j$ as RIS configuration.
- Record the received SNR as $\xi_j$.

**end for**
Step 4: Sort $\{\boldsymbol{x}^j\}_{j=1}^K$ in a descending order as $\{\boldsymbol{x}^{\sigma_j}\}_{\sigma_j=1}^K$ with respect to $\xi_j$.
Step 5: Select the best $J = \lceil \varphi K \rceil$ samples from $\{\boldsymbol{x}^{\sigma_j}\}_{\sigma_j=1}^K$, where $\varphi$ denotes the quantile and generally ranges from 0.01 to 0.1 [18], and then update the probability vector $\mathbf{P}^t$ with $P_n^t = \frac{\sum_{\sigma_j=1}^J x_n^{\sigma_j}}{J}$, $n = 1, \ldots, N$.
**if** $\mathbf{P}^t$ converges to a binary vector **then**
Break
**else if** $t = T$ **then**
Post-process $\mathbf{P}^t$ to be a binary vector with $P_n^t = 1$ if $P_n^t > 0.5$, otherwise $P_n^t = 0$, $n = 1, \ldots, N$.
**else**
Set $t = t + 1$ and go to Step 2.
**end if**
Step 6: Return $\mathbf{P}^t$ as the optimized RIS configuration $\boldsymbol{x}^*$.

***Results and outcomes***

Both simulations and experiments are conducted for performance evaluation of the proposed CE algorithm. For the simulations shown in Figure 3-12a, the average SNR is only -1.9 dB without RIS. The proposed CE algorithm increases the SNR to nearly 11 dB at 5 iterations, which then surpasses the benchmarks with a SNR advantage of around 7 dB. From experiment results shown in Figure 3-12b, the average SNR is only 4.8 dB without RIS, while the MH and SA converge to an inferior sub-optimal solution at around 8.3 dB. The proposed CE algorithm enhances the SNR to over 12 dB, which outperforms the benchmarks by around 4 dB.

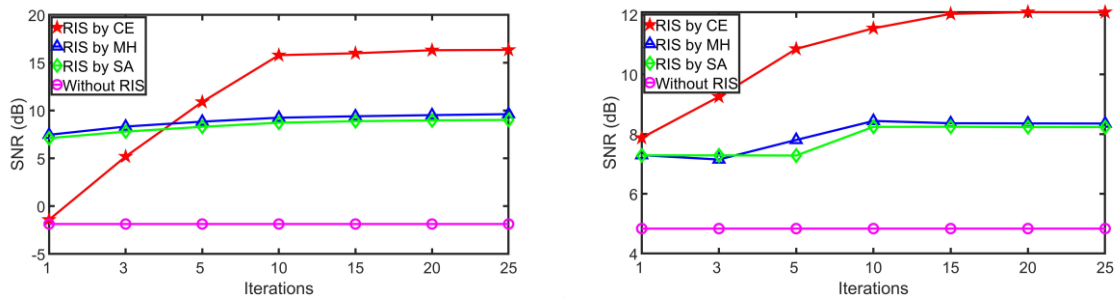


(a) simulations (b) experiments

**Figure 3-12 Performance on different numbers of iterations.**

Figure 3-13 validates that the average SNRs of all algorithms improve with an increasing number of RIS elements. The proposed CE method outperforms the benchmarks in terms of both SNR and channel hardening, and it shows greater advantages than the benchmarks with growing numbers of RIS elements. The practical experiments achieve stronger channel hardening than simulations. In Figure 3-13a, a curve of $N^2$ is also given, which demonstrates that the CE algorithm achieves a similar trend as indicated by the square law expectation [BS20] between the SNR and the $N^2$. Despite the fact that the SNR improvements in Figure 3-13b slightly deviate from the square law due to the potential influence of imperfect RIS element deactivation, the CE approach leads to significant SNR enhancement and channel hardening.

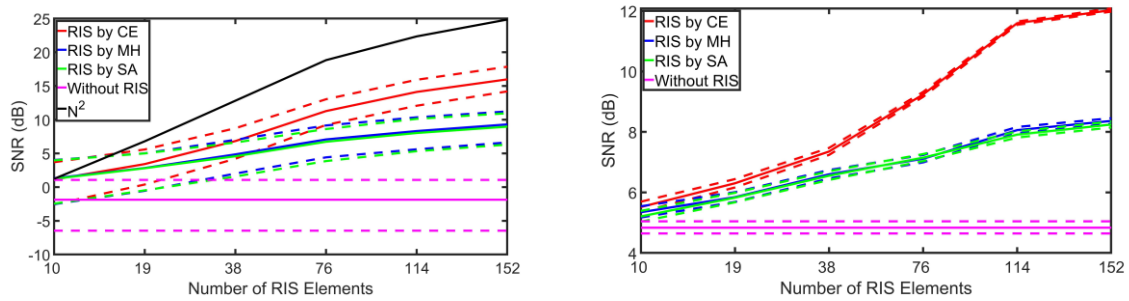


(a) simulations (b) experiments

**Figure 3-13 Performance on channel hardening.**

To further evaluate the channel hardening performance, Figure 3-14 demonstrates the ratio between the variance and the mean square of the collected SNRs with increasing numbers of RIS elements. Both simulation and experiment results indicate that the ratio generated by the CE algorithm and benchmarks generally keeps decreasing with larger N, and the proposed CE algorithm remains the lowest, which illustrates that the channel hardening performance is superior to the benchmarks. Additionally, the performance of the CE algorithm generally follows the trend of the curve of the theoretical scaled 1/N.

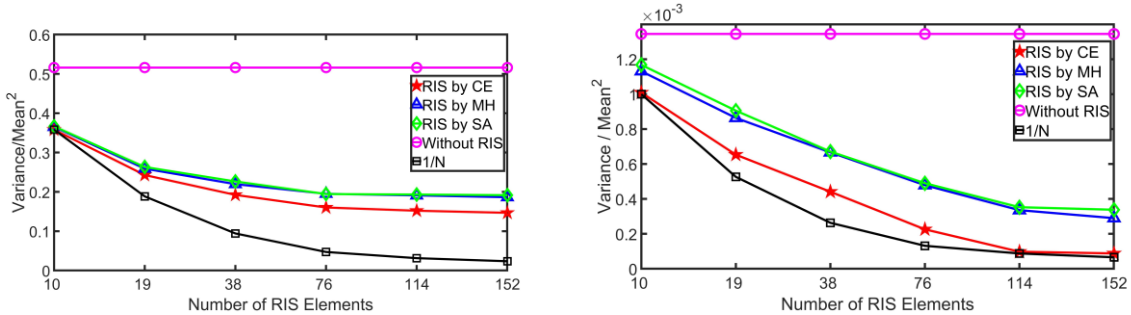


(a) simulations (b) experiments

**Figure 3-14 Performance on channel hardening (variance=mean^2).**

***Relation to other RISE-6G contributions***

This work studies the channel model free based solutions for the RIS optimization under laboratory environment, which complements to the model-based studies in WP3, and an additional Proof of Concept (PoC) prototype for the WP3 and WP6, e.g., for comparison purposes.

### 3.5.6 Non-coherent modulation schemes in RIS communications

***Motivation and context***

The exploitation of RISs is mainly based up to date on the classical Coherent Demodulation Scheme (CDS), where the knowledge CSI is essential for the optimised configuration of the RIS tunable elements, the precoding and combining matrices, as well as the demodulation of the signal at the receiving node. This processing task is not straightforward since a non-convex design optimisation needs to be solved, increasing the operational complexity of the RIS-empowered communication system. Furthermore, the overheads increase when OFDM transmissions are taken into consideration, where the complexity of the channel estimation and optimisation scales with the number of subcarriers [ZZ20]**,** and coherence time is always assumed to be long enough to cope with the channel training and uplink/downlink data transmission stages.

On the contrary, the Non-CDS (NCDS) is an alternative demodulation scheme that does not require CSI. NCDS is more robust than CDS for low SNR scenarios, where the latter scheme additionally suffers from noise pollution in the channel estimates. Motivated by the above, this contribution investigates the use of the NCDS strategy of DPSK method in the presence of RIS for SIMO OFDM systems [CAG22a], [CAG22b]. DPSK is robust in very fast time-varying channels because it only requires that the channel response is quasi-static over two contiguous symbols. This combination requires neither channel estimation nor solving a non-convex optimisation problem. Consequently, the channel training stage is no longer required and the side link to control the RIS is removed, since the passive elements of the RIS can be configured by any random phases. Hence, the proposed solution is not only able to improve the efficiency of the system, but it is also capable of reducing the processing complexity, especially for broadband multicarrier waveforms, simplifying the massive deployment of RISs.

The analysis conducted in [CAG22a], [CAG22b] includes the characterisation of the expected SINR, considering both an idealistic and a realistic channel model and provides approximate analytical expressions for the Symbol Error Probability (SEP). The numerical evaluation shows that the analysis is backed by the simulated scenarios and illustrates the superiority of the proposed NCDS system over a relevant CDS one. Besides, the performance of the proposed NCDS does not suffer from any performance penalisation when low resolution quantisation (even at 1 bit) is considered for the RIS phase configurations, unlike CDS.

***Methodology***

Two channel models are considered:

1. *Independent and Identically Distributed (IID) channel model:* As a benchmark, we consider the case where the elements of the channel frequency response for both links (BS-RIS and RIS-UE) are IID. This channel model is used for the purpose of upper-bounding the performance of the proposed NCDS, and comparing it with a more realistic geometric wideband channel model. The small-scale fading of the respective channels is modelled according to the Rayleigh distribution.
2. *Geometric wideband channel model:* For a more realistic performance evaluation, the two links (BS-RIS and RIS-UE) are characterized with a geometric wideband model made up of the superposition of several separate clusters, where each of them has a different value of delay and gain. Moreover, each cluster is comprised of a certain number of rays with different angles of arrival and departure. The delays and geometrical positions of each cluster/ray are typically characterised by the Delay and Angle Spreads (DS and AS), respectively. The recommended channel model for 5G is used [3GPPr16].

The DPSK scheme involves encoding the constellation symbols at the transmitter in the time domain along each subcarrier, so that the first symbol constitutes a reference symbol. The rest of the symbols in the burst are encoded as the product of the previous encoded signal with the current symbol to be sent (scaled accordingly to satisfy power constraints). Note that a single reference symbol is only required at the beginning of the burst in order to allow the differential demodulation, which represents a negligible overhead. At the receiver's end, the decoding can be expressed as a summation of four terms that include the useful symbol to be decided (polluted by the effective RIS-empowered cascaded channel), the cross-interference produced by the noise and the received differential symbol in two time instants, as well as a term resulting exclusively by the noise. The decoding procedure first decodes the known reference symbol at the beginning of the burst to deduce the effective channel coefficients and then proceeds to decoding the rest of the symbols by used the decoding symbols of the previous steps. Note that the proposed scheme does not need knowledge of the CSI, nor does it require optimisation of the RIS configuration. Therefore, random RIS profiles are utilised and are reconfigured after each channel coherence frame ends.

*Analytical expressions for the SINR and the SEP*

The SINR for the SPDK scheme under IID channels can be expressed as (Eq. 22 in [CAG22a] with a change of notation for consistency purposes)

$$\gamma_{IID} = \frac{N\,N_R}{N\ +\ N_R\ +\ 1\ +\ n_1 + \frac{n_2}{N}},$$

where $N_R$ is the number of receive antennas, and $n_1$, $n_2$ are constant terms depending on the noise levels and transmission power. The form of the above expression indicates that not only the number of the receiver antennas improves the system performance, but also the number of the RIS elements helps to reduce the interference and noise terms, by providing an additional spatial diversity gain. Consequently, the RIS is able to improve the overall performance of the system. Furthermore, as clearly indicated from the numerator, the performance of the system will be high, even though the number of antennas and/or the number of the RIS elements are not very large, since these values are multiplied.

Considering the 5G compatible geometric model, the analytic expression for the SINR in this case may be expressed as (Eq. 29 in [CAG22a] with a change of notation)

$$\frac{1}{\gamma_{geo}} = 1 + \frac{Q_4}{N^2{N_R}^2{n_3}^2} - \frac{2Q_2}{N\,N_R n_3} + \frac{1}{N^2{N_R}^2{n_3}^2}(2Q_2 n_4 + N_R{n_4}^2) \geq \frac{1}{\gamma_{IID}},$$

where, $Q_2$ and $Q_4$ quantify channel gains and $n_3$, $n_4$ denote noise-related terms, illustrating that the ideal IID channel model constitutes an upper bound of the achievable SINR. Obviously, the spatial correlation of the antennas at the receiver and the RIS passive elements is limiting the performance of the system for this geometric wideband channel model as compared to the IID case. Similarly to the previous case, both the number of antennas and the number of passive elements is contributing to enhance the SINR.

The analysis of Section 4 of [CAG22a] provides an expression for the SEP of the decoded symbol under the DPSK scheme, however, since it is not straightforward to express in closed form, it is skipped from the present text for brevity. The SEP values of the numerical evaluation below are evaluated numerically via numerical integration methods.

In terms of computational complexity, assuming bursts of $T$ symbols per channel frame, the encoding process requires $T$ complex products for the encoding phase and $(N_R + 1)(T - 1)$ complex products at the decoder, which is of the same order as the $N_R T$ products required by the OFDM CDS, while the latter also supposes a computational complexity of polynomial relation to $N$ for the iterative optimisation approach, as well as an added overhead for the channel estimation process.

***Results and outcomes***

Figure 3-16 illustrates the SINR performance as a function of the UE transmit power of the proposed NCDS with 8 - DPSK for both the IID Rayleigh and the geometric wideband channel models considering 4 receiving antennas and different values for RIS elements (denoted with *M* in the legend) and AS systems. As clearly shown, the performance for the IID channel model corresponds to the best case for all simulated RIS element values. On the other hand, for the case of geometric wideband channel, the performance depends on the spatial correlation. When the angular positions of the clusters/rays are separated (i.e., high AS), the performance is better compared to the low AS case. Evidently, his improvement becomes even better for large RIS sizes. It is also shown in this figure that the SINR analysis presented above (shown with black solid lines) accurately characterizes the RIS-empowered system performance.

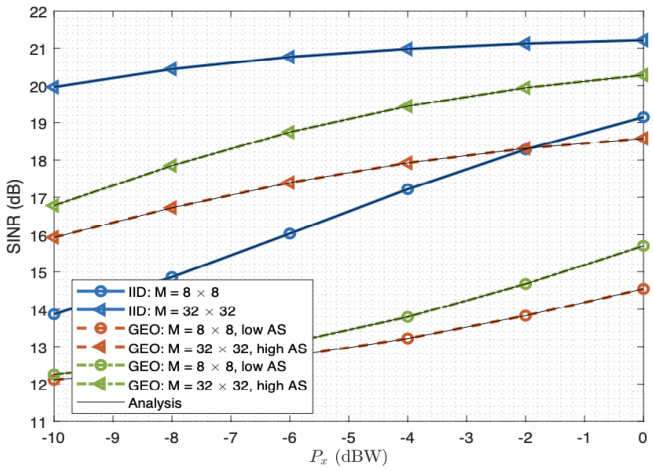


**Figure 3-16 SINR performance of NCDS in IID and geometric channels considering different RIS sizes and ASs.**

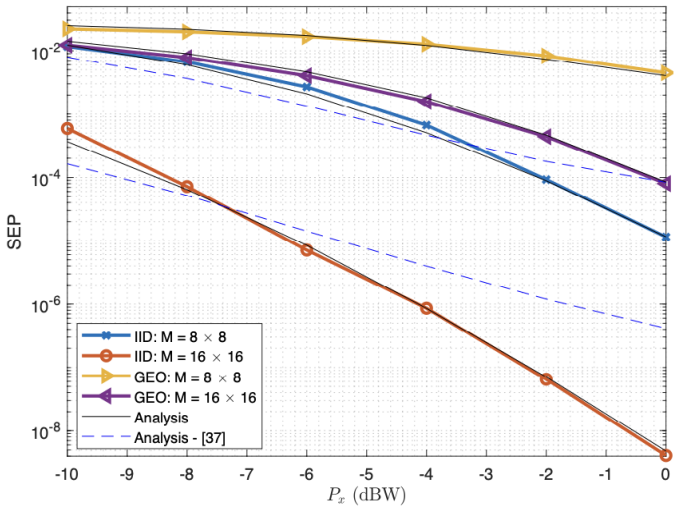


**Figure 3-15 SEP performance of the proposed NCDS with 4-DPSK NCDS in IID and geometric channels considering different RIS sizes.**

The SEP of 4-DPSK modulation for the proposed NCDS is demonstrated in Figure 3-15 for both considered channel models with 16 receive antennas, high AS, and different numbers of RIS elements. Similarly to the previous figure, RISs with more elements result in improved performance and the IID channel yields better performance than the geometric one. The approximated SEP values of the analysis are plotted in dotted lines, showcasing that the analysis is accurate enough.

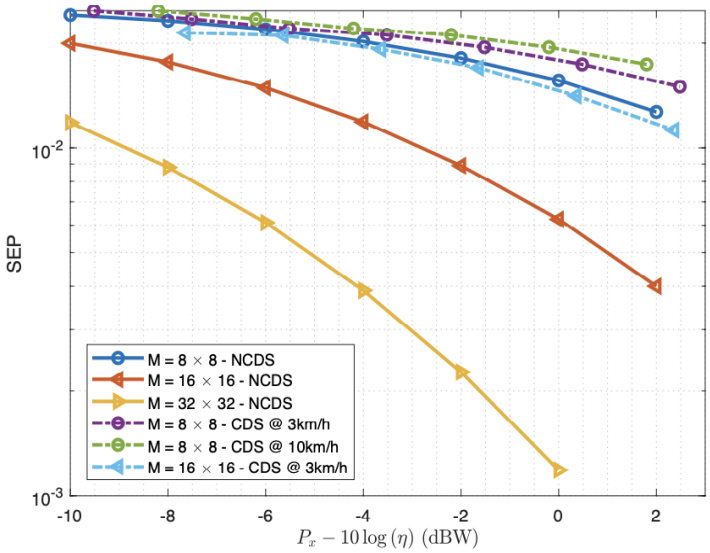


**Figure 3-17 SEP performance comparison between the proposed NCDS and the baseline CDS.**

Finally, a comparison of the NCDS approach along with the baseline CDS is showcased in Figure 3-17 over different mobility scenarios, accounting for channel estimation overheads, that result in penalised factors for the CDS case to account for the time slots spent for channel estimation and optimisation, thus allowing for a fair comparison. The results illustrate that the proposed NCDS scheme significantly outperforms CDS for large RIS size. Moreover, even for the small RISs, the NCDS outperforms CDS, due to the fact that the latter is not able to obtain accurate channel estimates due to the presence of noise. This happens because the UE's transmit power is in general limited, as also are the number of resources that can be devoted for CSI estimation while maintaining a reasonable efficiency.

***Relation to other RISE-6G contributions***

The majority of the contributions in this deliverable that focus on the rate-enhancing problem in general involve solving optimisation problems based on information relating to the users or the system (e.g., instantaneous CSI, statistical CSI, user positions, etc.) and therefore introduce unavoidable measurement and computational delays. In contrast, the analysis of this contribution offers an alternative for high-mobility scenarios where the estimation process may pose significant overheads.

### 3.5.7 Capacity analysis of large-RIS-systems

***Motivation and context***

RIS optimisation techniques, such as those proposed in this deliverable or works appearing in literature primarily focus on per-channel frame configuration of the profile of the metasurface. This operation may entail substantial overheads in terms of channel acquisition and often assumes that both the computation and the configuration switching delays occupy a negligible part of the channel frame. As the maturity level of the metasurface prototypes as well as the development of relevant infrastructure and algorithms increases, it remains unclear whether such requirements can be satisfied in all deployment scenarios. This problem is magnified by the fact that the number of RIS elements is expected to grow in very large scales.

Taking the above into consideration, this contribution [MAD23] provides a performance analysis of multi-RIS systems in terms of achievable capacity, as the number of BS and RIS elements becomes asymptotic. The main result of this endeavour a closed form expression for the RIS configuration that is asymptotically optimal when only statistical CSI is considered.

***Methodology***

Using tools from random matrix theory and statistical physics, analytic expressions for the ergodic MI and its variance are presented, by considering the limit of of large antenna numbers and large numbers for the reflecting elements of the RISs (Eqs. 8-13 in [MAD23]). Following the central limit theorem, the distribution of the MI performance converges weakly to a Gaussian distribution (Remark 2 in [MAD23]). The asymptotic properties of the correlation matrices corresponding to the incoming and outgoing EM waves to and from the RISs (Proposition 2 in [MAD23]), which allows for the solution of the capacity-maximisation objective function to be expressed in terms of the asymptotic form of the eigenvectors of the channel correlation matrices. This leads to a closed-form expression for the optimal RIS phase shifts, using only knowledge of the statistical properties of the channel matrix. Concretely, for LoS channels, the covariance matrices are unit-rank and the capacity expression can be approximated using the first eigenvectors of the cascaded channel, which are shown to be Fourier modes. Let $\boldsymbol{q}_{tk,1}$ and $\boldsymbol{q}_{rk,1}$ be the wavevectors that correspond to the projection on the surface of each $k$-th RIS of the mean direction of arrival and departure of the EM wave's energy. Setting the phases of each $k$-th surface as

$$\varphi_{k,n} = (\boldsymbol{q}_{tk,1} - \boldsymbol{q}_{rk,1})^T \boldsymbol{x}_n$$

is asymptotically optimal. This result holds as an approximation even for the cases where the channel is not pure LoS, but it might be LoS-dominant.

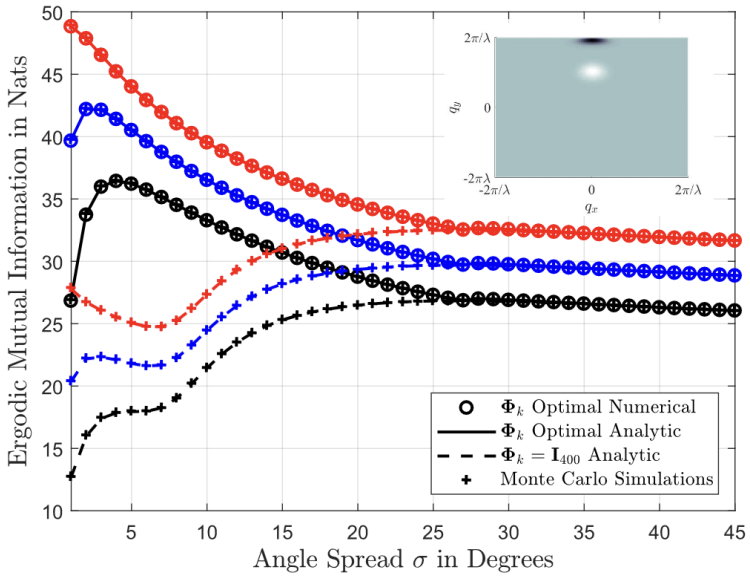


**Figure 3-18 Performance evaluation of the closed-form expression for the ergodically optimal RIS configuration.**

***Results and outcomes***

A comparison of the above analytic expression with numerical optimisation algorithms and Monte Carlo simulations has been conducted, with the results indicating the applicability of the closed-form expression despite small numbers of BS and UE antenna arrays used. The results are depicted in Figure 3-18, where 8 and 4 antennas has been set for the BS and receiver(s), respectively. The RIS has $N = 400$ elements, black lines indicate 1 UE, blue lines indicate 2 UEs, while red lines indicate 3 UEs. The inset figure depicts the distribution of the eigenvalues of the incoming (white ellipsis) and outgoing (black ellipsis) EM waves with incoming angle 30° and outgoing angle 70°, respectively, as well as angle spread of 5°. The numerical results additionally illustrate that ergodic RIS optimisation (irrespective of the algorithmic

approach used) is more beneficial in small angle spreads, which corresponds to pure-LoS and LoS-dominated environments. In rich scattering environments (high angle spread), the optimised RIS performance offers a smaller increase compared to fixed-profile or randomly tuned RIS.

***Relation to other RISE-6G contributions***

This contribution offers a solution for RIS tuning with minimal computational overheads when statistical CSI information is only available. As a result, it is complementary to most algorithmic approaches presented in this deliverable that are designed to operate on a per-channel-frame basis. The deployment and signalling of the implemented method follow that of contribution of Section 6.14 of D4.3.

### 3.5.8 On the maximum achievable Sum-Rate of the RIS-aided MIMO broadcast channel

***Motivation and context***

In [PTD22], we investigate the achievable sum rate optimization in a BC in the presence of RISs. We solve this problem by exploiting the well-known duality between the Gaussian MIMO BC and the MAC, and we correspondingly derive three algorithms which optimize the users' covariance matrices and the RIS phase shifts in the dual MAC.

We consider a BC in which one BS simultaneously serves $\boldsymbol{K}$ users, as shown in Figure 3-19. Both the BS and the users are equipped with multiple antennas, such that the BS and the $\boldsymbol{k}$-th user have $\boldsymbol{N_t}$ and $\boldsymbol{n_k}$ antennas, respectively. The BS antennas are placed in a uniform linear array (ULA) with inter-antenna separation $\boldsymbol{s_t}$. In a similar manner, all the antennas of a single user are placed in a ULA with inter-antenna separation $\boldsymbol{s_r}$. To improve the system performance, $\boldsymbol{N_s}$ RISs are also present in the considered communication environment. Each RIS consists of $\boldsymbol{N_{ris}}$ reflecting elements which are placed in a uniform rectangular array (URA), so that the separation between the centres of adjacent RIS elements in both dimensions is $\boldsymbol{s_{ris}}$.

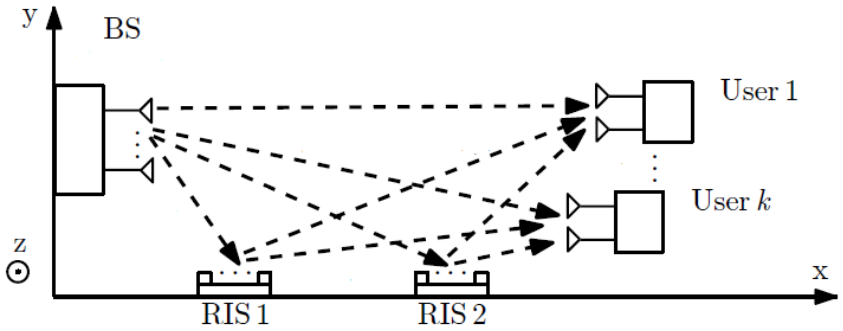


**Figure 3-19: Aerial view of the considered communication system for the case of 2 RISs.**

***Methodology***

The achievable rate optimization problem for the RIS-assisted MIMO BC can be expressed as

$$\max_{S,\theta} \sum_{k=1}^{K} R_{\pi}(k)$$

$$S.t. \sum_{k=1}^{K} Tr(S_k) \leq P;\ S_k \geq 0, \forall k,$$

$$|\theta| = 1$$

where $\boldsymbol{R_{\pi}(k)}$ the achievable rate for the $\boldsymbol{k}$-**th** user, $\boldsymbol{S_k}$ the input covariance matrix of user $\boldsymbol{k}$, $\boldsymbol{\theta}$ the phase shifts of the RIS elements and $\boldsymbol{P}$ the maximum total power at the BS.

Due to the non-convexity of the optimization problem and the possibility that a local optimization method may be trapped in a bad local optimum, we propose three different iterative algorithms which operate in the dual MAC, each of which provides a locally optimum solution.

The first algorithm, which we call the Alternating Optimization (AO) algorithm, optimizes the users' covariance matrices and the phase shifts of the RIS elements in an alternating manner. The users' covariance matrices are obtained by a dual decomposition method with a block coordinate maximization (BCM), while the phase shifts of the RIS elements are computed sequentially and formulated in a closed-form expression.

As it can be desirable to increase the time efficiency of the aforementioned sequential optimization, we introduce the approximate AO algorithm, which uses a gradient-based method for optimizing simultaneously the phase shifts of the RIS elements.

Finally, the alternating projected gradient method (APGM) algorithm applies a gradient-based method for optimizing the users' covariance matrices and the phase shifts of the RIS elements.

***Results and outcomes***

We plot in Figure 3-20 the average performance of the proposed algorithms over 100 channel realizations. For each channel realization, we also compute the best performance of the three algorithms when they are convergent, which is dubbed "Best" in Figure 3-20. We notice that the algorithms achieve different sum-rates. Therefore, in systems with low degrees of freedom, all three algorithms need to be run to increase the probability that the maximum sum-rate is obtained. In general, through a large number of numerical experiments, we have observed that the APGM algorithm usually provides good trade-offs between the achievable sum-rate and complexity, and thus it is the recommended choice in most scenarios (see [[PTD22]]).

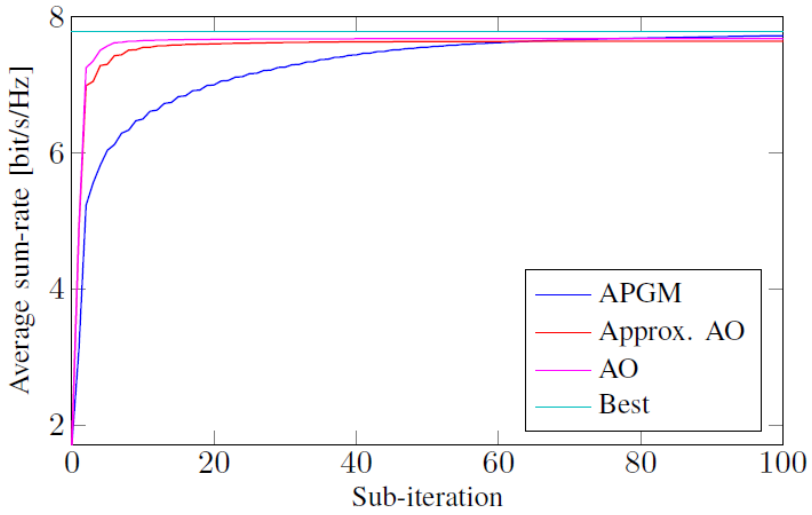


**Figure 3-20 Average achievable sum-rate of each proposed algorithm and their best sum-rate performance**

***Relation to other RISE-6G contributions***

Simulation results show that the proposed algorithms tend to converge to the same achievable sum-rate overall but may produce different sum-rate performance for some specific situations, due to the non-convexity of the considered problem. Also, the gradient-based optimization methods are generally more time efficient. In addition, we demonstrate that the proposed algorithms can provide a significant gain in the RIS-assisted BC with multiple RISs and that the gain depends on the placement of the RISs.

### 3.5.9 Extra degrees of freedom in RIS tuning via rotation and movement

***Motivation and context***

While RIS configuration selection, as well as suitable location for positioning RISs have been studied in the literature, the problem of rotating the surface to favourable propagation control has not been widely considered. To that end, this contribution [JAS22] studies the extra degrees of freedom in the overall system performance brought by optimising the mechanical rotation of the surface in terms of the channel capacity. This analysis extends to the related problem of location-selection. Although the RIS location has a big impact on the performance, the results showcase that the RIS rotation plays a more important role - i.e., a considerable improvement can be obtained by properly rotating the RIS rather than moving it over a wide area. For instance, we can achieve more than 200% performance improvement through rotating the RIS by 42.14°, while an 150% improvement is obtained by shifting the RIS over 400 meters.

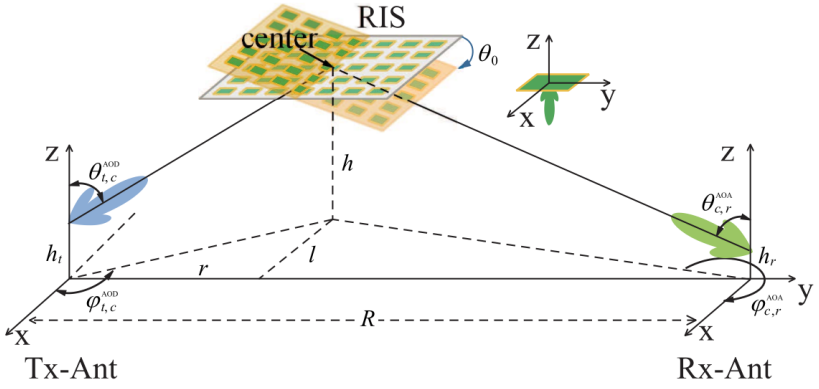


(a) Diagram of RIS rotation

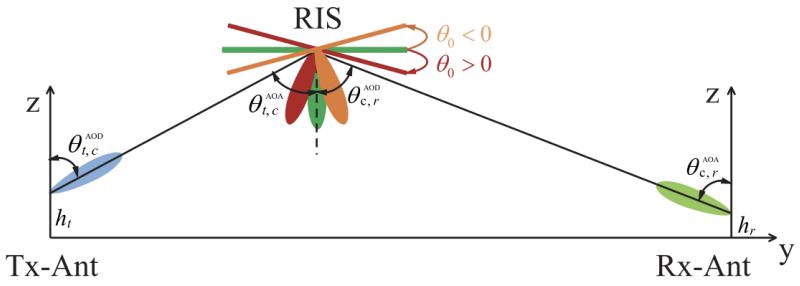


(b) Front view of the system

**Figure 3-21 Overview of the RIS rotation and position system under examination.**

***Methodology***

The analysis entails expressing the gains of the composite RIS channels in terms of the power patterns of the BS, UE and RIS antennas, which in turn depend on the AoAs and AoDs of the impinging/outgoing signals. This illustrates that the composite channel gain is maximised when the AoAs/AoDs of the RIS coincide with the directions of the main lobes of the BS and UE. By considering the latter as fixed, a closed form expression is derived about the RIS rotation angles that achieve the optimal capacity (Theorem 3 in [JAS22]). The upper bound of the optimal capacity can be expressed as in Eq. 25 of [JAS22]. The geometry and basic notation used in this contribution is given in Figure 3-21.

Next, the problem of optimal location of the RIS is considered, by assuming that the RIS can be located along the BS-UE line carrier and that its lower- and upper- bounded. When the altitude of the RIS is relatively low, its optimal position along the BS-UE carrier can be derived in closed-form, and particularly, when the selected height is much smaller than the BS-UE distance, the RIS is preferably deployed directly above the TX or the BS (Corollary 4 in [JAS22]). In the general case, however, the optimal position selection cannot be given in closed form, therefore, a simplified exhaustive algorithm is used in

the performance analysis which identifies effective position regions, i.e., sets of positions where the expected SNR is above a given threshold.

***Results and outcomes***

As numerical evaluation, the effects of the RIS rotation, position, and antenna directivity have been considered, along with their interplays. To evaluate the performance brought only by rotating the surface, Figure 3-22 depicts the ergodic capacity achieved as a factor of rotation angle for three different BS-UE distances, $r$. The rotation angle of the RIS plays a critical role in the achieved capacity of the system.

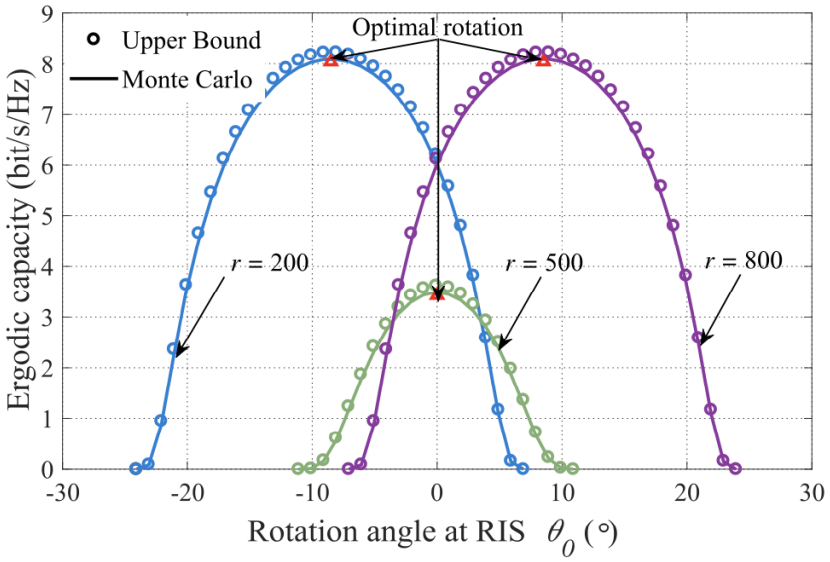


**Figure 3-22 Achieved capacity as a function of RIS rotation angle for different horizontal RIS positions.**

Further evaluating the RIS rotation angle over different RIS positions, as in Figure 3-23, the benefits of appropriate RIS positioning are illustrated. In a similar manner, Figure 3-24 showcases the performance increase brought to the system by more directive RIS radiation patterns (with the directivity factor denoted as $q_u$).

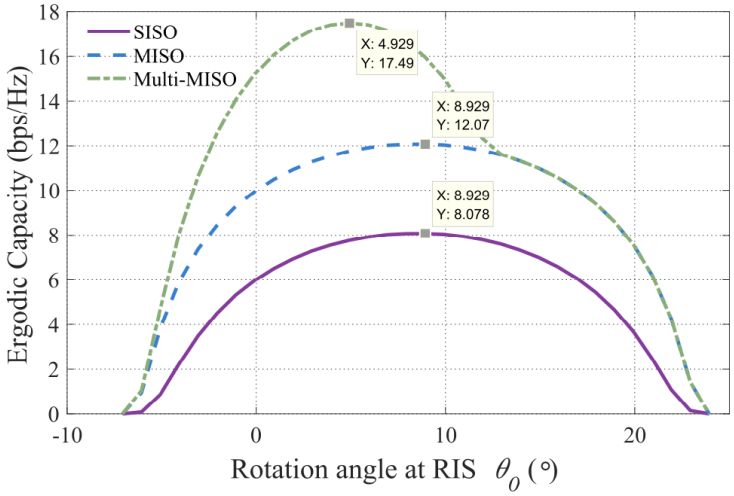


**Figure 3-23 Achieved capacity as a function of RIS rotation angle for different RIS positions and antenna configurations.**

Finally, Figure 3-25 compares the ergodic capacities of different locations under three cases: (i) no rotation at the BS, UE antennas and RIS (as a baseline), (ii) the optimal rotations at the antennas: both the BS and UE are with optimal rotations pointing to the RIS centre, while RIS is in the initial direction without rotation; (iii) all three nodes are in optimal rotations. When the antennas and RIS rotate with optimal

angles, the performance surpasses those in the other two cases. There is also a big gap between the performance with only optimal rotation at the antennas and that with optimal rotations at the antennas and RIS. This proves the necessity of appropriately adjusting the antennas and RIS rotations in guaranteeing a high performance.

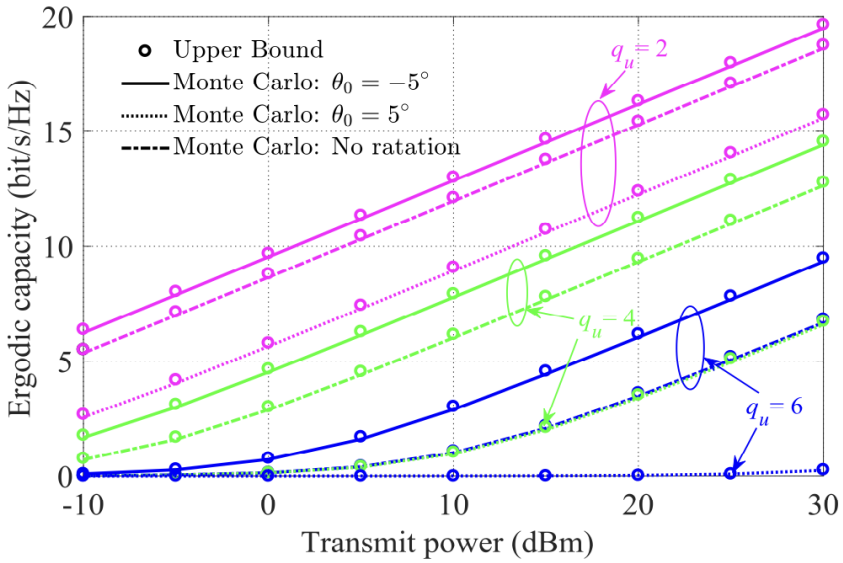


**Figure 3-24 Achieved capacity over transmit power under different RIS beam directivity values.**

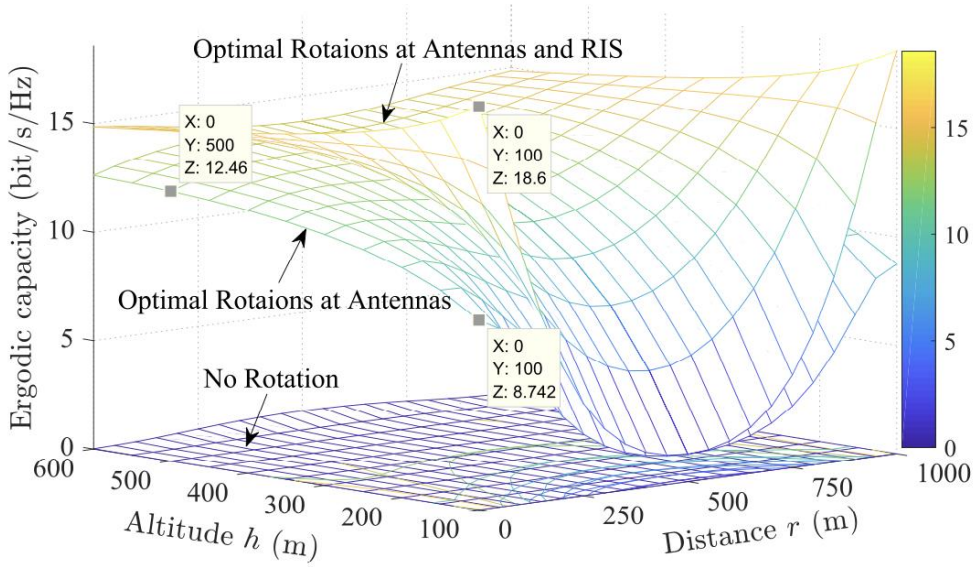


**Figure 3-25 Impact of RIS position and rotation of RIS, BS, and UE antennas in the ergodic capacity.**

***Relation to other RISE-6G contribution***

This contribution is complementary to the phase configuration optimisation approaches proposed in this deliverable. In practice, the rotation optimisation approach supposes a fixed, directive-beam RIS, which may be satisfactory for many use cases.

# 4 Design of Multi-User Techniques for RISE Communications

A complete design of multi-user communication techniques requires accounting for the different aspects of access, channel estimation, communication parameters optimization and data transmission. Differently from standard communications, RISs configuration design needs to be addressed in RIS-aided systems considering the impact that the configuration can have in the various operations. Indeed, RISs configuration can be optimized to increase the performance of a data transmission but can also be used to perform opportunistic variation of the environment improving the performance of various operations. In this section, we present the design of the various phases of RIS-aided wireless communications.

## 4.1 RIS-aided access procedures

The access procedure regards the admission of one or more users to the network. As discussed in D4.2, the approach of 5G NR makes use of Downlink (DL) synchronization signals transmitted by the BS. The users attempting network access listen to the incoming signal, try to decode the information within, and try to connect to the BS using synchronization and access messages. In case of MIMO BS, the DL synchronization signals are transmitted multiple times, while the beamforming of the BS sweeps to a certain number of beamformer vectors enabling it to cover the area of interest.

As presented in D4.2 and D4.3, similar procedures can be employed by the RIS-aided network, in which the RIS may sweep through a set of possible configurations [CSL22], [CSL23]. During the sweeping, a DL transmission phase occurs, in which the BS transmits synchronization signals to let the UEs learn which configuration provides a sustainable SNR. Exploiting this information, each UEs can send data signals during the access (UL) phase. Here, we stress the necessity of a careful design of: 1) the set of configurations available at the RIS, and 2) the estimation techniques at the UE. Regarding the RIS configuration design, a set of codebooks for DL and UL phases must be designed. Generally, the configurations are known to the RIS and the BS, so that the RIS can trigger the procedure, and the BS can use the configuration knowledge to perform further processing/estimation in the access phase. In principle, the DL codebook should contain enough configurations to illuminate at least the whole area of interest. Sweeping through configuration generates spatial diversity and may reduce the number of collisions. On the other hand, having many configurations increases the time for the configuration estimation phase, thus reducing the available throughput. Hence, the design of codebook and estimation techniques must consider this trade-off. Preliminary results on this method were given in D4.2/Section 4.4.3. This method and its result are further analysed in Section 4.4.1 of this deliverable.

When multiple RISs are deployed, a further possibility is to combine the scheduled transmission with random access [CYH22]. In this case, a frame structure considers both the scheduled users' transmission and contended users' transmission, the latter comprising the UEs requesting the access. At the beginning of the frame, DL training sequences are sent by the BS -- like synchronization signals – and are used by all the users to estimate the channel. Then, the resource allocation is made in a centralized way for the scheduled users, while the contended UEs schedule the use of resources and RISs through distributed optimization. More details are given in Section 4.4.2.

## 4.2 CSI estimation in multi-user RIS networks

CSI estimation might be the bottleneck in the design of communication techniques for RIS-aided systems. The presence of the RIS constrains the system to estimate multiple channels simultaneously, whose dimension increases with the number of elements of the RIS. On the other hand, a large number of elements is desirable to reach a certain gain provided by the RIS. Therefore, the need for fast and accurate CSI estimation techniques is of fundamental importance.

One solution analysed in D4.2/Section 4.4.1 is considering the different time-horizon that static and dynamic channel have. When the RIS and the BS are static, the BS-RIS channel changes slowly with respect to the RIS-UE channel. Exploiting this feature, a solution based on parallel decomposition and bilinear

estimation of the channel has proven to reach good performance with very fast convergence, being able to track time varying channels [YAK22].

It is well known that the use of message passing techniques in combination with the exploitation of the sparsity structure of the channel can improve the CE performance. Different procedures based on this principle has been design for RIS-aided networks, considering narrowband transmission with multiple RISs [MLY23], and broadband transmission with single-RIS [MSL23]. These techniques show better NMSE performance with respect to algorithms in literature, allowing the reduction of overhead generated by the transmission of pilot sequences. Further details are given in Sections 4.4.3 and 4.4.4.

When considering RISs capable of sensing operations (i.e., HRIS), specific techniques can be designed to exploit the possibility of acquiring individual channels at the RIS [ZSA23]. An analysis on the benefits of the use of HRIS for CSI acquisition in given in Section 4.4.5.

## 4.3 Transmission parameter optimization in RIS-aided networks

The general problem of optimizing the beamforming for both BS and RIS has been described in Section 3.1; here, we discuss the considerations for optimizing the transmission parameter in realistic scenarios, showing strategies based on different information acquired by the decision maker.

### 4.3.1 CSI-based optimisation

As mentioned, CSI acquisition is a complex task for the RIS-aided networks. However, when the CSI of the *separate links* (e.g., BS-RIS and RIS-UEs) is available, the optimization of the RIS configuration become an easier task. Nevertheless, the decision maker usually needs to optimize RIS configuration together with other transmission parameters, such as BS beamformer or resource block allocation, while targeting a specific goal.

For example, D4.2/4.4.4-4.4.5-4.4.6 present different solutions able to maximise the sum rate based on CSI knowledge, in different scenarios. With the same aim, new solutions envisioning the use of distributed optimization of the available resources when multiple RISs have been recently investigated [KSI+22], [KDA22]. Further details on the specific solutions can be found in Section 4.4.7.

The spatial diversity brought by the RIS can also be exploited to slice different kinds of service. On this matter, solution for multiplexing eMBB and URLLC exploit the knowledge of the eMBB CSI to assist URLLC communication, even when the CSI of the latter is unknown at the transmitter [SCK23a]. Indeed, the knowledge of the CSI of a subset of users is enough to let the RIS loads configurations that nullify the interference on other transmissions. Further details are given in Section 4.4.6.

If a HRIS can be deployed, application of self-configuration design can be considered to avoid deploying new infrastructure and to reduce the burden of explicitly controlling the RIS [ADS22]. Moreover, novel solutions incorporating energy harvesting (EH) can be included [ADS23]. Through the acquisition of the separate links CSI, the HRIS can self-configure to provide boosted connectivity towards UEs, while maximize its own EH. Further details are given in Section 4.4.8.

### 4.3.2 Localization-based optimization

Recently, many works have shown that transmission parameter optimization design can be made using the information related to the receiver position, overcoming the need of CSI estimation. Localization-based solutions are particularly suitable when the coherence time of the channel is short, i.e., in scenarios where the acquired CSI can easily be outdated and/or inaccurate.

In D4.2/4.4.2-4.4.5, two solutions based on classical optimization methods and machine learning techniques were developed. In this deliverable, we present two novel solutions that optimise the communication resources based on localization information [SKP23], [SCK23a]. Section 4.4.9 presents a resource allocation solution that can robustly allocate the time and frequency resources of a RIS-aided OFDM transmission based on the (perfect) UE positioning. Section 4.4.10 deals URLLC traffic, allowing a low-

complexity minimum power solution that uses imperfect tracking information to optimize RIS beamforming and transmit power.

### 4.3.3 Mixed strategies

Recently, new design mixing localization-based and CSI-based optimization have been developed. In general, the idea is to reduce the overhead of the CSI acquisition by using positioning to perform a rough beamforming optimization of the RIS. Then, CSI is acquired under the same RIS configuration, and the BS transmission parameters are optimised [JAS22], [ZPR23]. Section 4.4.11 describes the solution, also analysing the impact of electromagnetic interference. Section 4.4.12 investigate the protocol data frame and the algorithmic requirements needed to apply CSI-localization-based mixed strategies.

## 4.4 Contributions from RISE-6G

Table 4-1 lists all relevant contributions from RISE-6G in the design of multi-user techniques for RISE systems. The table specifies the scope of the algorithm proposed, which information is based on, and the setting of the scenario. Moreover, the last column specifies where to find the contribution (deliverable and section numbers), considering that the contributions listed in D4.2 are not reported here if no updates were provided.

**Table 4-1 Contribution of RISE-6G on design of multi-user techniques**

| Title | Scope | Based on | #BS | #RIS | LoS/ NLoS | Continuous/ quantized phase-shift | Deliverable/ Section no. |
|---|---|---|---|---|---|---|---|
| Tensor-based Channel Tracking for RIS-Empowered Multi-User MIMO Wireless Systems | Fast CSI estimation | Transmission of pilot, parallel factor decomposition and bilinear estimation | 1 | 1 | LoS/ NLos | Continuous | D4.2/4.4.1 |
| Sum-Rate Optimization of Reconfigurable Intelligent Surfaces Based on Statistical Position Information | Maximize the throughput | Statistical positioning information | 1 | 1 | LoS/ NLos | Continuous | D4.2/4.4.2 |
| RIS Orchestration algorithms for online configuration tuning based on Reinforcement Learning | Online configuration optimization | Reinforcement Learning and Multi-Armed Bandit approaches | 1 | Multiple | LoS/ NLoS | Quantized | D4.2/4.4.4 |
| Supervised learning of optimal phase configuration based on user positions | Phase shift of multiple RIS at once | Deep Neural Network learning approach | 1 | Multiple | LoS/ NLoS | Quantized | D4.2/4.4.5 |

| | | | | | | | |
|---|---|---|---|---|---|---|---|
| Reconfiguration of the physical layer for multi beamforming | Multi beamforming toward different receivers | LoS beamforming | 1 | 1 | LoS | Continuous | D4.2/4.4.6 |
| Random Access Protocol with Channel Oracle Enabled by a Reconfigurable Intelligent Surface | Access of new and intermittently active users | Sweeping through a RIS codebook | 1 | 1 | LoS | Continuous | D4.4/4.4.1 (Updated from D4.2/4.4.3) |
| Multi-RIS Massive Access Protocol via Scheduling and Contention | Multiple access and scheduling | Centralised scheduling and distributed contention policies | 1 | Multiple | LoS/ NLoS | Any | D4.4/4.4.2 |
| Generalized Unitary Approximate Message Passing for Double Linear Transformation Model | Generalize narrowband CSI estimation method | UL pilot transmission | 1 | 1/ Multiple | LoS/ NLoS | Any | D4.4/4.4.3 |
| Direct Tensor-Based Estimation of Broadband mmWave Channels With RIS | Broadband CSI estimation method for the double-path BS-RIS-UE | UL pilot transmission | 1 | 1 | LoS/ NLoS | Any | D4.4/4.4.4 |
| Channel Estimation with Simultaneous Reflecting and Sensing Hybrid Reconfigurable Intelligent Metasurfaces | CSI estimation method for hybrid RISs | Simultaneously receiving and reflecting RIS | 1 | 1 | LoS | Continuous | D4.4/4.4.5 |
| Uplink Multiplexing of eMBB/URLLC Services Assisted by Reconfigurable Intelligent Surfaces | Multiplexing UL traffic with different QoS | Simultaneously receiving and reflecting RIS, interference nulling | 1 | 1 | LoS | Continuous | D4.4/4.4.6 |

| | | | | | | | |
|---|---|---|---|---|---|---|---|
| RIS-Empowered Multi-user communications: Distributed sum-rate maximization of cellular communications with multiple RISs | Distributed resource allocation for RIS-aided communications | Distributed optimization and successive concave approximation | Multiple | Multiple | LoS/NLoS | Continuous | D4.4/4.4.7 |
| ARES: Autonomous RIS solution with Energy harvesting and Self-configuration towards 6G | Joint self-configuration and energy self-sufficiency. | Sensing with directional power measurements of the UEs and BS transmission. Collection of a portion of the energy impinging on the HRIS for energy harvesting. | 1 | 1 | LoS/NLoS | Quantized | D4.4/4.4.8 |
| Localization-based OFDM framework for RIS-aided systems | OFDM-like multi-user resource allocation | (perfect) UE localization information | 1 | 1 | LoS/ NLoS | Continuous | D4.4/4.4.9 |
| RIS-aided URLLC with imperfect device tracking | Power control to satisfy URLLC requirements | (imperfect) UE localization information | 1 | 1 | LoS/ NLoS | Continuous | D4.4/4.4.10 |
| Two-Timescale Design for Reconfigurable Intelligent Surface-Aided Massive MIMO Systems with Imperfect CSI | CSI estimation for spatially independent and spatially-correlated Rician fading models | on some predefined pilot signals | 1 | 1 | LoS/ NLoS | Continuous | D4.4/4.4.11 |
| RIS area illumination strategies | Beamforming toward user location or target area | User position estimation and blockage areas | 1 | 1 | LoS | Continuous | D4.4/4.4.12 |

### 4.4.1 Random access protocol with channel oracle enabled by a Reconfigurable Intelligent Surface

***Motivation and context***

RISs represent a revolutionary advancement for the next generation of wireless systems, empowering them to manipulate radio waves and create intelligent radio environments with low-energy consumption. While existing literature primarily focuses on the PHY layer aspects and the modelling of related electromagnetic phenomena in RIS-assisted communication systems, integrating RIS into higher-layer protocols to harness the full potential of PHY benefits remains an underexplored area. One compelling challenge in incorporating RIS into higher layers is addressing the random access (RA) problem. In this scenario, individual resource allocation and coordination among UEs are unfeasible. We encounter two intriguing questions:

1. How can we effectively coordinate transmissions to avoid collisions, ensuring that only one UE transmits during a given period?
2. When collisions occur, what is the optimal approach for retransmitting packets?

We focus on a system model motivated by an application in an industrial scenario, as shown in Figure 4-1, where the coverage of an AP can be extended by using RISs without the need to install multiple APs.

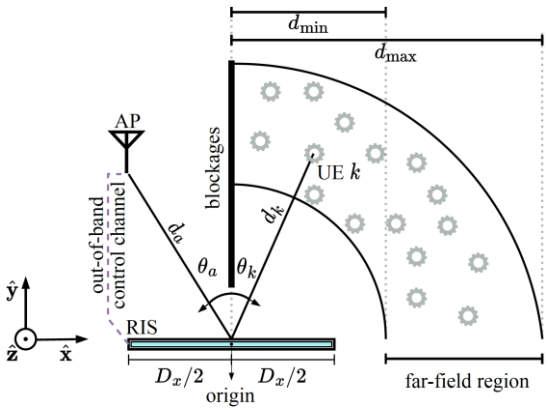


**Figure 4-1 System model of an industrial application scenario with one RIS and multiple UEs trying to connect to the AP [CSL23]**

***Methodology***

The proposed RIS-assisted random access protocol is visually depicted in

Figure 4-2. The structure consists of two independent modules: **A. Channel Oracle** and **B. Access**. Drawing inspiration from the carrier sensing approach, our protocol's core concept revolves around enabling each UE to develop a model for channel coefficient variations across the reflected angular space controlled by the RIS. The Channel Oracle module facilitates this distributed learning process, considering that the RIS control lies with the AP, not the UEs. Leveraging the output from the Channel Oracle, the Access module guides how the UEs attempt to transmit packets to the AP over the multi-access channel. Notably, the AP needs more prior information about the UEs and retains control over the RIS. The dependency on the Channel Oracle output is crucial for the UEs to benefit from the environment control facilitated by the RIS. Without it, the Access module could be replaced with conventional protocols. The Access module is more frequently employed in practice than the Channel Oracle module. In summary, the protocol works as follows:

**Channel Oracle:** the AP sends pilots while the RIS sweeps through a set of configurations; this enables the UE to learn a model that tells it how its channel is affected by the RIS.

**Access:** the UE exploits the model learned during the Channel Oracle to design access policies so that it can choose when to send packets. At the same time, the RIS is controlled to sweep again through another set of configurations.

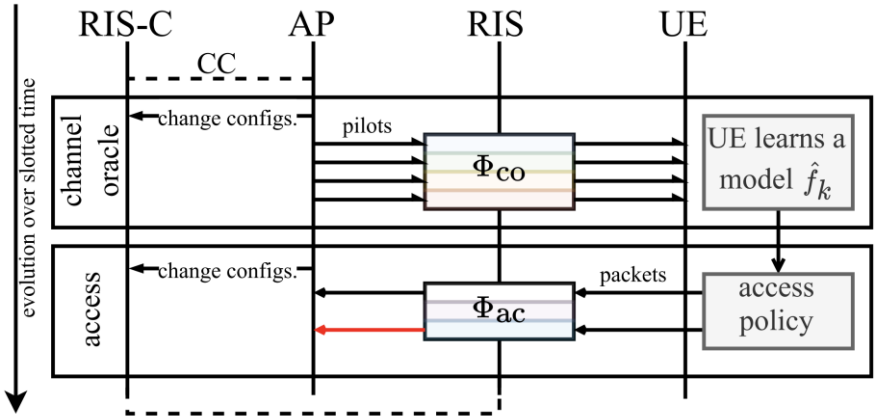


**Figure 4-2 Time diagram of the proposed RIS-assisted random access protocol. The RIS-C denotes the RIS controller, connected to the AP via the control channel (cc). Operations occur sequentially in time following the top-down direction. The protocol is comprised is comprised of two modules: channel oracle and access. The red arrow illustrates collision since, hypothetically, another UE decided to send a packet during the same access configuration [CSL23]**

We provide concrete designs for the Channel Oracle and Access modules. We design the configuration codebook for the Channel Oracle module to guarantee that the UEs learn good models. We relate the size of this codebook with the performance of the model. We design the access module to ensure good SNR conditions for all the UEs in the coverage area and reduce the probability of collisions among UEs.

The work also proposes how to acknowledge the UEs that their packets were decoded correctly when using the RIS. For more practical details about the protocol, refer to the work in [CSL23].

***Results and outcomes***

The evaluation presented in Figure 4-3(a) assesses the expected overall throughput for the proposed RIS-assisted protocol with three different access policies, assuming a switching time equal to 0. The switching time tells how long it takes for the RIS to load the configuration into its elements. The access policies are as follows and are based on transmitting replicas of the same packet:

1. *R*-configuration-aware random policy (*R*-CARAP). Each UE samples *R* access configurations randomly and without replacement from the access configuration codebook by using a probability mass function to evaluate the UE's channel gain of each configuration in the codebook.
2. *R*-greedy-strongest-configurations access policy (*R*-GSCAP). This access policy works by susceptibly getting the R best configurations concerning their channel gain.
3. Strongest-minimum access policy (SMAP). In this heuristic policy, the UE transmits just two replicas: one at the strongest access configuration and another at the access configuration, ensuring a minimum SNR so the AP can decode the UE's packet.

Notably, our random-access protocol consistently outperforms the baseline, regardless of the access policy employed. The R-GSCAP access policy stands out, offering an impressive 66.18% higher throughput than the baseline on average.

In Figure 4-3(b), we explore the impact of control commands and hardware operation at the RIS on the throughput. We observe that a switching time equal to the symbol time renders the protocol impractical due to significant overhead from sweeping over access configurations. Consequently, from a protocol standpoint, rapid-switching RIS and a CC between the AP and the RIS are desirable. To mitigate the impact of switching time, one potential approach is to reduce the size of the access codebook, which may lead to more collisions on average.

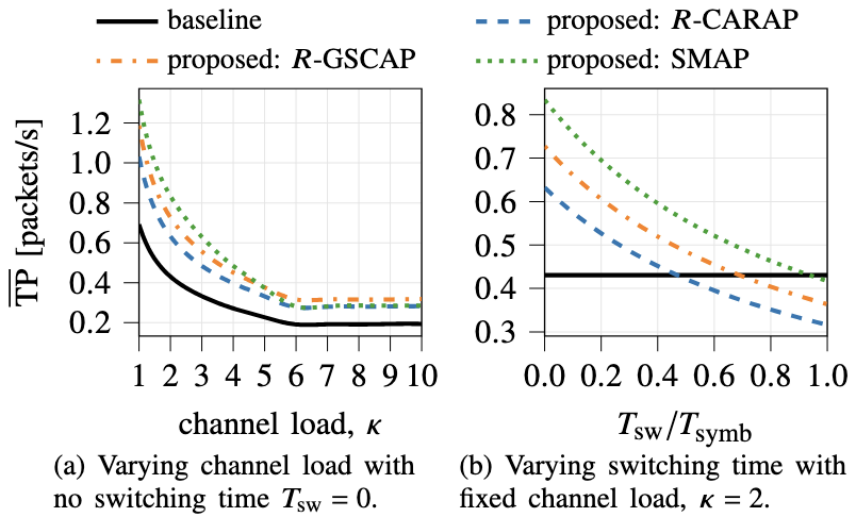


(a) Varying channel load with no switching time $T_{sw} = 0$.
(b) Varying switching time with fixed channel load, $\kappa = 2$.

**Figure 4-3 Performance of the proposed methods [CSL23]**

***Relation to other RISE-6G contributions***

The proposed random-access procedure can retrieve information on the CSI of the users for every configuration of the RIS involved in the access phase through the oracle procedure. At the end of the access phase, the BS is informed on which configuration each user prefers for transmission. This information can be used as initialization to RIS profile optimisation algorithms. Moreover, every configuration is related to a certain position in the space. Hence, a prior information on the location can be obtained and propagated to WP5 localization algorithms as initial point. Finally, the beam sweeping procedures exploited in this contribution are used in the field trials of WP7.

### 4.4.2 Multi-RIS Massive Access Protocol via Scheduling and Contention

***Motivation and context***

Next Generation Multiple Access (NGMA) protocols will be designed to handle massive numbers of connections, heterogeneous data traffic, offering high spectral efficiency and ultra-low latency services. In that regard, the deployment of RISs has the potential to offer a new layer of reconfigurability in accommodating large numbers of users in different resource blocks, both in terms of RIS phase configuration for higher spectral efficiency, as well as considering yet unexplored multiple access schemes (Figure 4-4). This contribution concerns the design of a NGMA scheme under a MAC protocol incorporating RISs [CYH22] offering improved system throughput and access fairness while revealing an emerging trade-off relationship between the two objectives in practical scenarios of static users operating together with mobile ones.

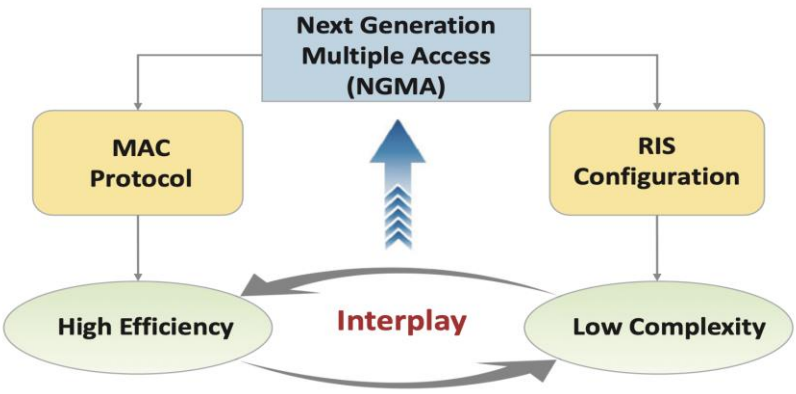

**Figure 4-4 RIS-aware MAC scheme for NGMA offering efficiency and complexity benefits.**

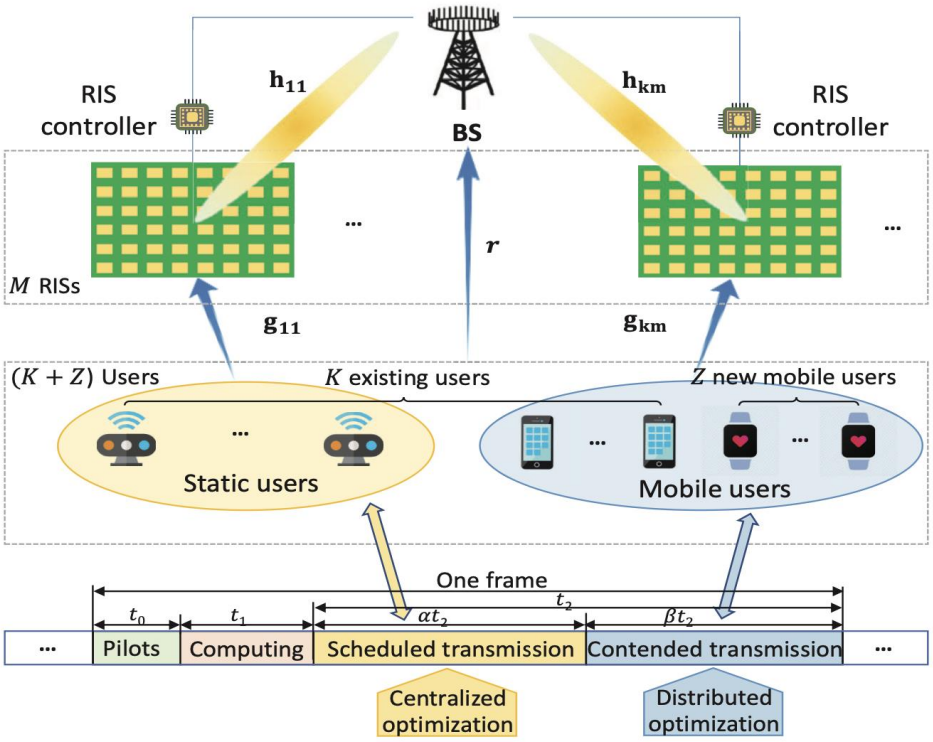


**Figure 4-5 The system considered in the MAC scheme including scheduled and contention transmission phases with multiple RISs serving static and mobile users.**

***Methodology***

The considered scenario assumes K users participating in all consecutive time frames, while Z new users are participating in individual frames. The users are split into groups of static and mobile devices, where the new users are assumed to be always mobile. The users are served by M RISs in their communication toward the BS. During a frame, based on pilot transmission and computation, static users communicate with the BS by scheduling M RISs, while mobile users communicate with the BS using these RISs by contention. The ratio of the transmission period of two types is β/α, which is optimised by the BS during the computing period. The overall system for a single time frame is given in Figure 4-5.

Specifically, after the pilot transmission stage, the BS performs a classification operation of their users according to their perceived mobility patters to predict which ones are mobile and which ones are static. For each of the static users, the individual links are then estimated. Based on the channel information, the BS computes the MAC protocol parameters and allocates the slots, power, and RIS usages for static users over non-overlapping sub-channels. The reflection parameters of the scheduled RISs are computed at the BS to support the transmission of all static users.

After the scheduled transmission phase elapses, the algorithm proceeds to a contended transmission mode solved via distributed optimisation. The unscheduled mobile users start their multiple access and compute the RIS configuration by themselves based on estimated CSI, which is calculated according to sub-channel and sensing. A distributed coordination function scheme is imposed for negotiating access with the BS which involves backoff and computing, request-to-send messages, and clear-to-send feedback, before the selected user is allowed to select RIS phase profiles and transmit their data on their occupied sub-channel.

The objective of the system is to maximise the total throughput which, given that Time-Division Multiple Access (TDMA) and Frequency-Division Multiple Access (FDMA) schemes, as well as the combination of scheduled and contended transmissions can be expressed as the constrained sum of the partial throughput of all users participating in the transmission schemes under the analysis provided in [CYH22]. This problem can be decomposed into partial sub-problems, so that an alternating optimisation scheme is employed to attain satisfying solutions, incorporating both centralised RIS configuration methods as well as distributed configuration algorithms.

***Results and outcomes***

Introducing RISs enhances the quality of wireless links, thereby attaining the following benefits of the MAC protocol.

1. *MAC efficiency improvement*. On the one hand, a low-complexity RIS configuration will reduce the computing cost; On the other hand, the access latency of static and mobile users can be reduced by the low-complexity scheduling and the low-contention collision, respectively. Thus, the efficiency of the MAC protocol is improved.
2. *MAC fairness improvement*. Because of the separation of static and mobile users and the low-complexity operation on them, the fairness of users can be enhanced.

A scenario of a network consisting of a BS, 2 RISs having 128 elements each and 200 users is evaluated in [CYH22] by using as two baselines schemes the strategy of performing centralised multiple access across all static and mobile users (Scheme 1), as well as operating in a purely distributed/contention mode (Scheme 2). The impact of the presence and the number of RISs, along with their numbers of elements is also studied. The results are presented in Figure 4-6 and Figure 4-7 below:

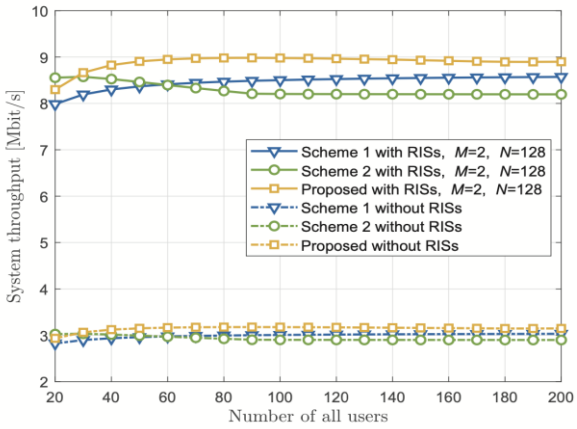


**Figure 4-6 Comparison of the total throughput between the proposed system and the baselines while also considering the case of no RISs.**

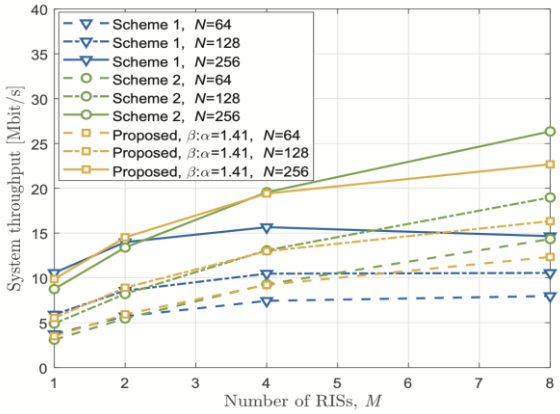


**Figure 4-7 Comparison of the total throughput between the proposed system and the baselines for different numbers of RISs, different numbers of elements per RIS, and different ratios of scheduling vs contention.**

***Relation to other RISE-6G contributions***

The protocol aspects and the signalling characterisation of this NGMA scheme have been studied under D4.3. Moreover, this MAC scheme is based on multi-RIS optimisation techniques, therefore the various RIS tuning procedures proposed in the current deliverable may be incorporated in the proposed scheme with little or no modifications of the overall algorithm. The exact methodology depends on the characteristics of the system and the kind of information that can be collected, as well as the capabilities of the RISs, including the potential phase configuration profiles and reconfigurability delays.

### 4.4.3 Generalized unitary approximate message passing for double linear transformation model

***Motivation and context***

The double linear transformation model $Y = AXB + W$ plays an important role in a variety of science and engineering applications, where $X$ is estimated through known transformation matrices $A$ and $B$ from the noisy measurement $Y$. Our aim in this paper is to develop a generalized algorithm with low complexity and high robustness for the target model, which can be employed in channel estimation problem of RIS-aided MISO system and multi-RIS-aided MISO system (as depicted in Figure 4-8). The great significance of the proposed algorithm is that it is not only applicable to RIS-assisted communication, but to any problem that satisfies the double linear transformation model.

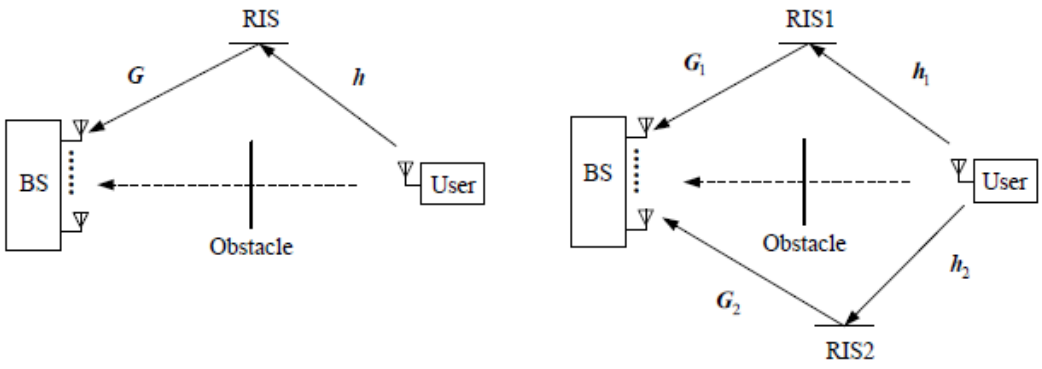


**Figure 4-8 System model. (a) Single RIS aided communication system. (b) Multi-RISs aided communication system [MLY23]**

***Methodology***

Decoupling $X$ from the double linear transformation model is a hard task due to the high complexity brought by the multiplication of the unknown matrix (vector) with the transformation matrix (M-UMTM). The proposed algorithm, termed as GD-UAMP, applies the ``three-step approximation'' method to derive a tractable simplification of the combined message passing (MP) BP-EP rule and the double unitary transformation to enhance the robustness. We further implement the EP rule that can fit arbitrary input messages, broadening the use of the proposed algorithm. As a generalized algorithm, GD-UAMP can be applied to address the generalized Bayesian inference problem, i.e., the arbitrary prior probability of $X$ and likelihood function of $Z$, where $Z = AXB$ is the noiseless measurement.

The interested reader can refer to [MLY23] for all the details on the system model, problem formulation, and algorithmic solutions.

***Results and outcomes***

The RIS-aided wireless communication signal model coincides with the double linear transformation model; thus, the channel estimation problem can be solved by our generalized algorithm. We apply the proposed algorithm to RIS-aided MISO system (Figure 4-9 and Figure 4-10) and multi-RIS-aided MISO system (Figure 4-11 and Figure 4-12) to evaluate the effectiveness of the proposed algorithm.
In Figure 4-9, we compare the NMSE performance among various channel estimation methods. It can be seen that the proposed DUAMP-SBL algorithm exhibits the optimal performance among all estimation algorithms. In Figure 4-10, we evaluate the impact of pilot overhead on the NMSE. It is intuitive that the

performance of DUAMP-SBL is superior to the other algorithms. LS fails when L > 64 since the algorithm cannot guarantee the unique solution with insufficient observations. Both AMP-based algorithms and V-OMP take full advantage of the angular sparsity of the channel, thus reducing the pilot overhead. In Figure 4-11, we compare the NMSE performances of the various algorithms. First, the DUAMP-SBL algorithm provides the superior performance for both H1 and H2 as expected. In addition, the estimation of H1 is more accurate than that of H2. It is due to the fact that H1 has more variables to be estimated than H2 in the angular domain. Figure 4-12 shows the NMSE performance with respect to the pilot overhead. First, it can be observed that the proposed algorithm outperforms the benchmark in all cases. Although the performance of EM-GM-VAMP improves rapidly with increasing pilot overhead, it is still lower than that of the proposed DUAMP-SBL. In addition, DUAMP-SBL can achieve almost the same level of estimation accuracy as that of V-OMP with half of the pilot consumption, leading to a huge reduction in pilot overhead.

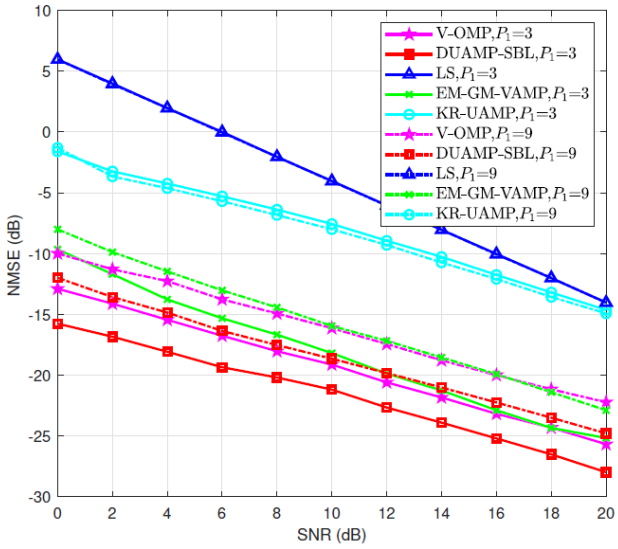


**Figure 4-9 NMSE performance of the single RIS-aided MISO system vs. SNR [MLY23]**

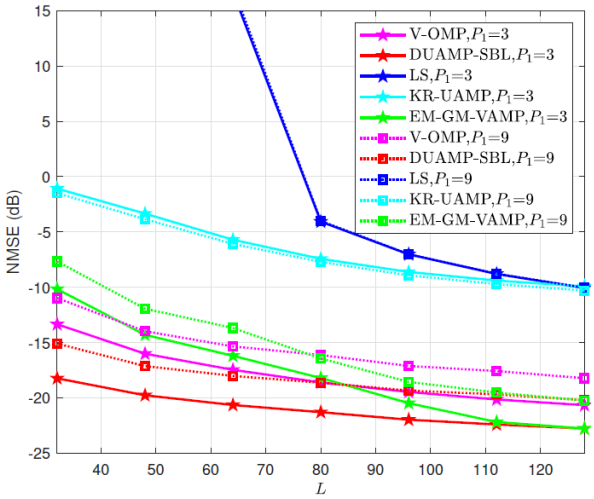


**Figure 4-10 NMSE performance of the single RIS-aided MISO system vs. the pilot overhead ($L$) [MLY23]**

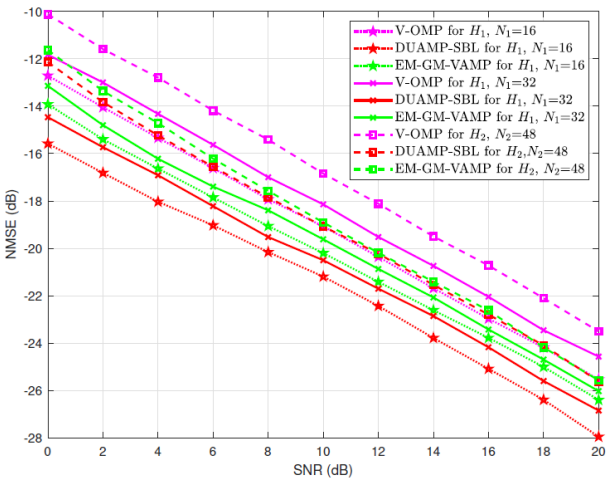


**Figure 4-11 NMSE performance of the multi-RIS-aided system vs. SNR [MLY23]**

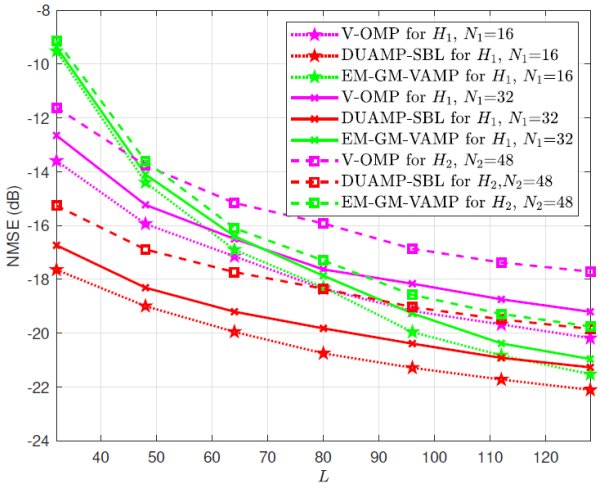


**Figure 4-12 NMSE performance of the multi-RIS-aided system vs. the pilot overhead ($L$) [MLY23]**

***Relation to other RISE-6G contributions***

Channel estimation is a fundamental task for RIS-aided communication. The proposed algorithm is mainly applicable to the channel estimation problem in narrowband RIS-aided systems. Broadband RIS-aided channel estimation algorithm can be found in [MSL23].

### 4.4.4 Direct tensor-based estimation of broadband mmWave channels with RIS

***Motivation and context***

RIS has generated a lot of interest in relation to the next generation of wireless communication, as it offers the possibility to control part of the wireless propagation environment and potentially boost the communication performance. The use of RIS brings new challenges related to the acquisition of CSI since plenty of RIS reflecting units increase the dimension of the CE problem. Due to the presence of double paths channel, i.e., from the UE to the RIS and from the RIS to the BS, the passive capabilities of the RIS, and the large quantity of channel coefficients to be estimated, a single training sequence is not enough to separately infer the channel paths and solve the CE problem. This method is developed to estimate the double-path channel using direct tensorial computation. This contribution investigates the mmWave due the limited number of paths characterizing the spectrum, simplifying the computational complexity of the solution. This solution can be easily extended for the sub-6GHz spectrum.

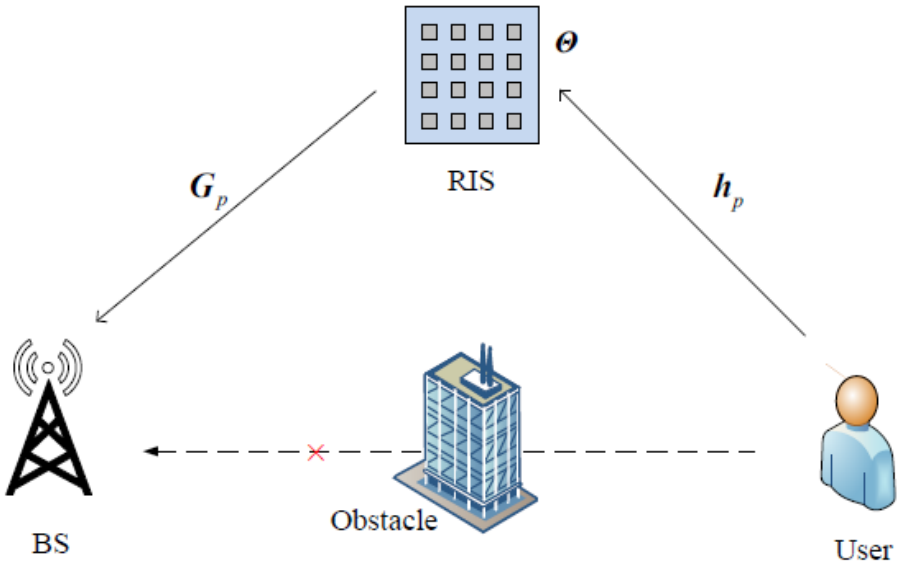


**Figure 4-13 System model [MSL23]**

***Methodology***

We address the channel estimation problem in mmWave systems aided by RIS and propose a peak detection-message passing (PDMP) algorithm and a peak detection-average (PDAVE) algorithm. The angle and delay parameters of the channel are estimated from the multi-dimensional structure of the received tensor by exploiting the properties of the array steering vector (ASV). Different from the common-used canonical polyadic decomposition (CPD) method, the proposed algorithm directly obtains the angle and delay parameters from the multi-dimensional structure of the tensor rather than from the factor matrices Finally, the channel gain is further estimated by employing the message passing method.

The interested reader can refer to [MSL23] for all the details on the system model, problem formulation, and algorithmic solutions.

***Results and outcomes***

In the simulation, we analyse two different cases: angle separation (AS), i.e., the different angle and delay parameters in different main lobes, and without angle separation assumption, marked by ``NAS", benchmarking against the SCPD algorithmic in literature [ZWS22].
In Figure 4-14, we compare the performance with respect to the number of available subcarriers $P$, where SNR$=0$ dB and time-slots $Q=16$. We find that the proposed algorithm exhibits the best results even under the ``NAS" assumption. It is interesting that the accuracy of the SCPD gets worse as the number of subcarriers increases, while the performances of PDMP and PDAVE improve. The behaviour of the SCPD comes from the fact that there are more variables to be estimated as the subcarriers increases; otherwise, in PDMP and PDAVE, the higher the number of subcarriers, the better the performance due to the averaging operations. In Figure 4-15, we compare the performance of the proposed algorithm as a function of the SNR, where $Q=16$, $P=256$. The proposed algorithm still exhibits the best performance, especially in the low SNR regime. In SCPD, the delay and angle parameters are obtained from intermediate estimations, whose procedure suffers from the presence of noise. For the proposed algorithm, they are directly estimated from overall tensor, where the averaging operation improves estimation performance. Figure 4-16 shows the NMSE performance as a function of the number of time slots, where SNR$=0$ dB and $P=256$. The proposed algorithm shows excellent performance, even when few time slots are available. Although the performance of SCPD increases rapidly with the growth of the number of time slots, its performance is significantly lower than the proposed algorithms.

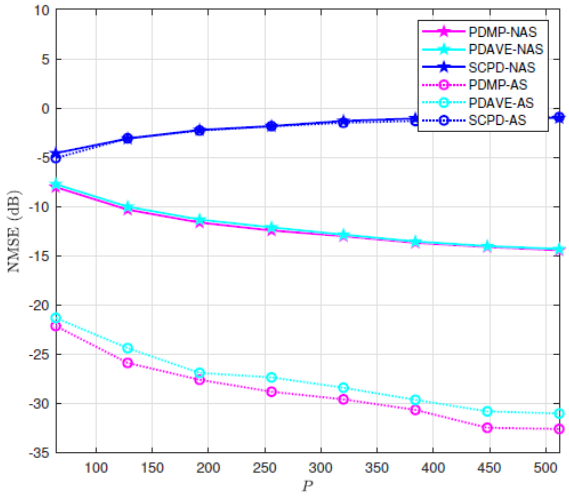


**Figure 4-14 NMSE vs. number of subcarriers (*P*) [MSL23]**

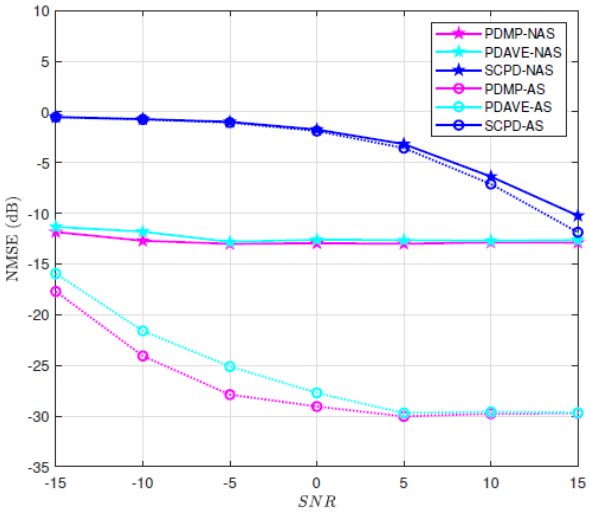


**Figure 4-15 NMSE vs. SNR [MSL23]**

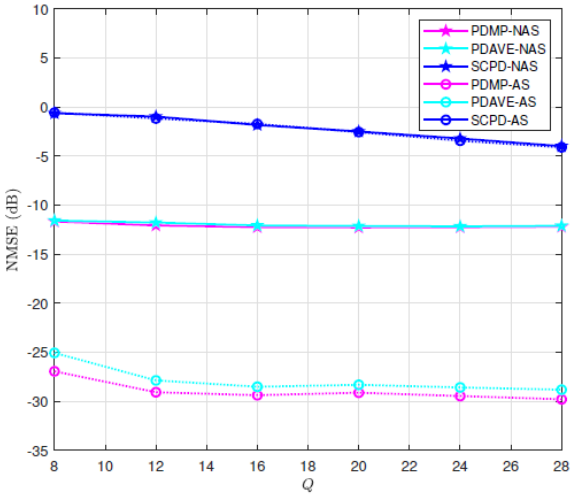


**Figure 4-16 NMSE vs. time slots (*Q*) [MSL23]**

***Relation to other RISE-6G contributions***

Channel estimation is a fundamental task for RIS-aided communication. The proposed algorithm is mainly applicable to the channel estimation problem in broadband OFDM-like RIS-aided systems. This method can used to feed the communication procedures and resource allocation techniques that requires CSI information in setting where the direct channel is blocked.

### 4.4.5 Channel estimation with simultaneous reflecting and sensing Hybrid Reconfigurable Intelligent Metasurfaces

***Motivation and context***

The process of channel estimation becomes more involved when RISs are deployed with multiple elements due to the high dimensionality of controllable paths. Therefore, simultaneously reflecting and sensing RISs (i.e., "Hybrid" (HRIS)) offer a high proposition of value due to their inherent capabilities in collecting and potentially processing impinging signals. To that end, this contribution [ZSA23**]** considers the algorithmic formulation of the channel estimation procedure for the uplink of a multi-user HRIS-empowered communication system. Considering first a noise-free setting, we theoretically

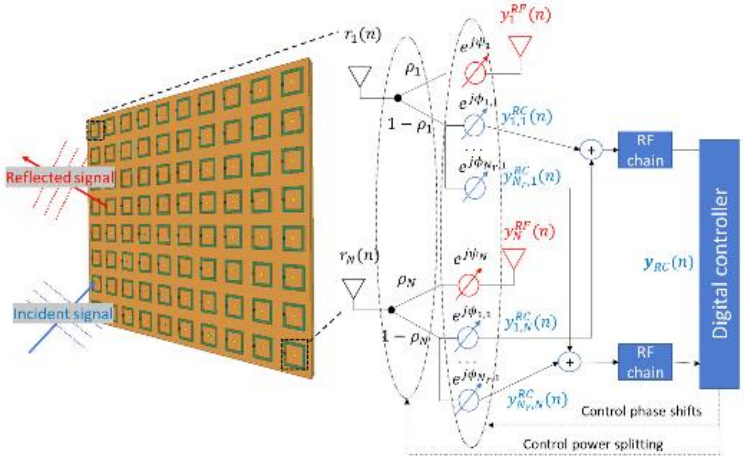


**Figure 4-17 A simple model for the proposed HRIS operation.**

quantify the advantage of HRISs in notably reducing the number of pilots needed for channel estimation, as compared to the case of purely reflective RISs. The MSE performance in estimating the individual channels at the HRISs and the BS is presented in closed-form, while a first-order differentiation algorithm is given to optimise the HRIS phase and power-splitting configuration for minimising the overall estimation error when noisy channels are considered.

***Methodology***

The exemplary system is composed of a MIMO BS where $K$ UEs send uplink pilot signals via the HRIS. The UE-BS link is assumed blocked and the controller colocated with the RIS decides on its receiving/reflecting configuration as well as the fraction of the signal power that will be absorbed. The considered HRIS-empowered multi-user MIMO communication system operating in the uplink direction. Since the HRISs architecture enables the metasurface to reflect the impinging signal in an element-by-element controllable manner, while simultaneously sensing a portion of it, this contribution presents a mathematical model of the hybrid meta-atom elements for HRIS-empowered wireless systems in a manner that is amenable to system design, as shown in Figure 4-17. The parameter $\rho_l$ models the portion of the impinging signal at the $l$-th meta-atom of the HRIS that gets tunably reflected, while $\psi_l$ and $\varphi_{r,l}$ model the meta-atom's controllable phase shift and the joint effect of its response together with the analog phase shift before the $r$-th receive RF chain, respectively. Specifically, for the $n$-th element, a portion of this signal, dictated by the parameter $\rho_n(n) \in [0,1]$, is reflected with a controllable phase shift $\psi_l(n) \in [0, 2\pi)$, and thus the reflected signal from the $l$ -th element at the $n$ -th time instant can be expressed as:

$$y_l^{RF}(n) = \rho_l(n)\, e^{j\,\psi_l(n)} r_l(n),$$

while the remainder of the observed signal is locally processed via analog combining and digital processing. The signal forwarded to the $r$-th RF chain via combining, with $r \in \{1,2,\ldots,N_r\}$, from the $l$-th element at the $n$-th time instant is consequently given by

$$y_{r,l}^{RC}(n) = (1-\rho_l(n))\, e^{j\,\varphi_{r,l}(n)} r_l(n),$$

where $\varphi_{r,l}(n) \in [0, 2\pi)$ represents the adjustable phase that models the joint effect of the response of the $l$-th -th meta-atom and the subsequent analog phase shifting.

The reconfigurability of HRISs implies that the parameters $\rho(n)$ as well as the phase shifts $\psi(n)$ and $\varphi(n)$ are externally controllable. It is noted that when an element is connected to multiple receive RF chains, then additional dedicated analog circuitry (e.g., conventional networks of phase shifters) is required to allow the signal to be forwarded with a different phase shift to each RF chain, at the possible cost of additional power consumption. Nonetheless, when each element feeds a single RF chain, then the model in Figure 4-17 can be realised without such circuitry by placing the elements on top of separated waveguides. Following the mathematical formulation of the paper for the case of the noise-free channels, it is proved that the true channels can be estimated perfectly when the number of pilots $\tau$ is greater than the fraction of the total RIS elements over the number of receiving elements, multiplied by the number of participating users. Proceeding to the case of noise in the channels, the estimation problem can be expressed as the sum of the MSEs of the estimations of the partial links. Note that the estimation of the UE-RIS links depends only on $\psi(n)$ and $\rho(n)$, while the estimation of the RIS-BS link depends additionally on $\varphi(n)$. Since those expressions are composed of differentiable analytical operations, the minimisation problem is tackled via gradient descent through automatic differentiation, setting a regularisation penalty for the violation of the constraints.

***Results and outcomes***

For the case of the absence of noise, this methodology demonstrates the intuitive benefit of HRISs in facilitating individual channel estimation with reduced number of pilots, as compared to existing techniques for estimating the cascaded UTs-RIS-BS channels (e.g., [WLC20])**.** For instance, for a multi-user MIMO system with $M = 16$ BS antennas, $N_r = 8$ HRIS RF chains, $K = 8$ UEs, and $N = 64$ HRIS elements, the adoption of an HRIS allows recovering the partial links separately using $\tau = 64$ pilots. By contrast, the method proposed in [WLC20] requires transmitting over 90 pilots to identify the cascaded channel coefficients. This reduction in pilot signals is directly translated into improved spectral efficiency, as less pilots are to be transmitted in each coherence duration.

Figure 4-18 demonstrates the effect of the power-splitting ratio of the HRIS architecture. When most of the signal power is absorbed (low ρ values), the UE-RIS links are estimated with higher precision compared to the RIS-BS link and vice-versa.

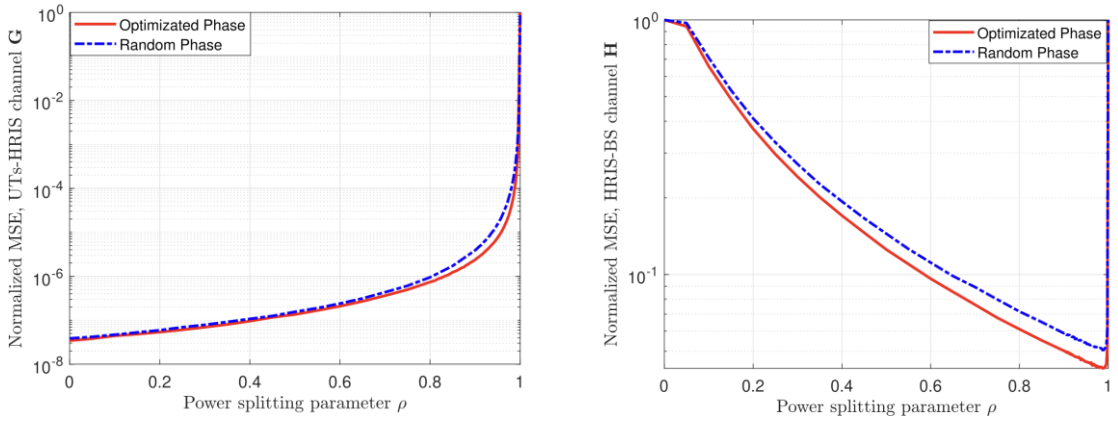


**Figure 4-18: Estimation performance of the partial UE-RIS (left) and RIS-BS (right) links for different power splitting parameter value choices.**

Figure 4-19 displays the evaluation of the HRIS architecture for channel estimation in comparison to the purely reflective RIS approach of **[**WLC20**],** for different system parameter values and alternative HRIS deployment (i.e., by setting the HRIS configuration and power-splitting randomly, or only partially connecting the receiving elements to RF chains). The HRIS proposal offers substantial benefits in terms of pilot lengths and total number of RIS elements, while requiring only limited number of RF chains.

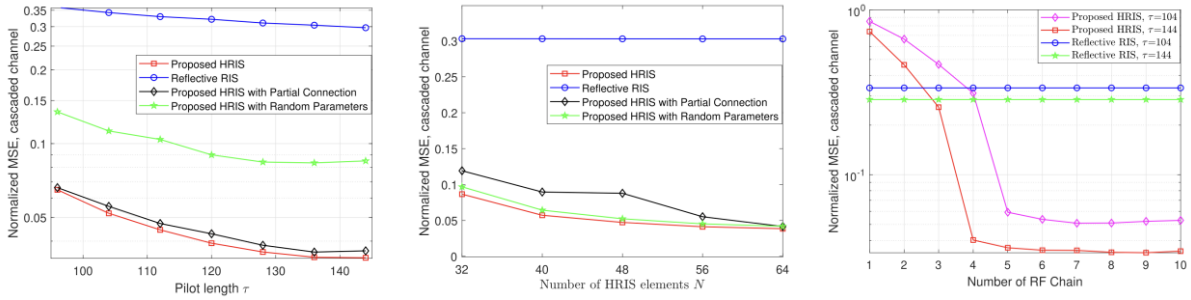


**Figure 4-19 Performance evaluation of the channel estimation procedure across different system parameter values.**

***Relation to other RISE-6G contributions***

This algorithmic approach and numerical analysis of channel estimation with an HRIS builds on top of the deployment scenario presented in the contribution of Section 6.13 of D4.3, utilising the signalling and data flow considerations specified therein. Similarly, the channel estimation procedure is one of the core components of the self-configuring RIS solution, presented as the contribution of Section 6.10 in D4.3.

### 4.4.6 Uplink multiplexing of eMBB/URLLC services assisted by Reconfigurable Intelligent Surfaces

***Motivation and context***

The fifth generation of wireless communication technology and beyond are envisioned to simultaneously support heterogeneous services with different QoS requirements and traffic characteristics. In particular, eMBB require extremely high data rates, while URLLC services demand high reliability and low latency. The contrast between the requirements of these two services makes it very challenging to jointly serve eMBB and URLLC UEs. In the uplink, this is even more difficult since UEs cannot communicate directly and, consequently, coordinate the access among themselves. Meanwhile, reconfigurable intelligent surfaces with their potential of enabling a programmable environment represent a promising technology to support the coexistence of eMBB and URLLC services.

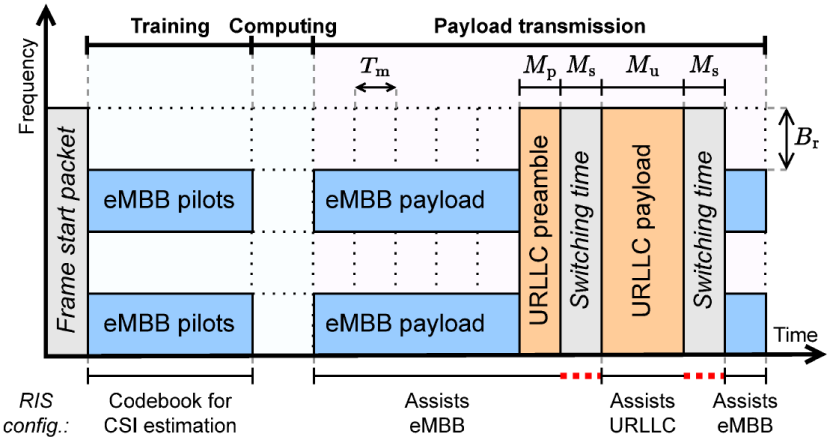


**Figure 4-20 Structure of the UL frame divided into training, computing, and payload transmission phases. The ongoing eMBB traffic is punctured by URLLC transmission.**

***Methodology***

In this contribution [SCK23b], we propose an UL RIS-assisted multiplexing scheme to support the coexistence of eMBB and URLLC traffic. The scheme is based on computing two RIS configurations. The first optimizes the QoS of the eMBB UE. The second configuration focuses on supporting the QoS of the URLLC UE based on the idea of interference nulling (IN), where reliable URLLC transmissions are made possible even in the presence of eMBB interference. At the BS, the computation of a RIS configuration to assist the URLLC transmission is challenging, since only eMBB CSI is available at the BS. The idea is to find a configuration that mitigates the interference caused by the eMBB traffic to the URLLC one. To that end, we present two methods for computing the URLLC-oriented configuration. The first one is a heuristic based on phasors rotation (PR). The second one is an alternating projection algorithm to approximate a configuration that nulls the eMBB interference (IN). Both strategies use only the CSI of the eMBB UE. Intuitively, the first method tries to cancel out the channel gain of the eMBB UE by compensating the phase shifts of the RIS elements via subtraction, while the second achieves it by relying on a conventional optimization method. The idea of IN using RIS is addressed in the recent literature [JY22], but it has not been applied before to support different service modes. To satisfy the URLLC low-latency requirement, our scheme relies on detecting the start of the URLLC traffic locally at a hybrid RIS, introducing minimum overhead and low computational complexity. Performance is analysed by evaluating the Spectral Efficiency (SE) of the eMBB UE and the outage probability and latency for the URLLC one.

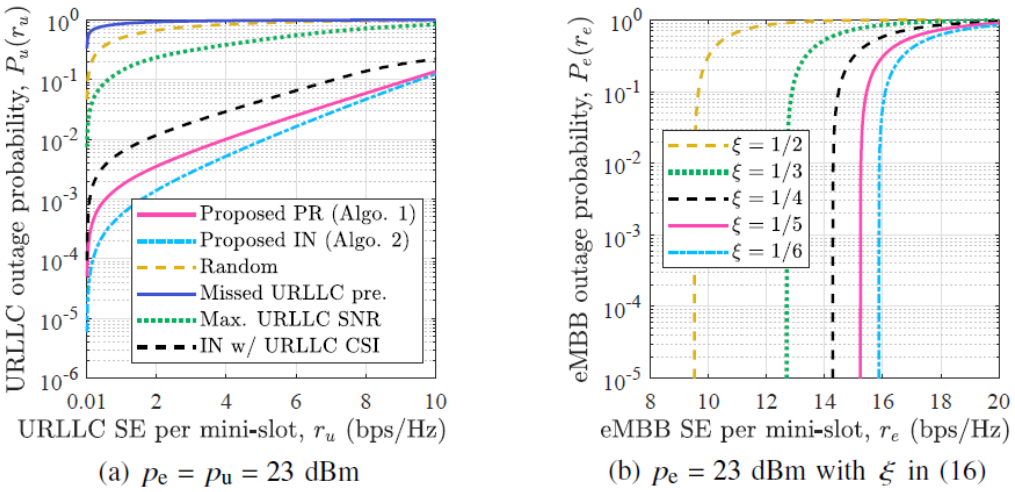


**Figure 4-21 Outage probabilities of URLLC UE (a) and eMBB UE (b). The RIS has $N = 100$ elements.**

***Results and outcomes***

Figure 4-21(a) presents the URLLC outage probability as a function of the spectral efficiency with eMBB and URLLC UEs using the same transmit power $p_e = p_u$. The performance of the configurations computed by the proposed PR and IN algorithms reveal that it is possible to improve the reliability of the URLLC transmission relying only on eMBB CSI. In fact, in the provided figure, the IN configuration improves the outage probability by up to 3 orders of magnitude compared to the random one. Comparing the PR and IN algorithms, IN presents outage probability up to 6 times lower. However, the PR algorithm yields a better trade-off due to its computationally simple implementation.

Figure 4-21(b) depicts the eMBB outage probability as a function of the spectral efficiency for different values of $\xi$ which is the fraction of the mini-slots punctured by URLLC (including the transmission of the URLLC preamble, payload, and RIS configuration switching) out of the total eMBB payload. Note that the outage probability improves as $\xi$ decreases, since the proportion of eMBB mini-slots free from URLLC traffic increases. Hence, given the sporadic behaviour of the URLLC traffic, high SE can be provided to the eMBB UE by optimizing the number of mini-slots in the payload transmission phase.

***Relation to other RISE-6G contributions***

The proposed technique can be generalized to provide a way of multiplexing the traffic of different users, where the CSI is available only for some of them. Since it follows a generic frame structure (including training, computation and payload phases) it can be implemented using control strategies and architectures introduced in D4.3. Similarly, for the training and CSI acquisition it can use the existing approaches, such as the ones presented in this deliverable.

### 4.4.7 RIS-empowered multi-user communications: Distributed sum-rate maximization of cellular communications with multiple RISs

***Motivation and context***

RISs are lately considered as a key enabling technology for future generation wireless communication networks, constituting a promising solution for realising smart radio propagation environments [RDP19]. The concept of RIS-enabled smart wireless environments necessitates the efficient orchestration of multiple RISs. However, the vast majority of the up-to-date optimization frameworks considers centralized approaches, which require large overhead (in terms of time and power consumption) of control information exchange usually in a central network orchestrator. In this contribution [KSI+22], [KDA22] , we instead investigate the impact of multiple distributed passive RISs, each one of them being controlled by a single-antenna BS that performs OFDM transmissions to its assigned single-antenna receiver, in the presence of *interfering neighbouring channels*. Referring to Figure 4-22, we consider the design of a multi-user RIS-empowered and OFDM-based wireless system comprising of $Q$ communicating pairs. We focus on the downlink direction and assume that each BS sends information to its associated UE using a common set of physical resources, e.g., time and bandwidth. The BS and the UE are both equipped with a single antenna, but the generalisation to the multiantenna case is straightforward. Also, we assume that each BS can control an RIS, which is placed closely to it to enhance the communication with its UE. The RISs are assumed to comprise $N$ passive reflecting elements, and are connected to a controller, which adjusts their pattern for desired signal reflection. We will refer to each BS-RIS-UE triplet as a "user".
In this context, the research question that we tackle is: How to derive a fully distributed algorithm for network resource optimization, where each BS can optimize its communication parameters (i.e., power allocation and RIS phase shifts) requiring only a limited exchange of information with other BSs?

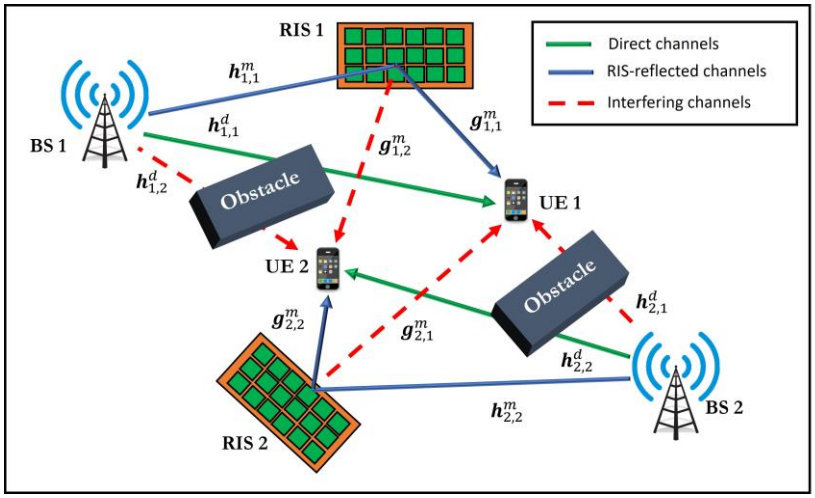


**Figure 4-22 Distributed scenario with RIS-aided interference channels, with Q=2 BS-RIS-UE triplets.**

***Methodology***

Differently from other studies, we consider that each RIS meta-atom element is dictated by a frequency selective profile, according to the Lorentzian frequency response, which is more accurate for the considered OFDM-based multi-carrier modulations, as recently presented in [KSI+22]. Based on the described system model, in [KDA22] we formulate a design optimization problem focusing on the overall sum-

rate's maximisation and having as free parameters the power allocation over the sub-carriers and the surfaces' reflection profiles. To solve the resulting problem, we develop a distributed optimisation framework and propose a Successive Concave Approximation (SCA) algorithm, which tackles the decoupling of the power allocation and the parameters of the Lorentzian responses.
Concretely, the achievable sum-rate performance objective under power and RIS reflectivity constraints is not jointly concave and, therefore, the problem has generally multiple local optima. The solution requires in general a centralised approach. Nevertheless, the solution the analysis of [KDA22] shows that the solution can be reached in a distributed fashion, by allowing a very limited exchange of control data among the users. For each user, a (strongly) concave surrogate is built for the objective function that can be computed thanks to limited exchange of information among users and can be easily optimised in an iterative fashion. To this aim, the original problem is rewritten as a summation of two (non-concave) terms, the first one expressing the user's achievable rate after all other participants have selected their parameters for the current iteration, while the second describes the sum-rate (accounting for interference) brought by the target user to the rest of the users. The first term is treated by a strongly convex surrogate function, while the second term is linearised, using the method of interference pricing vectors that quantify the amount of interference produced by the resource allocation of the user under investigation toward the other users. Considering interference prices into the overall optimisation help maximising the social sum-rate utility function thanks to cooperation among users, which avoid interfering too much with each other. Finally, the surrogate function is solved for the local power allocation and RIS phase shifts, accounting for the pricing vectors. The first sub-problem admits a multi-level water filling solution [PF05] and can be solved in closed form. For the Lorentzian-constrained RIS responses an iterative scheme based on the penalty dual decomposition method [SH20] is employed. Interestingly, the framework takes into consideration the exchange of interference prices, pursuing a fully non-cooperative approach, thus trading-off performance (in terms of sum-rate) with control information burden.

***Results and outcomes***

The considered approach has been evaluated in a system with Rayleigh channel fading, 16 OFDM sub-carriers and $Q = 2$ or $Q = 4$ BS-UE-RIS cells and 50 RIS elements. Its performance is given in Figure 4-23 having as baseline the case without RISs in any cell. It can be observed that, for all evaluated schemes, the total achievable sum-rates increase with transmit power, whereas in the high SNR regime (i.e., above 20 dBm), a saturation trend is present. This behaviour is expected by noting that the interference with the neighbouring users is inevitable. In addition, as illustrated, inserting one RIS for each user, even with a relatively small number of unit elements, leads to higher sum rate, confirming the benefits of the RIS technology.

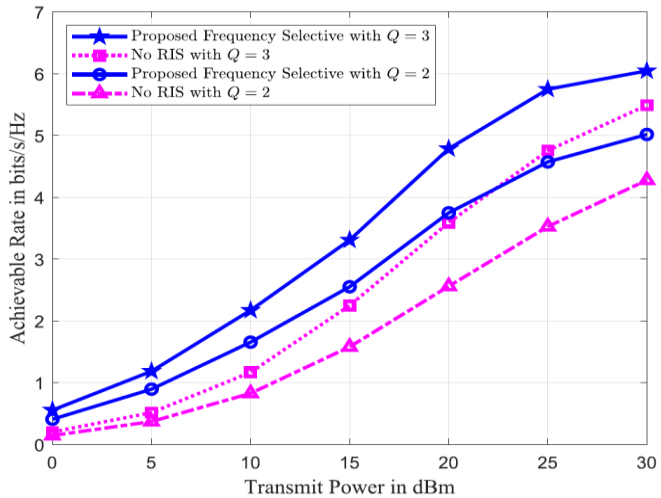


**Figure 4-23 Achievable sum-rate performance in bps/Hz as a function of the transmit power for each BS, for different number of users Q, with and without RISs.**

***Relation to other RISE-6G contributions***

This contribution is set on the decentralized deployment and control strategy, discussed in D4.3 and is designed to address the problem of information exchange between the nodes. The application scenario is related to the multi-cell and shared-RIS use-cases investigated under WP2. Since the optimization scheme of this approach depends on local CSI at each user, multi-user channel estimation techniques are assumed to be in use, such as those discussed in this deliverable, with special focus on the channel estimation using a simultaneously reflective and sensing RIS due to its lower overhead and the added benefit of estimating each individual link. The distributed algorithmic framework proposed in this contribution can be extended to tackle also other optimization problems involving RISs such as, e.g., RIS-empowered edge computing, distributed RIS-aided localization, and so on.

### 4.4.8 ARES: Autonomous RIS solution with Energy harvesting and Self-configuration towards 6G

***Motivation and context***

The necessity of a complex and fast control channel (CC) supporting real-time RIS configuration to adapt to the ever-changing channel conditions and the need for an extensive power distribution system supporting the energy requirements for operating the RIS hardware are two major challenges to be faced to pave the way for commercially viable RIS devices. In [ADS22], we first introduced the concept of self-configuring RIS to overcome the need for explicit CC availability. Starting from it, in [ADS23], we propose a novel RIS design named ARES: Autonomous RIS with EH and Self-configuration, which is capable of combining the self-configuring capabilities of HRISs with EH techniques.

ARES is the first fully autonomous RIS solution both from the control and the energy supply point of view. This facilitates the seamless installation of HRIS devices throughout the service area without requiring modification of the existing network infrastructure or power distribution system.

***Methodology***

In ARES we leverage the novel HRIS hardware architecture depicted in Figure 4-24. The HRIS consists of two branches: a reflection branch and an absorption branch. Each element of the RIS is equipped with a bank of directional couplers. These couplers re-route a fraction $\eta - 1$ of the impinging wave signal for reflection, while the remaining fraction $\eta$ is absorbed by the surface and routed through an RF circuit toward either a power detector or an energy harvesting module.

Both the reflection and absorption branches have tunable phase shift banks, which can be controlled independently. The phase shift bank at the reflection branch allows us to set the desired reflection beam pattern, while the phase shift bank in the absorption branch enable us to focus the absorption properties of the RIS toward intended directions.

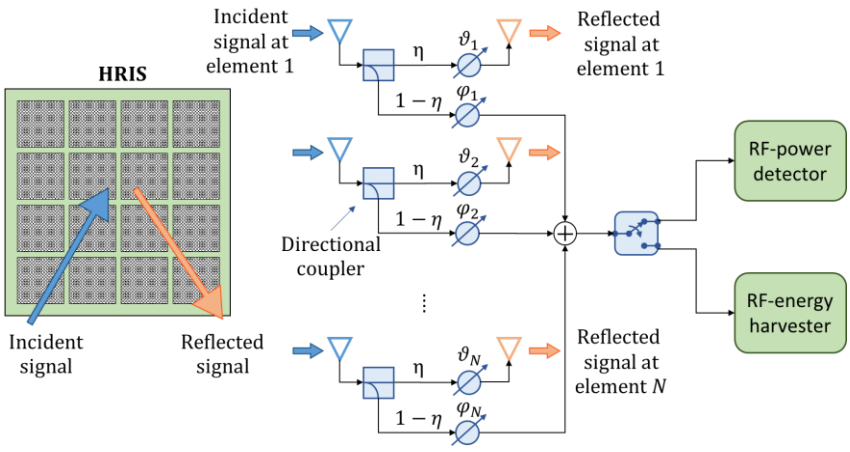


**Figure 4-24 Reference diagram of HRIS with EH capabilities.**

To acquire CSI, the RIS autonomously performs directional power sensing and constructs a power profile indicating the angle of arrival of the signals emitted by the communicating devices. With such information, we can retrieve the CSI of the RIS-BS and the RIS-UEs channels [ADS22]. In ARES, we exploit the so-obtained CSI both for communication and EH operation. Specifically, we optimize the configuration of the reflection branch to maximize the reflected path gain offered by the RIS, which supports communication between BS and UEs. Simultaneously, we optimize the phase shifters of the absorption branch to directionally focus the absorption properties of the RIS towards the sensed AoA directions, thus maximizing the harvested energy. The harvested energy is then collected in a rechargeable battery that powers the RIS hardware.

***Results and outcomes***

In this contribution, we show the performance of the charge/discharge process of the battery, modelled by means of an irreducible Markov Chain. This allows us to statistically evaluate the lifespan of the autonomous HRIS through the probability of falling to a low battery charge state corresponding to a minimum level Γ of energy available to operate the HRIS. When the level of energy stored in the battery falls below Γ, the battery is considered to be in a loss of charge (LoC) state. The probability of LoC as a function of the battery size is shown in Figure 4-25. From the results, the higher the battery size the lower the LoC probability.

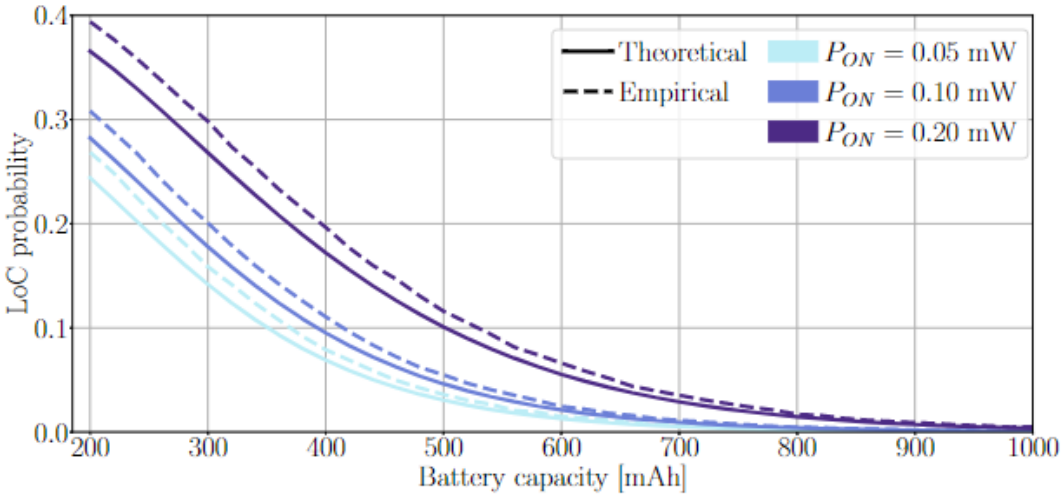


**Figure 4-25 Loss of charge probability against the battery capacity. N = 40 meta-atoms, Q = 2. The scenario includes K = 75 users with traffic ζ = 0.5.**

***Relation to other RISE-6G contributions***

The contribution shows the feasibility of fully autonomous HRIS with energy harvesting and self-configuration capabilities. Such devices do not require an explicit CC and the availability of a power supply at the deployment site to operate. This contribution enables agile and seamless RIS deployment, which is in line with the work package objective. Here, more focus is given on the algorithmic point of view of the contribution; the details on the EH results are given in D6.4, being one of the topics investigated in work package 6.

### 4.4.9 Localization-based OFDM framework for RIS-aided systems

***Motivation and context***

Efficient integration of RISs into the current wireless network standard is not a trivial task due to the overhead generated by performing CE. Indeed, in multi-user systems, RIS channel estimation procedures need pilot sequences whose length is proportional to the number of RIS elements and the number of UEs in the system.

Hence, the CE procedure may lead to an unfeasible overhead when serving a large number of users. Considering the relevance that integrated sensing and communication (ISAC) has gained to enable the connected intelligence promised by the 6G, it is natural to imagine the use of the localization information available in RIS-aided networks to help the scheduling decision: instead of wasting time for exchanging CE pilot sequences, the knowledge of the UEs position can be used to optimize the data transmission.

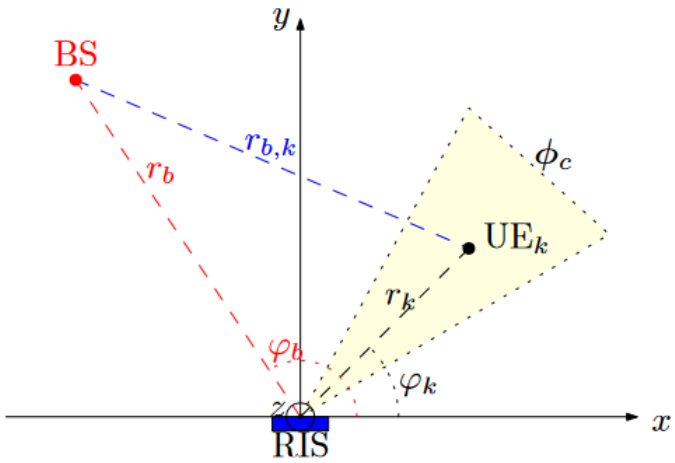


**Figure 4-26 Scenario under consideration [SKP23]**

***Methodology***

We consider an UL RIS-aided communication scenario shown in Figure 4-26, where a single-antenna BS, an RIS, and set of single-antenna UEs are present. The BS is assumed to have perfect knowledge of the UEs' position, and it uses this information to make scheduling decisions. Accordingly, an OFDM time-frequency is considered, where in every time slot a portion of OFDM symbols is reserved for data communication, while the others are reserved for localization waveform used to keep track of the user position. At the beginning of each time slot, the RIS loads a single configuration, which is kept for the whole time slot duration. The configurations are designed in order to cover the overall area of interest. UEs are multiplexed through orthogonal slot-RB allocation, as shown in the time-frequency example given in Figure 4-27. The resource allocation can then be made in a robust way considering the position information and the impact of the fading in the direct BS-UE channel. The interested reader can refer to [SKP23] to the details of implementation and design.

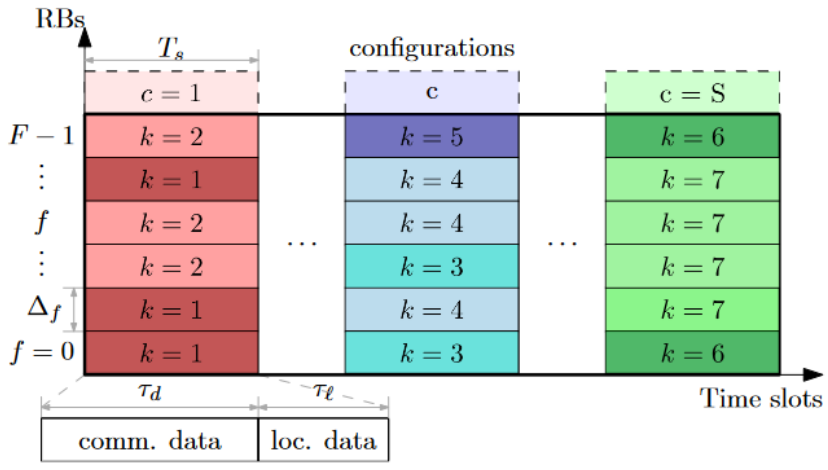


**Figure 4-27 Example of proposed OFDM data frame [SKP23]**

***Results and outcomes***

Numerical simulations are made to evaluate the proposed framework, considering a max-rate and a min-max resource allocation. A joint (jnt) and sequential (seq) time-frequency allocation schemes are presented. Moreover, the results are compared with a perfect CSI knowledge scenario (csi), where we account for the overhead needed for obtain the CSI information. Figure 4-28 shows the performance obtained by the max-rate allocation schemes, where (a) presents the goodput as a function of the number of users ($K$) when the Rician $\kappa$ factor is 9 dB, while (b) as a function of the Rician $\kappa$ factor when $K = 55$. Both localization-based paradigms outperform the CSI-based scheme. In particular, when the system is in an overloaded state, the CE overhead increases in a prohibitive manner. Figure 4-29 shows the performance of the min-max allocation, where (a) presents the Jain's fairness versus number of users $K$ when the Rician $\kappa$ factor is 9 dB, (b) shows the average goodput per user as a function of the Rician $\kappa$ factor when $K = 550$. In this case, the fairness performance of jnt and the csi are comparable, both outperforming seq for every number of users. Regarding the average goodput per user, the localization-based schemes outperform the CSI-based.

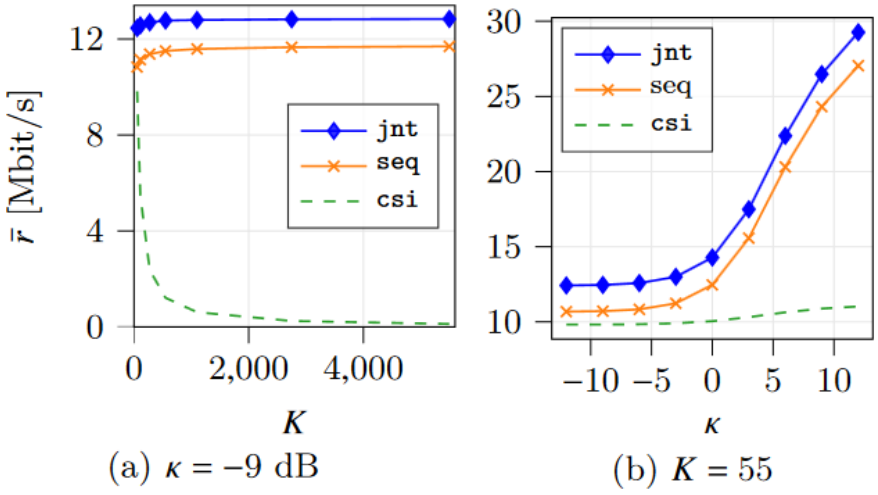


**Figure 4-28 Max-rate performance [SKP23]**

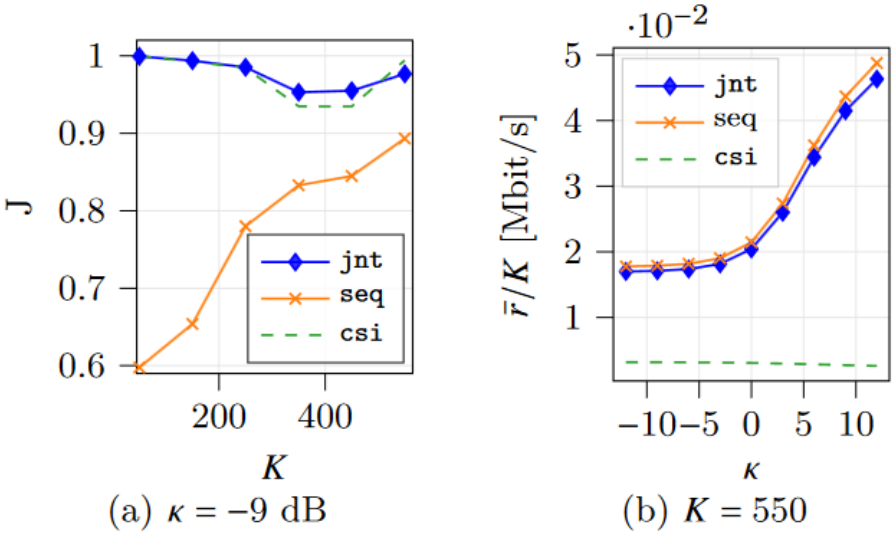


**Figure 4-29 Min-max performance [SKP23]**

***Relation to other RISE-6G contributions***

This contribution represents an attempt to bridge the development in localization estimation in WP5 with the multi-user RIS-aided transmission techniques developed in WP4, taking into account the possibility of using the standardized OFDM modulation of the 5G NR standard.

### 4.4.10 RIS-aided URLLC with imperfect device tracking

***Motivation and context***

The use of RIS technology to extend coverage and allow for better control of the wireless environment has been proposed in several use cases, including URLLC communications. However, the extremely challenging latency constraint makes explicit channel estimation difficult, so positioning information is often used to configure the RIS and illuminate the receiver device. This contribution analyses the effect of imperfections in the positioning information on the reliability, deriving an upper bound to the outage probability, which is in turn used to perform power control, efficiently finding the minimum power that respects the URLLC constraints under positioning uncertainty.

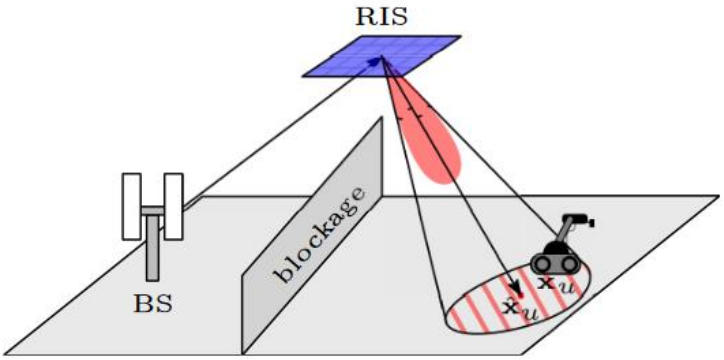


**Figure 4-30 Scenario of interest [SCK23a]**

***Methodology***

We consider an industrial DL URLLC communication scenario in which a single-antenna BS has to communicate to a single-antenna mobile UE, as shown in Figure 4-30. To ensure full coverage, a RIS is deployed on the ceiling of the factory. The BS performs tracking and it knows the mean value and the covariance matrix of the position of the UE, which uncertainty is a Gaussian distribution on the floor of the factory. Accordingly, the idea is to follow the UE movement pointing the beam of the RIS toward the direction $\hat{\theta}, \hat{\phi}$ (elevation, azimuth) corresponding to the mean value of the UE position. In order to fulfil URLLC requirement, robust power control is employed, according to the following steps:

1. The array factor (AF) gain provided by the RIS on the floor is approximated by concentric ellipses, as shown in Figure 4-31(a).
2. Binary search is performed to obtain the target reliable AF gain ($A_0$) among the possible ones, which involves the evaluation of the UE to be inside the ellipse (Gaussian integration on an ellipse), as shown in Figure 4-31(b).
3. Path loss is upper bounded by the farthest point on the ellipse on $A_0$.
4. Minimum power transmission is selected accounting for the inverse CDF of the fading.

The interested reader can refer to [SCK23a] for the details of the algorithm and the analysis.

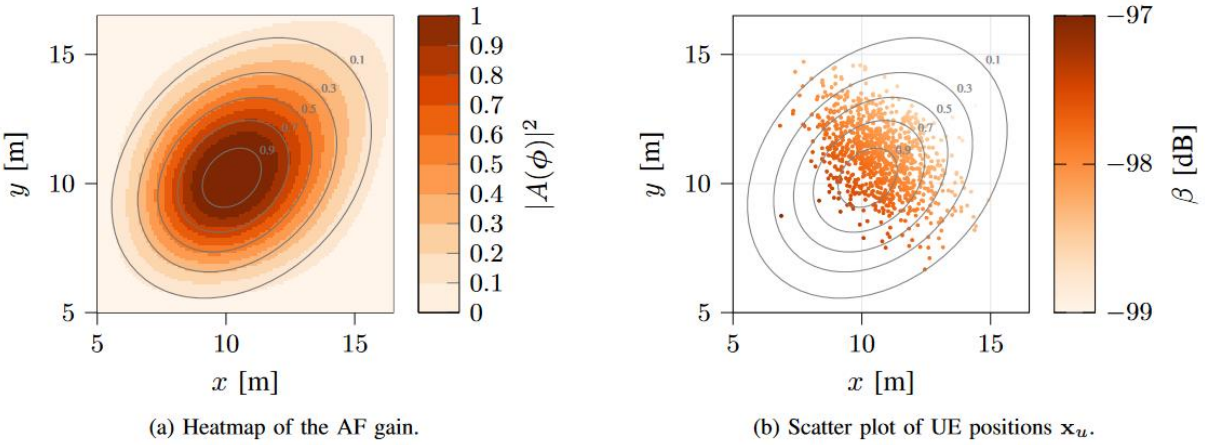


(a) Heatmap of the AF gain. (b) Scatter plot of UE positions $\mathbf{x}_u$.

**Figure 4-31 Region of influence of the AF for different $A_0$ using the ellipse approximation with $h = 25$ m, $\hat{\phi} = \pi/4$, $\hat{\theta} = \pi/6$ [SCK23a]**

***Results and outcomes***

The results are considered using different parametrization of the covariance matrix of the UE position through parameter Ψ, which represent three different behaviours when Ψ = 0, the uncertainty is a circularly symmetric Gaussian representing the error when the user is static; when Ψ = π/4 or −π/4, the major axis of the equiprobability ellipse is oriented toward Ψ, emulating the output error of common tracking filters when the UE is moving in direction Ψ. Figure 4-32 shows a heatmap of power consumption for the three values of Ψ: we can easily notice that power consumption is generally lower for Ψ = 0, and that the path loss is still the most important component: points farther away from the origin generally require a higher power. In the asymmetric error cases, the effect of the pointing is significant: if Ψ = π/4, the required power is minimal when $\hat{\phi}$ = Ψ, i.e., when the projected beam and the positioning error are aligned, and increases as the two ellipses rotate relative to each other. The opposite happens if Ψ = −π/4, as required power is maximal when the highest position error is orthogonal to the projected beam. In order to provide a meaningful comparison, we consider a fixed azimuth angle $\hat{\phi}$ = π/4 and consider performance as a function of $\hat{\theta} \in [0, 40°]$, in Figure 4-33. The results shows that the proposed solution slightly overestimates the required power, particularly in the cases with Ψ = ±π/4: the optimality gap is between 1.5 and 4.5 dB, as the upper bound to the outage probability is relatively tight, but still leaves some slack. Figure 4-33(b) confirms the conservative nature of the proposed solution: the outage probability, which should be close to 10−5, is between 25 and 60% lower.

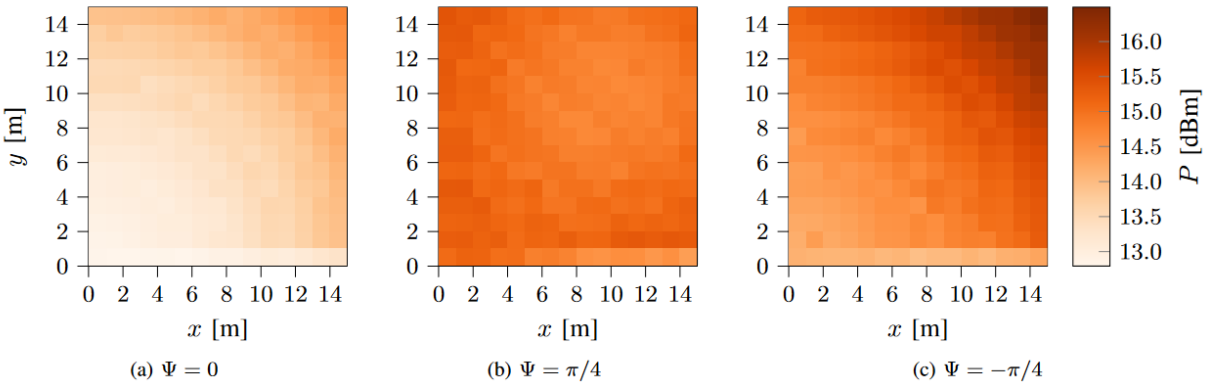


(a) $\Psi = 0$ (b) $\Psi = \pi/4$ (c) $\Psi = -\pi/4$

**Figure 4-32 Power consumption in the first quadrant of the area [SCK23a]**

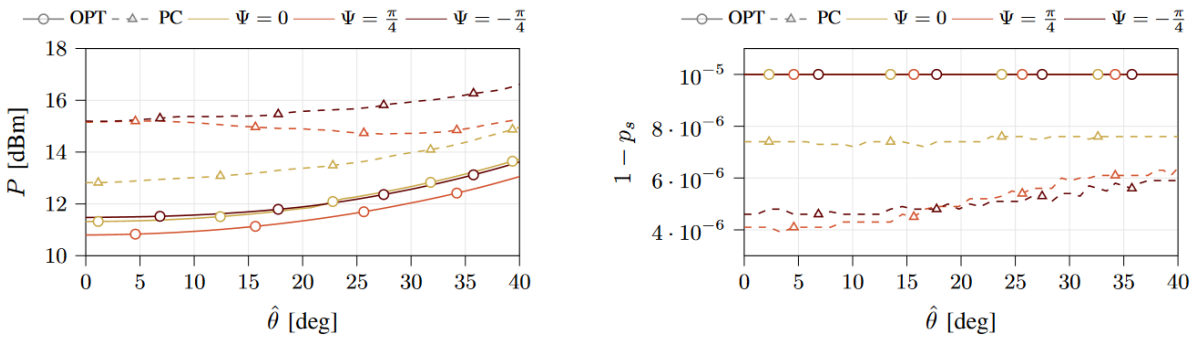


(a) Transmission power. (b) Outage probability.

**Figure 4-33 Performance as a function of $\hat{\theta}$ with $\hat{\phi} = \pi/4$ [SCK23a]**

***Relation to other RISE-6G contributions***

Similar to the contribution in Section 4.4.9, this work investigates how to exploit the localization capabilities of RIS-aided network studied in WP5 to provide communication performance. In particular, avoiding the CSI estimation, we are able to meet low-latency requirements, while using robust power control, communication reliability is assured.

### 4.4.11 Two-timescale design for RIS-aided massive MIMO systems with imperfect CSI

***Motivation and context***

[ZPR23] investigates the two-timescale transmission scheme RIS-aided massive MIMO systems, where the beamforming at the BS is adapted to the rapidly-changing instantaneous CSI, while the nearly-passive beamforming at the RIS is adapted to the slowly-changing statistical CSI. Specifically, we first consider a system model with spatially-independent Rician fading channels, which leads to tractable expressions and offers analytical insights on the power scaling laws and on the impact of various system parameters. Then, we analyse a more general system model with spatially-correlated Rician fading channels and consider the impact of Electromagnetic Interference (EMI) caused by other devices present in the considered environment. We consider the UL transmission of an RIS-aided massive MIMO system, where an RIS is deployed in the proximity of $\boldsymbol{K}$ users to assist their UL transmissions to the BS, as illustrated in Figure 4-34. For convenience, we denote the set of users as $\mathcal{K} = \{1, 2, \ldots, K\}$. The BS is equipped with $\boldsymbol{M}$ active antennas, the RIS comprises $\boldsymbol{N}$ nearly-passive reflecting elements, and the $\boldsymbol{K}$ users are equipped with a single transmit antenna.

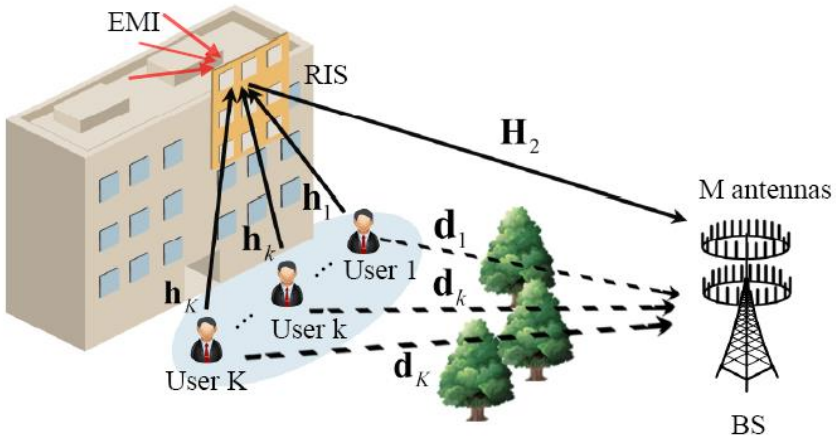


**Figure 4-34 An RIS-aided massive MIMO system**

***Methodology***

To begin with, we consider the spatial-independent Rician fading model. The aggregated channel is estimated by relying on the linear minimum mean square error (LMMSE) method and its performance in terms of MSE and NMSE is analysed. Under the assumption of maximal ratio combining (MRC) detectors, we derive closed-form expressions for the use-and-then-forget (UatF) bound of the achievable rate. The derived results hold for an arbitrary number of BS antennas and RIS elements. Then, we analyse the impact of important system parameters, the asymptotic behaviour of the rate, and the power scaling laws. We specialize our findings to the single-user case in order to obtain further engineering insights.

Next, we consider a more general system model that includes spatial correlation at the RIS and the EMI captured by the RIS. Also in this case, we compute the LMMSE channel estimates and formulate the UatF bound of the achievable rate in a closed-form expression. Our analysis shows that the presence of spatial correlation provides the RIS with an enhanced capability of customizing the wireless environment. On the other hand, the presence of severe EMI may result in different power scaling laws.

For both the spatially-independent and spatially-correlated channel models, we propose an accelerated gradient ascent-based algorithm to solve the minimum user rate maximization problem. We first apply a log-sum-exp approximation to obtain a smooth objective function. Then, we compute the gradient vectors with respect to the angle vectors. The performance loss in the projection is avoided since the objective function is periodic with the angles and the unit modulus constraint holds for all the angles. Besides, closed-form solutions are obtained in the special case of a single user.

***Results and outcomes***

Figure 4-35 compares the performance of the proposed method with two benchmark algorithms: the genetic algorithm (GA) and the gradient ascent method formulated in terms of the complex variables. In spatially-independent cases, it can be observed that the three algorithms provide almost the same performance. This is because the objective function possesses a simple and tractable form. Nevertheless, the proposed algorithm performs slightly better than the gradient ascent method applied to complex-valued variables. This is because the proposed method treats the angles as optimization variables and therefore avoids the performance loss due to the projection operation. In the presence of spatial correlation, the objective function of the optimization problem becomes more complex. In this case, the proposed method outperforms the other two methods especially when $\boldsymbol{N}$ is large (see [ZPR23]).

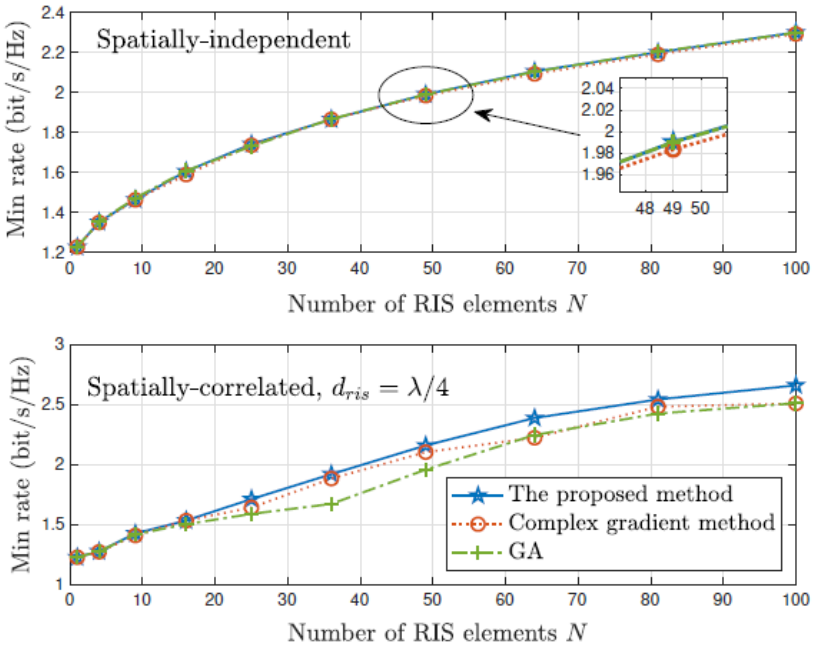


**Figure 4-35 Performance comparison between different optimization algorithms.**

***Relation to other RISE-6G contributions***

Numerical results show that, in the considered setup, the spatially independent model without EMI is sufficiently accurate when the inter-distance of the RIS elements is sufficiently large and the EMI is mild. In the presence of spatial correlation, we show that an RIS can better tailor the wireless environment. Furthermore, it is shown that deploying an RIS in a massive MIMO network brings significant gains when the RIS is deployed close to the cell-edge users.

### 4.4.12 RIS area illumination strategies

***Motivation and context***

Most algorithms developed for the optimization of RIS usually require knowledge of full CSI. However, the resulting acquisition overhead constitutes a major bottleneck for the realisation of RIS-assisted wireless systems in practice. In contrast, in this contribution [JAS22], focusing on downlink transmissions from a BS to a mobile UE that is located in a blockage region, we propose to optimize the RIS for illumination of the area centred around the UE. Hence, the proposed design requires the estimation of the UE's position and not the full CSI.

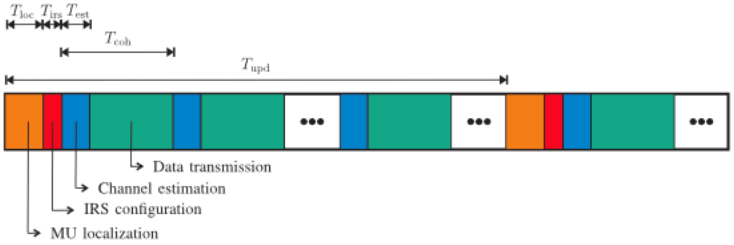


**Figure 4-36 Block diagram of the proposed RIS-assisted downlink transmission scheme, including the sub-blocks of UE localization, RIS phase-shift design, and pilot-assisted end-to-end channel estimation.**

***Methodology***

*Transmission scheme design*

The proposed RIS reconfiguration and channel estimation algorithm consist of the following three sub-blocks, which are illustrated in Figure 4-36:

- *Sub-Block 1 (UE Localization):* Since the RIS is deployed to have LoS connections to both the BS and the UE its location is assumed to be fixed. Since the BS is also a fixed node, their relative positions can be estimated once, and then, considered as known. However, the position of the UE varies due to its mobility which can be estimated using existing localization algorithms. Note that if the UE is in the far field of the RIS, it suffices for this localization sub-block to estimate the AoD from the RIS to the UE.
- *Sub-Block 2 (RIS Phase Shift Design):* We assume that the RIS phase-shift design is based only on the UE position or the required AoD in the case of far field. However, the RIS radiation pattern can be designed to be narrow or wide depending on the IRS configuration objective. This methodology assumes a system-defined parameter $\Delta$ (measured in meters) that specifies the width of the RIS radiation pattern and the illumination area. The exact approaches are discussed below.
- *Sub-Block 3 (End-to-End Channel Estimation):* Once the RIS is configured, the BS and the UE treat the surface as a part of the end-to-end wireless, which can be estimated using standard channel estimation techniques, alleviating the added complexity brought by the reconfiguration of the RIS. Note that this block is optional: The RIS phase shifts are already configured and remain fixed for multiple blocks (see the discussion below). Therefore, this channel estimation step is

design to aid the configuration of other system components, such as the BS and UE precoders/combiners, multi-user power and resource allocation strategies, etc. For simple systems (e.g., single-user or TDMA Single Input Single Output (SISO)), this step may be skipped – further reducing the overhead of this methodology.

We assume that the IRS is updated (using sub-blocks 1 and 2) once the current RIS illumination pattern cannot support the UE's QoS anymore. Thereby, we consider that the UE continuously calculates the average SNR (for which the fading is averaged out, and hence, it is determined by the LoS link), and once it falls below a certain threshold the UE sends a feedback message to the BS to initiate the UE localization and RIS phase shift update.

*RIS phase shift design*
The design of the RIS configuration can be configured in two modes:

*Beam focusing:* A beam steering (for far-field) or beam focusing (for near-field) configuration can be applied to construct a directive beam toward the position $\boldsymbol{p_r}$ of the user. Note that in the far-field regime, only the AoDs are required instead of the position. Concretely, the focusing phase shift of each point $\boldsymbol{p} = [\boldsymbol{0}, \boldsymbol{y}, \boldsymbol{z}]$ onto the RIS can be expressed as:

$$w_F(\boldsymbol{p}|\boldsymbol{p_r}) = -\boldsymbol{\kappa}\,\|\boldsymbol{p_r} - \boldsymbol{p}\| - \boldsymbol{\varphi}(\boldsymbol{p}),$$

where $\boldsymbol{\kappa}$ is the wavenumber and $\boldsymbol{\varphi}(\boldsymbol{p})$ denotes the phase of the incident wave onto point $\boldsymbol{p}$ of the RIS.

*Wide Illumination:* To illuminate the entire desired area, first the target region is partitioned into an we partition the IRS into sub-surfaces and split the targeted region into *N* sub-regions. Then, each element of the RIS applies wide-lobe beamforming toward that region. Assuming a square target area of L m2 and a widening parameter Δ, and denoting as $\boldsymbol{p_{ris}} = [x_i, y_i, z_i]$ the centre point of the RIS, we first define the (gradual) continuous mapping between each element of the RIS to the sub-region as

$$\mathcal{M}(\boldsymbol{p}) = \left[\frac{\boldsymbol{\Delta}}{\boldsymbol{L}}\boldsymbol{z} + x_i, \quad \frac{\boldsymbol{\Delta}}{\boldsymbol{L}}\boldsymbol{y} + y_i, \quad z_i\right],$$

and the beamforming pattern is expressed as

$$w_w(\boldsymbol{p}) = w_F(\boldsymbol{p}|\mathcal{M}(\boldsymbol{p})) - \boldsymbol{\kappa}\,\|\mathcal{M}(\boldsymbol{p}) - \boldsymbol{p_{ris}}\|,$$

where $\|\mathcal{M}(\boldsymbol{p}) - \boldsymbol{p_{ris}}\|$ is the reference distance from each sub-region to the RIS centre, whose contribution is removed from the directional beamforming expression. For a complete explanation of the mapping and the beamforming pattern, see [JAS22].

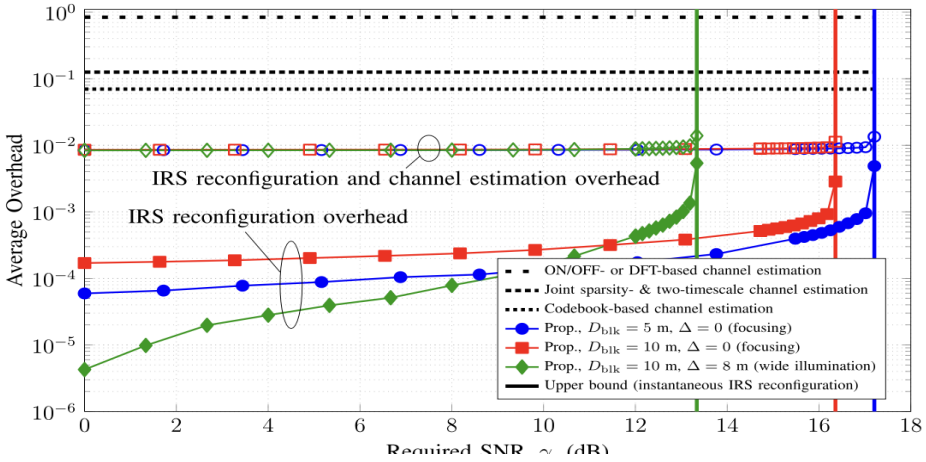


**Figure 4-37: Average overhead vs. the required SNR for the evaluation setup of the proposed area-illumination strategy.**

***Results and outcomes***

Figure 4-37 displays the overhead of only the RIS reconfiguration and the combined overhead of the RIS reconfiguration and channel estimation for the proposed methodology as a function of the required SNR for the system described in [JAS22]. The channel estimation overhead for the different benchmark schemes is included as a comparison [ZZ20], [HDH21], [WFD20], [JNS21]. The vertical lines represent the maximum SNR that is achievable for all points within the blockage area. Note that those values can be attained only via instantaneous IRS reconfiguration which relies on per-frame channel estimation approaches that introduce much greater overheads. Those result suggest that, unless the required SNR is extremely close the maximum achievable SNR (so that the estimation and configuration processes need to be repeated frequently), the RIS reconfiguration overhead is orders of magnitude less than the channel estimation overhead. In other words, at the cost of a negligible overhead, the proposed scheme can support SNRs which are quite close (e.g., within 1 dB) to the upper bound. Therefore, this contribution constitutes a low-overhead, practical solution for combatting blockage in systems with relatively low mobility and reasonable QoS requirements.

***Relation to other RISE-6G contributions***

This contribution considers a RIS configuration algorithm that operates at a lower granularity scale than those proposed for instantaneous RIS configuration in this deliverable. Its operation is based on the implementation of low-overhead user localization procedures, which are the topic of WP5. Once the RIS illumination patterns are configured, this strategy reduces the overhead of channel estimation methods. Note that different from the RIS-channel estimation procedures proposed in this deliverable and in D4.2, this strategy implies that the cascaded channel is estimated.

# 5 Design of Multi-User Techniques for RIS-Empowered Mobile Edge Computing

MEC is an enabler of several new services that require a fast, efficient, and reliable access to communication and computing resources, thanks to the deployment of the latter closer to the data source, at the edge of wireless networks. This convergence of communication and computing allows to continuously exchange and process data in real time, to enable, among several use cases, learning and inference in a timely and efficient manner, at the edge of wireless network, a concept also known as *edge intelligence*. Edge intelligence opens new challenges in service deployment and orchestration, as both communication and computing segments can highly affect the performance of learning and inference algorithms, including end-to-end energy and latency, but also learning and/or inference reliability (e.g., accuracy, confidence, etc.). In D4.2, different algorithms have been proposed to jointly orchestrate wireless and computing segments while dynamically reconfiguring RISs to increase wireless reliability and ensure a timely access to MEC resources ([DMC22], [AMD22], [BMD22], [MCK22]). The goal of this section is to extend previous results, by focusing on the typical –dimensional trade-off of edge intelligence, which entail energy, delay, and learning reliability, with the latter defined in several ways depending on the application. First, in Section 5.1.1, a model-based algorithm is proposed to enable energy-efficient edge inference with target delay and reliability constraints. Then, under the assumption that a full model of the system is not available a priori, Section 5.1.2 extends the study to a mixed model-based and data-driven optimisation, with deep reinforcement learning helping to overcome the limitations of the previous study.

## 5.1 Contributions from RISE-6G

The main contributions from RISE-6G in the design of RIS-Empowered MEC are listed below in Table 5-1. The table specifies the setting of the scenario and the KPI of the proposed algorithm. Moreover, the last column specifies where to find the contribution (deliverable and section numbers), considering that the contributions listed in D4.2 are not reported here if no updates were provided.

**Table 5-1: Contributions from RISE-6G on RIS-Empowered MEC**

| Title | Scope | Optimisation variables | # BS | # RIS | # UEs | Frequency band | Deliverable/ Section no. |
|---|---|---|---|---|---|---|---|
| Joint optimization and scheduling of communication and computation resources for RIS-empowered MEC | Minimise weighted energy of the system (UEs, AP, ES and RISs) under service delay constraints | Communication resources of UEs and BS, computation resources of the BS and phase shifts of RISs | 1 | multiple | multiple | any | D4.2/5.1.1 |
| RIS-empowered MEC over intermittent mmWave links | Minimise UEs' Tx power under service delay constraints | Uplink UEs' precoding matrices, RIS phase shifts and computation resources of the BS | 1 | 1 | multiple | mmWave | D4.2/5.1.2 |
| Adaptive federated Learning empowered by Reconfigurable Intelligent Surfaces | Minimise system energy under delay, accuracy, and reliability constraints | Uplink UEs communication resources, quantization bits, RISs phase shifts and computation resources of UEs and BS | 1 | multiple | multiple | any | D4.2/5.1.3 |
| Dynamic computation offloading over frequency-selective RIS-empowered communications | Minimise system power under delay and reliability constraints | UE' communication and computation resources and multi-carrier frequency selective RIS elements' responses | 1 | 1 | 1 | any | D4.2/5.1.4 |
| Model-based joint optimisation of RIS, wireless and computing resources for energy-efficient edge inference | Minimise devices energy consumption under delay and inference confidence constraints. | Devices transmit power, data compression, RIS phase shift, computing resources | 1 | 1 | multiple | any | D4.4/5.1.1 |

| | | | | | | | |
|---|---|---|---|---|---|---|---|
| Mixed model-based and data-driven joint optimization of RIS, wireless and computing resources for energy-efficient edge inference | Minimise devices energy consumption under delay and accuracy constraints | Devices transmit power, data compression, RIS phase shift, computing resources | 1 | 1 | multiple | any | D4.4/5.1.2 |

### 5.1.1 Model-based joint optimisation of RIS, wireless and computing resources for energy-efficient edge inference

***Motivation and context***

In the described context, when multiple users are served by a single RIS, the configuration of the latter determines the wireless communication perfomance and, indirectly, a trade-off between energy, latency, and reliability of learning and inference tasks run on data continuously collected and processed at the edge. In [MBD22], the authors propose an algorithm to dynamically and jointly optimise data encoding, wireless and computing resources, to minimise the energy consumption of multiple users, while guaranteeing per-user specific latency and inference reliability constraints. They show that a control of the inference confidence through a smart selection of data compression can help improving the trade-off between energy and delay. Indeed, compressing data for edge inference means reducing the communication overhead, but also potentially degrading the perfomance in terms of, e.g., accuracy. They focus on a neural network based classification of images collected by a set of end devices.

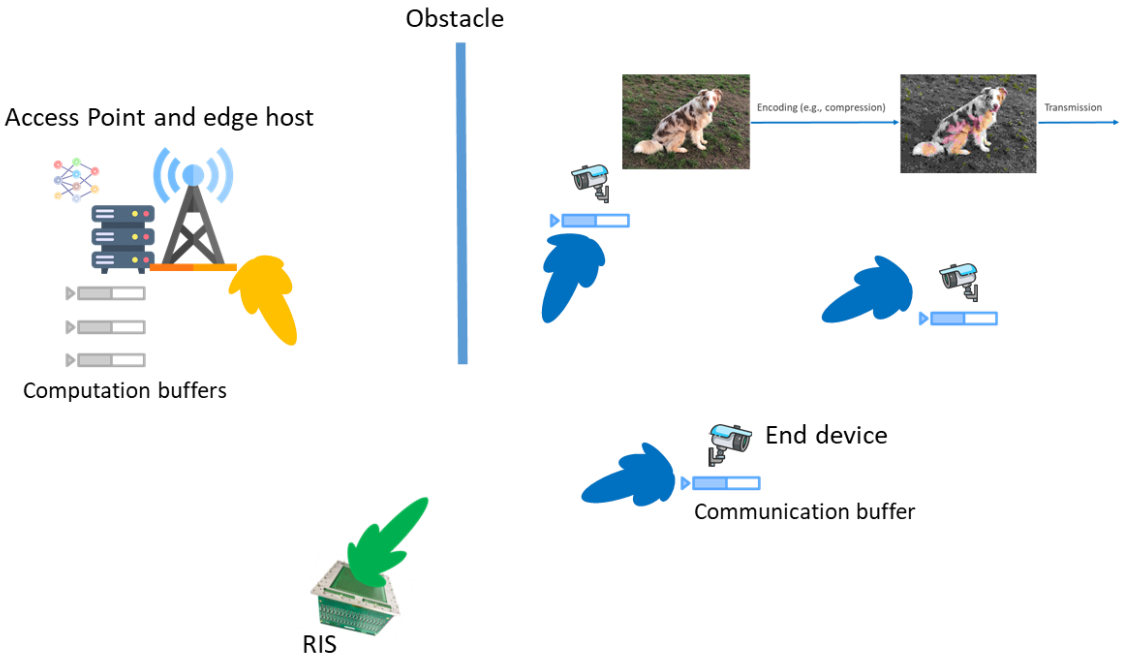


**Figure 5-1 Scenario for multi-user edge inference**

However, they only consider favorable propagation conditions (i.e., without blockages) that typically do not require the use of RISs. In this section, the work is extended to a MIMO mmwave communication scenario, in which the direct path between the users and the base station is blocked, so that the users need

to communicate through an RIS. The challenge is to dynamically reconfigure the RIS to serve the users with target performance that include end-to-end delay and inference confidence.
The scenario under investigation is composed of multiple users, an RIS, and an access point that gives access to a pool of computing resources (edge host), as in Figure 5-1. Each user generates images to be uploaded to the edge host for classification.

***Methodology***

Time is organised in slots, at the beginning of which a decision is taken to setup RIS configuration, scheduling of computing resources (i.e., amount of computing resources assigned to each user), data compression level (in this case, JPEG quality factor) and device transmit power to upload data. The goal is to minimise transmit energy of the devices under two long-term constraints: *i)* average end-to-end delay (comprising communication and computation), and ii) average inference confidence, measured by the entropy at the output of a neural network [MBD22], pre-trained and available at the edge host. More specifically, each device requires the entropy to be lower than a predefined threshold on average. To model the end-to-end system performance, we exploit the queueing model already presented in D4.2, with a buffer of data at each device waiting to be uploaded, and a buffer of data at the edge host, waiting to be processed. It is assumed that each device can transmit with a maximum transmit power, and the RIS configuration is selected from a pre-optimised codebook, and built from [CDS12]. At the same time, the edge host CPU is shared among the users through a dynamic CPU cycle frequency assignment. Obviously, the sum of CPU cycle frequencies assigned to all users cannot exceed the maximum computing power of the edge host. Stochastic Lyapunov optimisation [Nee10] is exploited to decouple the original long-term problem into a sequence of deterministic problems, to be solved at each slot, and requiring the knowledge of instantaneous context parameters such as the wireless channel states. More details of the proposed method can be found in [DMC22], [AMD22]. Here, the difference is that, at the same time, the data compression scheme is dynamically selected, and the RIS is optimised through the exploitation of the codebook.

***Results and outcomes***

To evaluate the performance of the proposed method, we consider a simple scenario with two users, with multiple antennas at each user and at the access point. More specifically, each user is equipped with a 4x4 planar array, the AP a 20x20 planar array, and the RIS is modelled as 10x10 planar array. The cartesian position of the users are (10,10) and (17,7), the AP is in position (0,10), and the RIS in position (10,0). In this way, both users are at the same distance from the RIS (10 m), with two different angles (0° and 45°), which is useful for our evaluation. Rician channels with Rice factor 10 and path loss exponent 3.5 are generated, each user is assumed to transmit toward the RIS, since the direct link with the access point is blocked, while the access point combiner is optimised to focus towards the RIS. The RIS codebook is capable of focusing in the range [-45°,45°], with a step of 5°. The total bandwidth is 2 GHz, equally shared among the two users, and a noise power spectral density of -174 dBm/Hz is considered. The maximum user transmit power is set to 20 dBm. From a computation perspective, the number of CPU cycles per classified pattern has been empirically evaluated to be, and the edge host CPU cycle frequency (to be shared among the users based on the optimisation) is assumed to be 3.6 GHz. The classification task runs over the CIFAR-10 dataset [Kri09].

As a first result, we evaluate the trade-off between total average energy consumption and average delay, for the two users requesting the service. In Figure 5-2a, this trade-off is shown for the two users requesting the same level of inference confidence, i.e., the highest possible confidence. In this case, the compression level is not dynamically optimised, and data are transmitted with the best quality factor, thus the highest communication overhead is incurred. The results are compared with a benchmark methos that randomly selects, from the RIS codebook, the two patterns that maximise the users' SNRs, respectively. In particular, with this benchmark selection, each user has 50% of chances of finding the RIS configured to best reflect its signal. At the same time, the resulting (moving) average entropy and classification accuracy (both averaged over a window of 1000 slots) are shown in Figure 5-2b and Figure 5-2c, respectively.

As we can notice, both cases reach the same values on average, however showing a different energy-delay trade-off (Figure 5-2a).

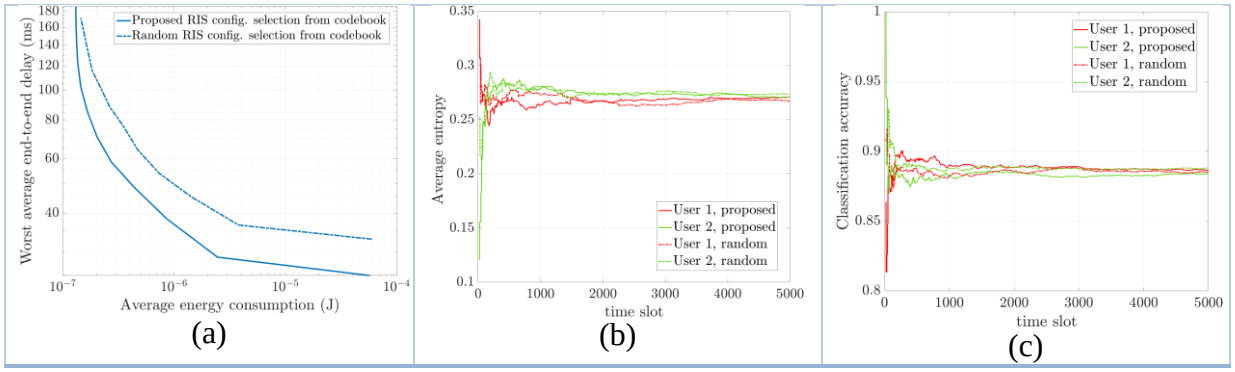


**Figure 5-2 (a) Trade-off energy-delay for two different strategies and different user requirements; (b) Per-user resulting average entropy; (c) Per-user resulting average classification accuracy**

However, the most interesting cases are represented by the scenarios in which different confidence levels are requested by the users. In Figure 5-3, we show the same results, in the case one user requests an average entropy below 0.35, while the other requests the average entropy to be below 0.7. in other words, the second user has a more relaxed constraint for its service. Results are again shown with the fully optimised system (i.e., smart RIS configuration selection) and the random selection benchmark. Besides the convergence of our algorithm to the desired solution in terms of inference confidence, it is worth noting how an optimised selection of the RIS configuration is beneficial to the energy-delay trade-off, showing thus the strong relation between lower layers and application performance. Indeed, although both users experience the same arrival rate and are at the same distance from the RIS, a selection from a codebook based on tha actual performance of the application (in this case, inference confidence) outperforms the benchmark strategy.

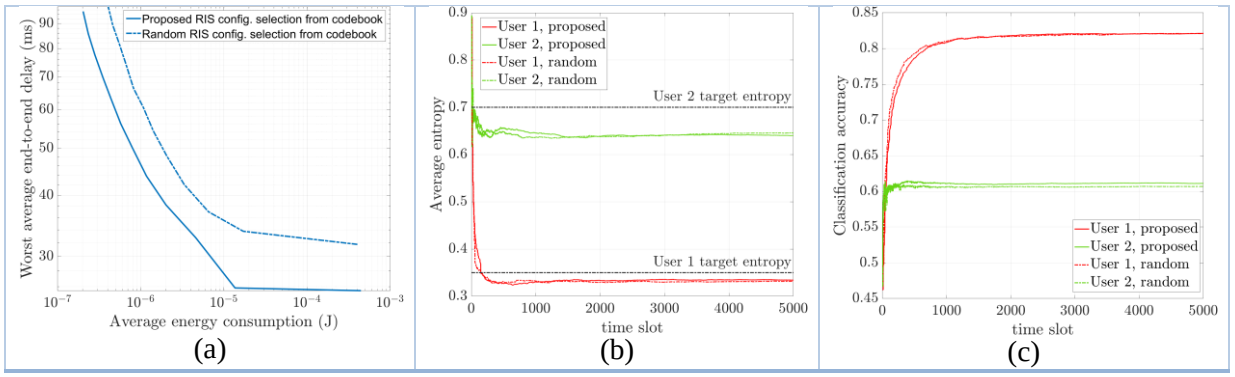


**Figure 5-3 (a) Trade-off energy-delay for two different strategies and different user requirements; (b) Per-user moving average entropy meeting the constraints; (c) Per-user moving average classification accuracy**

In this section, we presented an edge inference system optimised to reach target performance in terms of delay and inference confidence, while minimising end users' energy consumption. We solved a long-term problem via stochastic optimisation tools, showing through numerical results how a confidence-aware dynamic RIS configuration can help achieving a better energy-delay trade-off without impacting inference confidence and accuracy. The main limitation of the proposed method is the assumption of a full

system modelling, including the relation between data compression and inference performance. This limitation is mitigated in the next section, in which a mixed model-based and data-driven optimisation is proposed in a similar context.

### 5.1.2 Mixed model-based and data-driven joint optimisation of RIS, wireless and computing resources for energy-efficient edge inference

***Motivation and context***

As already mentioned in the previous section, model-based approaches are very powerful, as the hinge on the full description of the system that helps devising the best strategy under the considered constraints. However, modelling the full system is not always possible or, sometimes, the available model is too complex. In these cases, data-driven tools can help overcoming the limitations. One popular data-driven optimisation tool is Deep Reinforcement Learning (DRL), which allow multiple agents to learn a function linking environment states, actions, and rewards. This section briefly describes a Lyapunov-driven DRL method that solves a similar problem as the previous one. The technical details of the proposed solutions can be found in [SMD23]. The method mixes both model-based and data-driven approaches to benefit from their respective positive aspects and overcome their limitations.

***Methodology***

As in the previous section, a system with multiple users, an access point, an RIS, and an edge host is considered. The edge host runs the same classification task on images collected by the end devices (users) and transmitted to the access point through an uplink wireless communication. The goal is to minimise the devices' energy consumption under delay and inference accuracy constraints. Differently from the previous contribution, the fact of not having a model linking data compression and inference accuracy is overcome via the exploitation of a DRL algorithm that runs on top of the model-based Lyapunov optimisation method exploited previously. We consider an RIS whose elements' phases can be reconfigured between 0 and $2\pi$. From the DRL point of view, a Proximal Policy Evaluation (PPO) algorithm is used, as described in [SMD23] to optimise data compression and RIS reconfiguration. Then, once these variables are fixed, the remaining part is optimised through a typical (and low complexity) water-filling algorithm, as in [AMD22].

***Results and outcomes***

To illustrate the effectiveness our proposed methodology we conceive an edge inference scenario of image recognition, in the presence of an RIS, and an AP. A ResNet32 [HZR16] model is deployed on a mobile edge host (MEH) machine and trained to classify CIFAR-10 images, after being trained to approximately 92% accuracy (over the uncompressed images), offering a reasonable compromise between performance and E2E delay. For the shake of clarity of the results, we consider a single mobile user with no direct wireless link to the AP. The UE performs image compression on device using the JPEG protocol, so that compression values correspond to different compression qualities. In terms of inference reliability metric, we consider the average accuracy to provide interpretable thresholds and performance evaluations. While indeed, the accuracy of the network in unlabelled images cannot be known a priori, we have numerically quantified its average metric values for all possible JPEG compression levels of dataset's test set, to be used for performance evaluation. The rest of the parameter values are CPU cycles per classified pattern, Poisson arrivals with parameter 4, fmax = 3.6 GHz, maximum device transmit power 20 dBm, available bandwidth 100 MHz, required inference accuracy above 85%, Rice factor 25 dB, noise power −120 dB, operating frequency 5 GHz, UE-RIS attenuation: 62.60 dB, AP-RIS attenuation: 66.34 dB, maximum user movement displacement 5 m.

To assess the overall formulation, we numerically evaluate performance of the DRL's selections of RIS reflections and compression schemes. As baselines, we introduce the policies of always performing (i) maximum compression (which offers the minimum delay), (ii) no compression (offering maximum accuracy) and (iii) compression at a uniformly random level, while employing the rest of the optimization components and controlling the RIS reflections at random. We train a PPO instance with 5 layers of 32 neurons for its policy and value networks for 106 time steps, resetting the system at randomized episodes

of length 1500, using the final episode as evaluation. The training phases resulted in objective values orders of magnitudes lower than the baselines.

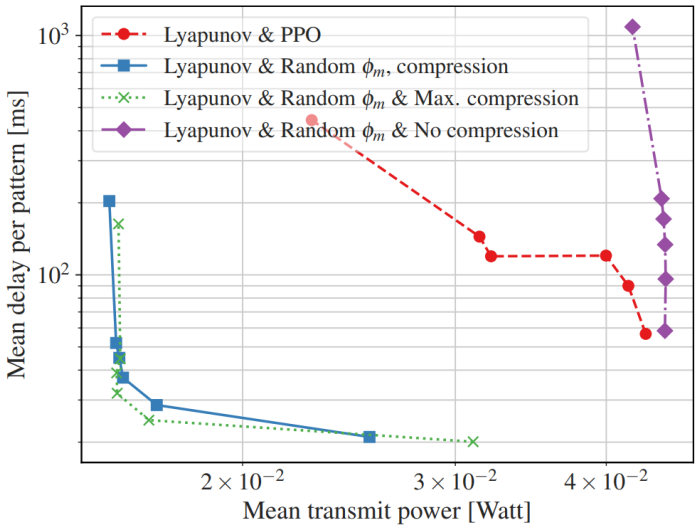


**Figure 5-4 Energy-delay-accuracy trade-off.**

The resulting accuracy offered by PPO ranges from 0.85 to 0.91 denoting that the DRL component always satisfies the desired constraint. The maximum and random compression schemes offer accuracy scores of 0.20 and 0.69, respectively. Figure 5-4 presents the achieved delay and mean transmit power offered by each method. Compared to the no compression approach, DRL can achieve up to 47% reduction in the average UE power consumption and up to 59% reduction in the maximum E2E delay. At the same time, it results from 45% to up to 2.5 times (in the most delay-sensitive cases) higher power consumption and 5 – 8 ms added delay in comparison to the full compression policy, but the latter falls extremely short of any practical accuracy constraints. Clearly, the system endowed with the Lyapunov-based techniques and DRL can automatically offer an excellent balance between performance (accuracy and E2E delay) and power consumption.

***Relation to other RISE-6G contributions***

This contribution builds on top of the Edge Inference proposed in the contribution of section 5.1.1 by setting an AI-enabled RIS controller which is designed to learn as the system evolves and is therefore more tailored to dynamic scenarios. Besides, the use of DRL as RIS and system controllers has been investigated under section 4.4.4 of D4.2, and the AI deployment strategy has been discussed in D4.3.

# 6 Conclusions and outlook

In the present deliverable, we reported major research advances and contributions for each of the four tasks of WP4 under examination. Specifically, going beyond the results already listed in D4.2, the main contributions and takeaways obtained by the RISE-6G consortium in D4.4 can be summarized as follows.

(1) In the context of RIS-aided multiple-access cellular networks, we have formalized the problem of jointly optimizing the BS and RIS active and passive beamforming, considering and end-to-end mutual coupling aware and electromagnetic-compliant channel model.

(2) In the context of controlling RISE wireless environments to improve the communication performance, we have illustrated how to shape the temporal channel statistics, such as the channel correlation.

(3) In the context of degree-of-freedom estimation and analytical approximation (in 2D) of channel strengths, based on the geometry in phase space of the set of rays connecting transmitter to receiver, we have provided an extended analysis that applies to a continuum limit of transmitter and receiver antennae.

(4) In the same context of point (3), we have extended our analysis to the case of complex and lossy metareflective environments, where ray density is variable in the set formed in the receiver phase plane by rays arriving from the transmitter, defining a local signal-to-noise ratio that is resolved in terms of angle of arrival as well as position.

(5) In the context of RIS reflectivity optimization for performance enhancement, we have proposed a model-free cross-entropy (CE) algorithm to optimize the binary RIS configuration for improving the signal-to-noise ratio (SNR) at the receiver.

(6) In the context of RIS optimization and signal demodulation, we have illustrated how the use of a Non-Coherent Demodulation Strategy of Differential Phase Shift Keying (DPSK) help reducing complexity and avoiding the typically required channel estimation procedure.

(7) In the context of capacity analysis of large-RIS-systems, we have provided a performance analysis of multi-RIS systems in terms of achievable capacity, as the number of BS and RIS elements becomes asymptotic.

(8) In the context of RIS-aided cellular networks, we have provided several alternating optimization methods for sum rate optimization considering a broadcast channel in the presence of RISs.

(9) In the context of optimal RIS placement and orientation, we have studied the extra degrees of freedom in the overall system performance brought by optimising the mechanical rotation of the surface in terms of the channel capacity.

(10) In the context of random access with RISs, we have proposed a RIS-assisted random access protocol with channel oracle that effectively coordinates transmissions to avoid collisions; when collisions occur, we illustrate an efficient approach for packet retransmission. The beam sweeping procedures exploited in this contribution are also used in the field trials of WP7.

(11) In the context of massive multiple access, we have designed a Next Generation Multiple Access protocol incorporating RISs, offering improved trade-off between system throughput and access fairness in practical scenarios of static users operating together with mobile ones.

(12) In the context of channel estimation in RIS-aided MISO system and multi-RIS-aided MISO systems, we have developed a generalized algorithm to solve a double linear transformation model with low complexity and high robustness. Interestingly, the proposed method has a broad applicability also to other contexts.

(13) In the context of RIS-aided mmWave channel estimation, we have designed novel tensor-based methodologies implementing a peak detection-message passing (PDMP) algorithm and a peak detection-average (PDAVE) algorithm that cope with double-path channels.

(14) In the context of RIS-aided channel estimation, we have illustrated the algorithmic formulation of the channel estimation procedure for uplink communication in a multi-user Hybrid RIS-empowered system.

(15) In the context of RIS-aided communications, we have proposed an UL multiplexing scheme to support the coexistence of eMBB and URLLC traffic, based on computing two RIS configurations to optimize the QoS of the eMBB UE and support the QoS of the URLLC UE.

(16) In the context of RIS-aided cellular communications, we have provided a distributed optimization framework for sum-rate maximization of a RISE system considering multiple passive RISs, each one of them being controlled by a BS that performs OFDM transmissions to its assigned receiver, in the presence of interfering neighbouring channels.

(17) In the context of autonomous RIS deployment, we have proposed a novel RIS design named ARES (Autonomous RIS with Energy Harvesting and Self-configuration), which can combine the self-configuring capabilities of Hybrid RISs with Energy Harvesting techniques.

(18) In the context of RISE communications, we have provided a localization-based OFDM framework, which exploits localization information available in RIS-aided networks to optimize data transmission and scheduling, while avoiding complex channel estimation procedures.

(19) In the context of RIS-aided URLLC, we have analysed the effect of imperfections in the positioning information (used to configure the RIS and illuminate the receiver device) on the reliability, deriving an upper bound to the outage probability, which is in turn used to perform power control under URLLC constraints.

(20) In the context of RISE communications, we have investigated a two-timescale transmission scheme for RIS-aided MIMO systems, where the beamforming at the BS is adapted to the rapidly changing instantaneous CSI, while the nearly passive beamforming at the RIS is adapted to the slowly-changing statistical CSI.

(21) In the context of RISE communications, we have developed a method for RIS optimization that does not require knowledge of full CSI, but rather only estimation of the UE's position, which is then used to optimize the RIS illumination toward the area centred around the UE.

(22) In the context of dynamic edge inference empowered by RISs, we propose a model-based algorithm to optimise data encoding, communication parameters (including RISs configuration), and computing resources, to minimise the energy consumption of multiple users, while guaranteeing per-user latency and inference reliability constraints.

(23) In the context of dynamic edge inference empowered by RISs, we have proposed a Lyapunov driven deep reinforcement learning method that learns over time communication and computation parameters, jointly with RISs configurations, with the aim of performing energy-efficient inference at the wireless network edge.

In conclusion, considering the large amount and variety of obtained results in all tasks of WP4, we believe that the planned objectives for deliverable D4.4 are all achieved.

## References

[3GPPr16] Study on channel model for frequencies from 0.5 to 100 GHz (Release 16). Technical Report 38.901, 3GPP, France, 2019.

[AAS21] I. Alamzadeh, G. C. Alexandropoulos, N. Shlezinger, and M. F. Imani, "A reconfigurable intelligent surface with integrated sensing capability," Nature Scientific Reports, vol. 11, no. 20737, pp. 1–10, Oct. 2021.

[ADD21] A. Abrardo, D. Dardari, M. Di Renzo and X. Qian, "MIMO Interference Channels Assisted by Reconfigurable Intelligent Surfaces: Mutual Coupling Aware Sum-Rate Optimization Based on a Mutual Imped-ance Channel Model," in IEEE Wireless Communications Letters, vol. 10, no. 12, pp. 2624-2628, Dec. 2021, doi: 10.1109/LWC.2021.3109017.

[ADS22] A. Albanese, F. Devoti, V. Sciancalepore, M. Di Renzo, and X. Costa-Ṕerez, "MARISA: A Self-configuring Metasurfaces Absorption and Reflection Solution Towards 6G," in IEEE INFOCOM 2022 - IEEE Conference on Computer Communications, 2022.

[ADS23] A. Albanese, F. Devoti, V. Sciancalepore, M. Di Renzo, A. Banchs, and X. Costa-Pérez, "ARES: Autonomous RIS solution with Energy harvesting and Self-configuration towards 6G." IEEE Transactions on Mobile Computing, under revision, 2023, [online] https://arxiv.org/abs/2303.01161.

[AES22] Albanese, A., Encinas-Lago, G., Sciancalepore, V., Costa-Pérez, X., Phan-Huy, D.-T., & Ros, S., "RIS-Aware Indoor Network Planning: The Rennes Railway Station Case," in Proceedings of the IEEE International Conference on Communications (ICC) 2022.

[AJH20] S. Alfattani, W. Jaafar, Y. Hmamouche, H. Yanikomeroglu, A. Yongac ̧oglu, N. D. Đ`ao, and P. Zhu, "Aerial platforms with reconfigurable smart surfaces for 5G and beyond," IEEE Communications Magazine, no. January, pp. 96–102, 2020.

[AJS22] Alexandropoulos, G. C., Jamali, V., Schober, R., & Poor, H. V. (2022, June). Near-field hierarchical beam management for RIS-enabled millimetre wave multi-antenna systems. In *2022 IEEE 12th Sensor Array and Multichannel Signal Processing Workshop (SAM)* (pp. 460-464).

[AMD22] F. Ezzahra Airod, M. Merluzzi, P. Di Lorenzo, and E. Calvanese Strinati, Reconfigurable Intelligent Surface Aided Mobile Edge Computing over Intermittent mmWave Links, in Proceedings of the IEEE International Workshop on Signal Processing Advances in Wireless Communication (SPAWC), 2022.

[APV21] N. Awarkeh, D. -T. Phan-Huy and R. Visoz, "Electro-Magnetic Field (EMF) a-ware beamforming assisted by Reconfigurable Intelligent Surfaces," 2021 IEEE 22nd Interna-tional Workshop on Signal Processing Advances in Wireless Com-munications (SPAWC), 2021, pp. 541-545.

[APV221] N. Awarkeh, D.-T. Phan-Huy, R. Visoz, M. di Renzo "A Novel RIS-Aided EMF-Aware Beamforming Using Directional Spreading, Truncation and Boosting," accepted to EuCNC 2022.

[APV222] N. Awarkeh, D.-T. Phan-Huy, M. di Renzo "A Novel RIS-Aided EMF Exposure Aware Approach Using an Angularly Equalized Virtual Propagation Channel," accepted to EuCNC 2022.

[ASA21] G. C. Alexandropoulos, N. Shlezinger, I. Alamzadeh, M. F. Imani, H. Zhang, and Y. C. Eldar, "Hybrid reconfigurable intelligent metasurfaces: Enabling simultaneous tunable reflections and sensing for 6G wireless communications," IEEE Communications Magazine, under revision, 2021, [online] https://arxiv.org/abs/2104.04690.

[ASC21] A. Albanese, V. Sciancalepore, and X. Costa-Perez, "SARDO: An Automated Search-and-Rescue Drone-based Solution for Victims Localisation," IEEE Transactions on Mo-bile Computing, pp. 1–12, 2021.

[ASH22] G. C. Alexandropoulos, K. Stylianopoulos, C. Huang, C. Yuen, M. Bennis, and M. Debbah, "Pervasive machine learning for smart radio environments enabled by reconfigurable intelligent surfaces," IEEE Proceedings, 2022.

[AV20] G. C. Alexandropoulos and E. Vlachos, "A hardware architecture for reconfigurable intelligent surfaces with minimal active elements for explicit channel estimation," in Proc. IEEE International Conference on Acoustics, Speech, and Signal Processing, Barcelona, Spain, 4–8 May 2020, pp. 9175–9179.

[AXW22] An, J., Xu, C., Wu, Q., Ng, D. W. K., Di Renzo, M., Yuen, C., & Hanzo, L. Codebook-Based Solutions for Reconfigurable Intelligent Surfaces and Their Open Challenges. *IEEE Wireless Communications*, 2022.

[BMD22] C. Battiloro, M. Merluzzi, P. Di Lorenzo, and S. Barbarossa, Dynamic Resource Optimization for Adaptive Federated Learning empowered by Reconfigurable Intelligent Surfaces, proc. of IEEE ICASSP, Singapore, June 2022.

[BS20] E. Björnson and L. Sanguinetti, "Rayleigh fading modeling and channel hardening for reconfigurable intelligent surfaces," IEEE Wireless Communications Letters, vol. 10, no. 4, pp. 830–834, Dec. 2020.

[BSD14] S. Barbarossa, S. Sardellitti, and P. Di Lorenzo, "Communicating while computing: Distributed mobile cloud computing over 5G heterogeneous networks," IEEE Signal Proc. Mag., vol. 31, no. 6, pp. 45–55, 2014.

[CAG22a] K. Chen-Hu, G. C. Alexandropoulos, and A. García Armada, "Non-coherent modulation with random phase configurations in RIS-empowered cellular MIMO systems,"

*ITU Journal on Future and Evolving Technologies*, vol. 3, no. 2, pp. 1–14, September 2022.

[CAG22b] K. Chen-Hu, G. C. Alexandropoulos, and A. García Armada, "Non-Coherent MIMO-OFDM uplink empowered by the spatial Diversity in reflecting surfaces," in *Proc. IEEE Wireless Communications and Networking Conference*, Austin, USA, 10–13 April 2022, pp. 1–6.

[CBG23] Creagh, S.C., Blakaj V. and Gradoni, G., 2023. Communication in phase space. To be submitted to IEEE Journal on Selected Areas in Communications.

[CDS12] A. Clemente, L. Dussopt, R. Sauleau, P. Potier and P. Pouliguen," Focal Distance Reduction of Transmit-Array Antennas Using Multiple Feeds," in IEEE Antennas and Wireless Propagation Letters, vol. 11, pp. 1311-1314, 2012, doi: 10.1109/LAWP.2012.2227105.

[CDS23] Croisfelt, V., Devoti, F., Saggese, F., Sciancalepore, V., Costa-Pérez, X. and Popovski, P., 2023. "An Orchestration Framework for Open System Models of Reconfigurable Intelligent Surfaces." *arXiv preprint arXiv:2304.10858*.

[CG23a] Creagh, S.C. and Gradoni, G., 2023. Slepian Eigenvalues for Near-Field Communication. To be submitted to Annals of Physics.

[CG23b] Creagh, S.C. and Gradoni, G., 2023. Slepian eigenvalues as tunnelling rates. Annals of Physics, 449, p.169204.

[CMG23] Creagh, S.C., Miller, D. and Gradoni, G., 2023. Electromagnetic Information Theory in Phase Space: A Quantum Tunnelling Approach, IEEE VTC 2023 Spring, Florence, 20-23 June 2023.

[CSL22] V. Croisfelt, F. Saggese, I. Leyva-Mayorga, R. Kotaba, G. Gradoni and P. Popovski, "A Random Access Protocol for RIS-Aided Wireless Communications," *2022 IEEE 23rd International Workshop on Signal Processing Advances in Wireless Communication (SPAWC)*, Oulu, Finland, 2022, pp. 1-5, doi: 10.1109/SPAWC51304.2022.9833984.

[CSL23] Croisfelt, V., Saggese, F., Leyva-Mayorga, I., Kotaba, R., Gradoni, G., & Popovski, P. "Random Access Protocol with Channel Oracle Enabled by a Reconfigurable Intelligent Surface." in *IEEE Transactions on Wireless Communications*, 2023 doi: 10.1109/TWC.2023.3268765. *arXiv preprint arXiv:2210.04230*.

[CYH22] X. Cao, B. Yang, C. Huang, G. C. Alexandropoulos, C. Yuen, Z. Han, and H. V. Poor, "Massive access of static and mobile users via reconfigurable intelligent surfaces: Protocol design and performance analysis," *IEEE Journal on Selected Areas in Communications*, vol. 40, no. 4, pp. 1253–1269, Apr. 2022.

[CYZ23] Tianrui Chen, Minglei You, Yangyishi Zhang, Gan Zheng, Jean Baptiste Gros, Geoffroy Lerosey, Youssef Nasser, Fraser Burton, and Gabriele Gradoni, "Model-free Optimization and Experimental Validation of RIS-assisted Wireless Communications under Rich Multipath Fading", IEEE Wireless Communications Letters, under review.

[DKM05] P.-T. De Boer, D. P. Kroese, S. Mannor, and R. Y. Rubinstein, "A tutorial on the cross-entropy method," Annals of Operations Research, vol. 134, no. 1, pp. 19–67, Feb. 2005.

[DMC22] P. Di Lorenzo, M. Merluzzi, E. C. Strinati, and S. Barbarossa, "Dynamic edge computing empowered by reconfigurable intelligent surfaces," EURASIP Journal on Wireless Communications and Networking, vol. 2022, no. 1, Dec. 2022.

[DMS22] F. Devoti, P. Mursia, V. Sciancalepore and X. Costa-Pérez, "Taming Aerial Communication with Flight-assisted Smart Surfaces in 6G Era", in IEEE Vehicular Technology Magazine (to appear), 2023.

[GD21] G. Gradoni, and M. Di Renzo, End-to-End Mutual Coupling Aware Communication Model for Reconfigurable Intelligent Surfaces: An Electromagnetic-Compliant Approach Based on Mutual Impedances. IEEE Wireless Communications Letters, 2021

[GRT21] R. Gupta, D. Reebadiya, S. Tanwar, "6G-enabled Edge Intelligence for Ultra -Reliable Low Latency Applications: Vision and Mission," Computer Standards & Interfaces, vol. 77, pp. 103521, 2021.

[HDH21] C. Hu, L. Dai, S. Han, and X. Wang, "Two-timescale channel estimation for reconfigurable intelligent surface aided wireless communications," *IEEE Trans. Commun.*, vol. 69, no. 11, pp. 7736–7747, Nov. 2021.

[HHA20] C. Huang, S. Hu, G. C. Alexandropoulos, A. Zappone, C. Yuen, R. Zhang, M. Di Renzo, and M. Debbah, "Holographic MIMO surfaces for 6G wireless networks: Opportunities, challenges, and trends," IEEE Wirel. Commun., vol. 27, no. 5, pp. 118–125, Oct. 2020.

[HJU09] R. Hunger, M. Joham, and W. Utschick, "On the MSE-duality of the broadcast channel and the multiple access channel," IEEE Trans. Signal Process., vol. 57, no. 2, pp. 698–713, Feb. 2009.

[HYS20] H. Lu, Y. Zeng, S. Jin and R. Zhang, "Aerial Intelligent Reflecting Surface: Joint Placement and Passive Beamforming Design With 3D Beam Flattening," in IEEE Transactions on Wireless Communications, vol. 20, no. 7, pp. 4128-4143, July 2021

[HZA19] C. Huang, A. Zappone, G. C. Alexandropoulos, M. Debbah and C. Yuen, "Reconfigurable Intelligent Surfaces for Energy Efficiency in Wireless Communication," in IEEE Transactions on Wireless Communications, vol. 18, no. 8, pp. 4157-4170, Aug. 2019, doi: 10.1109/TWC.2019.2922609.

[HZR16] K. He, X. Zhang, S. Ren, J. Sun, "Deep Residual Learning for Image Recognition," in Conference on Computer Vision and Pattern Recognition (CVPR), Jun. 2016.

[ICS23] Inacio de Souza, J. H.; Croisfelt, V.; Saggese, F.; Abrão, T.; Popovski, P. "Randomized control of wireless temporal coherence via reconfigurable intelligent surface," 2023 *IEEE International Conference on Communications Workshops (ICC Workshops), Rome, Italy. (arXiv preprint arXiv:2302.00074)*

[JAB22] M. Jian, G. C. Alexandropoulos, E. Basar, C. Huang, R. Liu, Y. Liu, and C. Yuen, "Reconfigurable intelligent surfaces for wireless communications: Overview of hardware designs, channel models, and estimation techniques," TUP and ITU Intelligent and Converged Networks, vol. 3, no.1, pp. 1-32, March 2022.

[JAS22] V. Jamali, G. C. Alexandropoulos, R. Schober, and H. V. Poor, "Low-to-zero-overhead IRS reconfiguration: Decoupling illumination and channel estimation," *IEEE Communications Letters*, vol. 26, no. 4, pp. 932–936, Apr. 2022

[JNS21] V. Jamali, M. Najafi, R. Schober, and H. V. Poor, "Power efficiency, overhead, and complexity tradeoff of IRS codebook design—Quadratic phase-shift profile," *IEEE Commun. Lett.*, vol. 25, no. 6, pp. 2048–2052, Jun. 2021.

[JY22] T. Jiang and W. Yu, "Interference nulling using reconfigurable intelligent surface," IEEE J. on Sel. Areas in Commun., vol. 40, no. 5, pp. 1392–1406, May 2022.

[KDA22] K. Katsanos, P. Di Lorenzo, and G. Alexandropoulos, Distributed Sum-Rate Maximization of Cellular Communications with Multiple Reconfigurable Intelligent Surfaces, proc. of IEEE SPAWC, 2022.

[Kri09] A. Krizhevsky, "Learning multiple layers of features from tiny images," pp. 32–33, 2009. [Online]. Available: https://www.cs.toronto.edu/~kriz/learning-features-2009-TR.pdf

[KSI+22] K. D. Katsanos et al., "Wideband multi-user MIMO communications with frequency selective RISs: Element response modeling and sumrate maximization," in Proc. IEEE ICC, Seoul, South Korea, May 2022.

[MAD23] A. L. Moustakas, G. C. Alexandropoulos, and M. Debbah, "Reconfigurable intelligent surfaces and capacity optimization: A large system analysis," *IEEE Transactions on Wireless Communications*, to appear, 2023.

[MAM22] F. Maresca, A. Albanese, P. Mursia, V. Sciancalepore, and X. Costa-Pérez, "A Frequency-Agnostic RIS-based solution to control the Smart Radio Propagation Environment," accepted for publication in 23rd IEEE International Workshop on Signal Processing Advances in Wireless Communications (SPAWC), 2022.

[MCK22] M. Merluzzi, F. Costanzo, K.D. Katsanos, G. C. Alexandropoulos, P. Di Lorenzo, Power Minimizing MEC Offloading with QoS Constraints over RIS-Empowered Communications, in Proceedings of the IEEE Global Communications Conference (GLOBECOM), 2022.

[MDB21] Mattia Merluzzi, Paolo Di Lorenzo, and Sergio Barbarossa, "Wireless edge machine learning: Resource allocation and trade-offs," IEEE Access, vol. 9, pp. 45377–45398, 2021.

[MBD22] M. Merluzzi, C. Battiloro, P. Di Lorenzo and E. C. Strinati, "Energy-Efficient Classification at the Wireless Edge with Reliability Guarantees," 2022 IEEE International Conference on Communications Workshops (ICC Workshops), Seoul, Korea, Republic of, 2022, pp. 109-114, doi: 10.1109/ICCWorkshops53468.2022.9814659.

[MFC21] E. Moro, I. Filippini, A. Capone and D. De Donno, "Planning Mm-Wave Access Networks With Reconfigurable Intelligent Surfaces," 2021 IEEE 32nd Annual International Symposium on Personal, Indoor and Mobile Radio Communications (PIMRC), 2021, pp. 1401-1407.

[MLY23] L. Mo, X. Lu, J. Yuan, C. Zhang, Z. Wang and P. Popovski, "Generalized Unitary Approximate Message Passing for Double Linear Transformation Model," in IEEE Transactions on Signal Processing, vol. 71, pp. 1524-1538, 2023, doi: 10.1109/TSP.2023.3269151.

[MPS23] P. Mursia, S. Phang, V. Sciancalepore, G. Gradoni and M. D. Renzo, "SARIS: Scattering Aware Reconfigurable Intelligent Surface Model and Optimization for Complex Propagation Channels," in *IEEE Wireless Communications Letters*, doi: 10.1109/LWC.2023.3299304.

[MSB18] M. Mozaffari, W. Saad, M. Bennis, Y. H. Nam, and M. Debbah, "A tutorial on UAVs for wireless networks: Applications, challenges, and open problems," IEEE Communications Surveys and Tutorials, vol. 21, no. 3, pp. 2334–2360, 2018.

[MSG21] P. Mursia, V. Sciancalepore, A. Garcia-Saavedra, L. Cottatellucci, X. C. Pérez and D. Gesbert, "RISMA: Reconfigurable Intelligent Surfaces Enabling Beamforming for IoT Massive Access," in IEEE Journal on Selected Areas in Communications, vol. 39, no. 4, pp. 1072-1085, April 2021, doi: 10.1109/JSAC.2020.3018829.

[MDS21] P. Mursia, F. Devoti, V. Sciancalepore and X. Costa-Pérez, "RISe of Flight: RIS-Empowered UAV Communications for Robust and Reliable Air-to-Ground Networks," in IEEE Open Journal of the Communications Society, vol. 2, pp. 1616-1629, 2021.

[MSL23] L. Mo, F. Saggese, X. Lu, Z. Wang and P. Popovski, "Direct Tensor-Based Estimation of Broadband mmWave Channels With RIS," in IEEE Communications Letters, vol. 27, no. 7, pp. 1849-1853, July 2023, doi: 10.1109/LCOMM.2023.3270513.

[NTH19] A. Ndikumana, N. H. Tran, T. M. Ho, Z. Han, W. Saad, D. Niyato, and C. S. Hong, "Joint communication, computation, caching, and control in big data multi-access edge computing," IEEE Transactions on Mobile Computing, pp. 1–1, 2019.

[Nee10] M. J. Neely, Stochastic Network Optimization with Application to Communication and Queueing Systems. M. & C. Publishers, 2010

[PF05] D. P. Palomar and J. R. Fonollosa, "Practical algorithms for a family of waterfilling solutions," *IEEE Trans. Signal Process.*, vol. 53, no. 2, pp. 686–695, Feb. 2005.

[PHS05] C B Peel, B M Hochwald, and A L. Swindelhurst, "A Vector-Perturbation Technique for Near-Capacity Multiantenna MultiUE Communication - Part I: Channel Inversion and Regularization," IEEE Trans. Commun., vol. 53, no. 1, pp. 195–202, Jan. 2005.

[PSZ21] X. Pang, M. Sheng, N. Zhao, J. Tang, D. Niyato, and K.-K. Wong, "When UAV Meets IRS: Expanding Air-Ground Networks via Passive Reflection," IEEE Wireless Communications, vol. 28, no. 5, pp. 1–7, 2021.

[PTD22] N. S. Perović, L.-N. Tran, M. Di Renzo and M. F. Flanagan, "On the Maximum Achievable Sum-rate of the RIS-aided MIMO Broadcast Channel," IEEE Transactions on Signal Processing, vol. 70, pp. 6316 - 6331, 2022.

[RDP19] M. Di Renzo, M. Debbah, D.-T. Phan-Huy, A. Zappone, M.-S. Alouini, C. Yuen, V. Sciancalepore, G. C. Alexandropoulos, J. Hoydis, H. Gacanin, J. de Rosny, A. Bounceu, G. Lerosey, and M. Fink, "Smart radio environments empowered by AI reconfigurable meta-surfaces: An idea whose time has come," *EURASIP Journal on Wireless Communications and Networking*, 129, pp. 1–20, May 2019.

[QD21] X. Qian and M. D. Renzo, "Mutual Coupling and Unit Cell Aware Op-timization for Reconfigurable Intelligent Surfaces," in IEEE Wireless Communications Letters, vol. 10, no. 6, pp. 1183-1187, June 2021, doi: 10.1109/LWC.2021.3061449.

[SAH22] K. Stylianopoulos, G. C. Alexandropoulos, C. Huang, C. Yuen, M. Bennis, and M. Debbah, "Deep contextual bandits for orchestrating multi-UE MISO systems with multiple RISs," IEEE International Conference on Communications, Seoul, South Korea, 16–20 May 2022.

[SCK23] Saggese, F., Croisfelt, V., Kotaba, R., Stylianopoulos, K., Alexandropoulos, G. C., & Popovski, P. (2023). A Framework for Control Channels Applied to Reconfigurable Intelligent Surfaces. *arXiv preprint arXiv:2303.16797*.

[SCK23a] Saggese, F., Chiariotti, F., Kansanen, K., & Popovski, P. "Efficient URLLC with a Reconfigurable Intelligent Surface and Imperfect Device Tracking." 2023 IEEE International Conference on Communications Workshop, Rome, Italy (arXiv preprint arXiv:2211.09171).

[SCK23b] J. H. I. de Souza, V. Croisfelt, R. Kotaba, T. Abrão and P. Popovski, "Uplink Multiplexing of eMBB/URLLC Services Assisted by Reconfigurable Intelligent Surfaces," Submitted to IEEE Global Communications Conference (GLOBECOM), 2023, *arXiv preprint arXiv:2305.04629*.

[SH20] Q. Shi and M. Hong, "Penalty dual decomposition method for nons- mooth nonconvex optimization —Part I: Algorithms and convergence analysis," *IEEE Trans. Signal Process.*, vol. 68, pp. 4108–4122, Jun. 2020.

[SKP23] Saggese, F., Kansanen, K., & Popovski, P. "Localization-based OFDM framework for RIS-aided systems." 2023 IEEE International Conference on Communications Workshops (ICC Workshops), Rome, Italy (arXiv preprint arXiv:2303.12763.)

[SMD23] K. Stylianopoulos, M. Merluzzi, P. Di Lorenzo and G. C. Alexandropoulos, "Lyapunov-Driven Deep Reinforcement Learning for Edge Inference Empowered by Reconfigurable Intelligent Surfaces," ICASSP 2023 - 2023 IEEE International Conference on Acoustics, Speech and Signal Processing (ICASSP), Rhodes Island, Greece, 2023, pp. 1-5, doi: 10.1109/ICASSP49357.2023.10095112.

[SSH04] Q. H. Spencer, A.L. Swindlehurst, and M. Haardt (2004). Zero-forcing methods for downlink spatial multiplexing in multiUE MIMO channels. IEEE Transactions on Signal Processing, 52(2), 461–471.

[SSH22] K. Stylianopoulos, N. Shlezinger, P. del Hougne, and G. C. Alexandropoulos, "Deep-learning-assisted configuration of reconfigurable intelligent surfaces in dynamic rich-scattering environments," IEEE International Conference on Acoustics, Speech, and Signal Processing, Singapore, 22–27 May 2022.

[TKB22] R. A. Tasci, F. Kilinc, E. Basar, and G. C. Alexandropoulos, "A new RIS architecture with a single power amplifier: Energy efficiency and error performance analysis," IEEE Access, 2022.

[WFD20] P. Wang, J. Fang, H. Duan, and H. Li, "Compressed channel estimation for intelligent reflecting surface-assisted millimeter wave systems," *IEEE Signal Process. Lett.*, vol. 27, pp. 905–909, 2020.

[WHA21] L. Wei, C. Huang, G. C. Alexandropoulos, C. Yuen, Z. Zhang, and M. Debbah, "Channel estimation for RIS-empowered multi-UE MISO wireless communications," IEEE Transactions on Communications, vol. 69, no. 6, pp. 4144–4157, June 2021.

[WHG22] L. Wei, C. Huang, Q. Guo, Z. Yang, Z. Zhang, G. C. Alexandropoulos, C. Yuen, and M. Debbah, "Joint channel estimation and signal recovery for RIS-empowered multi-UE communications," IEEE Transactions on Communications, under revision.

[WLC20] Z. Wang, L. Liu, and S. Cui, "Channel estimation for intelligent reflecting surface assisted multiuser communications: Framework, algorithms, and analysis," *IEEE Trans. Wireless Commun.*, vol. 19, no. 10, pp. 6607–6620, Oct. 2020.

[WZ19] Q. Wu, and R. Zhang, "Intelligent Reflecting Surface Enhanced Wireless Network: Joint Active and Passive Beamforming Design", IEEE Transactions on Wireless Communications, vol. 18, no. 11, pp. 5394-5409, Nov. 2019.

[XH21] F. Xin and Y. Huo. "An Overview of Low latency for Wireless Communications: An Evolutionary Perspective," 2021 Online: https://arxiv.org/abs/2107.03484

[XYH22] X. Cao, B. Yang, C. Huang, G. C. Alexandropoulos, C. Yuen, Z. Han, H. V. Poor, and L. Hanzo., "Massive Access of Static and Mobile Users via Reconfigurable Intelligent Surfaces: Protocol Design and Performance Analysis," in IEEE Journal on Selected Areas in Communications, vol. 40, no. 4, pp. 1253-1269, April 2022, doi: 10.1109/JSAC.2022.3145908.

[YAK22] Yuan, J., Alexandropoulos, G. C., Kofidis, E., Jensen, T. L., & De Carvalho, E. "Tensor-based channel tracking for RIS-empowered multi-user MIMO wireless systems." 2022, arXiv preprint arXiv:2202.08315

[YH07] M. A. Yurkin and A. G. Hoekstra, "The discrete dipole approximation: An overview and recent developments," J. Quantitative Spectrosco-pyan d Radiative Transfer, vol. 106, no. 1, pp. 558–589, 2007.

[ZZ20] B. Zheng and R. Zhang, "Intelligent reflecting surface-enhanced OFDM: Channel estimation and reflection optimization," *IEEE Wireless Com- mun. Lett.*, vol. 9, no. 4, pp. 518–522, Apr. 2020.

[ZZD22] Y. Zhang, J. Zhang, M. Di Renzo, H. Xiao and B. Ai, "Reconfigurable Intelligent Surfaces With Outdated Channel State Information: Centralized vs. Distributed Deployments," in IEEE Transactions on Communications, vol. 70, no. 4, pp. 2742-2756, April 2022, doi: 10.1109/TCOMM.2022.3146344.

[ZSA23] H. Zhang et al., "Channel Estimation With Hybrid Reconfigurable Intelligent Metasurfaces," in IEEE Transactions on Communications, vol. 71, no. 4, pp. 2441-2456, April 2023, doi: 10.1109/TCOMM.2023.3244213.

[ZPR23] K. Zhi et al., " Two-Timescale Design for Reconfigurable Intelligent Surface-Aided Massive MIMO Systems With Imperfect CSI," IEEE Transactions on Information Theory, vol. 69, no. 5, pp. 3001 - 3033, May 2023.

[ZWS22] X. Zheng, P. Wang, J. Fang and H. Li, "Compressed channel estimation for IRS-assisted millimeter wave OFDM systems: A low-rank tensor decomposition-based approach", IEEE Wireless Commun. Lett., vol. 11, no. 6, pp. 1258-1262, Jun. 2022